E.O. Paton Electric Welding Institute of the National Academy of Science of Ukraine
International Association «Welding»

The Paton Welding Journal

01
2023

International Scientific-Technical and Production Journal ◊ Founded in January 2000 (12 Issues Per Year)

Address of Editorial Board
E.O. Paton Electric Welding Institute, 11 Kazymyr Malevych Str. (former Bozhenko), 03150, Kyiv, Ukraine
Tel./Fax: (38044) 205 23 90, E-mail: journal@paton.kiev.ua
https://patonpublishinghouse.com/eng/journals/tpwj

State Registration Certificate 24933-14873 ПР from 13.08.2021
ISSN 0957-798X, DOI: http://dx.doi.org/10.37434/tpwj

Subscriptions, 12 issues per year:
$384 — annual subscription for the printed (hard copy) version, air postage and packaging included;
$312 — annual subscription for the electronic version (sending issues in pdf format or providing access to IP addresses).

Representative Office of «The Paton Welding Journal» in China:
China-Ukraine Institute of Welding, Guangdong Academy of Sciences
Address: Room 210, No. 363 Changxing Road, Tianhe, Guangzhou, 510650, China.
Zhang Yupeng, Tel: +86-20-61086791, E-mail: patonjournal@gwi.gd.cn

The content of the journal includes articles received from authors from around the world in the field of welding, metallurgy, material science and selectively includes translations into English of articles from the following journals, published by PWI in Ukrainian:
- Automatic Welding (https://patonpublishinghouse.com/eng/journals/as);
- Electrometallurgy Today (https://patonpublishinghouse.com/eng/journals/sem);
- Technical Diagnostics & Nondestructive Testing (https://patonpublishinghouse.com/eng/journals/tdnk).

CONTENTS

ORIGINAL ARTICLES

---

*Translated Article(s) from «Automatic Welding», No. 01, 2023.
**Translated Article(s) from «Automatic Welding», No. 12, 2022.
***Translated Article(s) from «Technical Diagnostics & Nondestructive Testing», No. 4, 2022.

DOI: https://doi.org/10.37434/tpwj2023.01.01

STUDIES OF STRUCTURAL FEATURES OF JOINTS OF RAILS OF R260MN GRADE IN FLASH-BUTT WELDING

V.I. Shvets, O.V. Didkovskyi, I.V. Zyakhor, E.V Antipin, L.M. Kapitanchuk

E.O. Paton Electric Welding Institute of the NASU
11 Kazymyr Malevych Str., 03150, Kyiv, Ukraine

ABSTRACT

The properties and features of the microstructure of joints of the rail steel of R260MN grade with an elevated content of manganese produced by flash-butt welding with pulsating flashing were investigated. The formation of martensitic-austenitic structures due to non-uniform distribution of austenitic stabilizing manganese is shown. A number and sizes of isolated martensitic-austenitic structures is insignificant and does not critically affect the joint test results. The control of the segregation inhomogeneity of manganese is achieved by improving the metallurgical process.

KEYWORDS: flash-butt welding, rails of R260MN grade, hardness distribution, martensitic-austenitic structures, segregation inhomogeneity

INTRODUCTION

An increase in speed and load capacity of trains requires improvement of service characterisitcs of the rails. The possibilities of heat treatment of pearlite rail steels are limited. One of the ways to solve this problem is to improve the chemical composition of rail steel by changing the ratio of basic elements (carbon, manganese, silicon) and additional alloying. In pearlite rail steel of M76 grade, the content of carbon is estimated in the amount of 0.69–0.82 %, manganese — 0.75–1.05 % and silicon — 0.18–0.4% (Table 1). Carbon, manganese and silicon increase the resistance of overcooled austenite. The pearlite transformation occurs in the area of lower temperatures with the formation of lamellar structures with a high dispersion and, accordingly, strength. Vanadium, titanium and niobium microalloying provides a dispersion hardening of pearlite with a simultaneous decrease in the interlamellar distance and refinement of the microstructure [1, 2]. In the rail steels of grades E76F, K76F, M76F and E76T, K76T, the service characteristics are noticeably increased. The known are pearlite rail steels of grades M76KhSF and E76KhSF, where as alloying elements vanadium and chromium were used. Alloying with chromium improves the hardness of rails that increases their wear resistance.

In the course of works on the improvement of rail steels, the possibilities of increasing carbon content over eutectoid (> 0.82 %) was considered. The content of carbon in such rails of grade AREAL 136HE-370 produced by the Japanese corporation Nippon Steel & Sumitomo metal group amounts to 0.99–1.0 %. In [3], we showed that in flash-butt welding (FBW) of rails of hypereutectoid composition, a redistribution of carbon in the microstructure of joints occurs. The decay of hypoeutectoid carbide phase is accompanied by the formation of carbon inclusions. The latter causes a decrease in carbon content in the matrix and the formation of the structure of the joint similar to that of pearlite rails of the hypoeutectoid composition. It should be noted that in the area of coarse grain in the joint, the hardness as compared to the base metal is slightly reduced and amounts to *HV* 3900 MPa. The reason for this is the lack of hypoeutectoid carbide phase on the boundaries of primary austenitic grains.

One of the directions of improving the wear resistance of pearlite surface hardened rails was an increase in the content of manganese, which increases by calcination. These include rails of R260MN grade, the upper limit of the content of manganese is 1.34 wt.% (Table 1).

At the PWI, the technology of flash-butt welding of high-strength rails R260 and R350NT with pulsating flashing was developed and successfully used that provides stable mechanical properties at the level of the base metal. According to the thermokinetic curves, the decay of austenite in the thermodeformational conditions of FBW of the mentioned rail steels, the formation of martensite in the joints does not occur [4]. The microstructure of the joints is pearlite, which differs in different areas of HAZ with a degree of dispersion. The properties of joints meet the requirements of European standards [5, 6].

Using previous developments after optimization of the mode, welding of the batch of rails of R260MN(60E1) grade produced by the metallurgical company ArcelorMittal was carried out. The tests of welded joints on fatigue, static bending and hardness distribution carried out at the Rails Expertise Centre SNCS (France) recognized that the parameters and test results meet the requirements of the European

Table 1. Chemical composition of rail steels (wt.%)

	C	Mn	Si	P	S	Cr	Al	Ni	Ti	V
M76	0.71–0.82	0.75–1.05	0.25–0.45	≤0.035	≤0.04	–	–	–	–	–
AREAL 136 HE-X (NipponSteel, Japan)	0.99–1.00	0.69–0.71	0.50–0.52	≤0.030	–	0.21–0.22	≤0.005	–	–	0.04
R260	0.60–0.82	0.65–1.25	0.13–0.60	<0.03	<0.03	<0.15	<0.004	<0.1	<0.025	<0.03
R260MN standards of manufacturer ArcelorMittal, Spain	0.66	1.34	0.27	0.018	0.008	0.03	0.001	0.22	0.22	0.04
Rail R260MN(60E1) which was investigated	0.75	1.45	0.28	0.017	–	0.35	–	0.03	–	–

standard [7]. At the same time, a small number of structural components were found in the microstructure of joints of some batches of rails, whose hardness is ~ 776–900 *HV* 0.1, which does not meet the requirements of the European standard.

The aim of this work was to find the features of the microstructural state of HAZ of joints of rails of R260MN(60E1) grade.

PROCEDURE AND EQUIPMENT

The joints of rails of R260MN(60E1) grade with the content of manganese of 1.45 wt.% (Table 1) were considered. The joints were produced in the K1000 machine for flash-butt welding with pulsating flashing. After optimization of the mode, the recommended parameters should be within the following ranges: welding time — 70–90 s, welding current — 360–390 A, tolerance for flashing — 10–14 mm, value of the upsetting — 11–14 mm.

The macrostructure of the joints was detected in accordance with the requirements of GOST R51685–2013 on a full-profile template, cut out in the transverse direction. The etching of polished specimens was carried out with an aqueous out polished of chlorine iron.

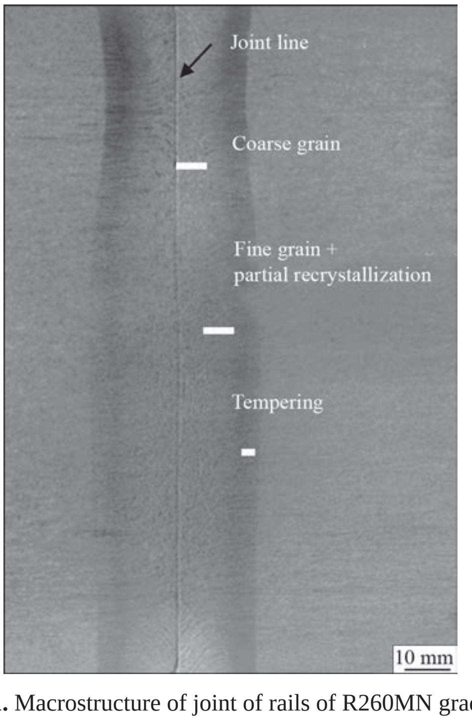

Figure 1. Macrostructure of joint of rails of R260MN grade

Metallographic examinations were performed in the optical NEOPHOT 32 microscope equipped with a digital camera. Microstructure was revealed by etching of preliminary polished specimens in a 4 % alcohol HNO_3 solution. To analyse the microstructure and determine the chemical composition of the structural components, the Auger-microprobe JAMP 9500F of JEOL Company (Japan) and X-ray energy dispersion spectrometer JNCA Penta FET x3 of Oxford Instrument Company were used. The energy of the primary electron beam was 10 keV at a current of 0.5 nA for SEM and EPMA methods. Before examinations, the surface of the specimens was subjected to cleaning directly in the analysis chamber of the device by etching with argon ions Ar+ with the energy of 1 keV during 10 min. The rate of etching over the reference SiO_2 specimen was 4 nm/min. The vacuum in the analysis chamber was within $5\cdot10^{-8}$–$1\cdot10^{-5}$ Pa.

The Vickers hardness was measured in the hardness meter NOVOTEST TC-GPB with a load of 292.4 N (30 kg). The distribution of hardness in the joint was investigated at a distance of 5 mm from the rolling surface of the rail.

RESEARCH RESULTS AND DISCUSSION

Metallographic examinations of joint macrostructure showed (Figure 1) that the HAZ is symmetric relative to the weld line. Its width was 30–40 mm and is within the limits admitted by the European standard [7] – 20–45 mm. The macrostructure of the HAZ is typical for similar joints of pearlite rail steels and consists of a weld zone, to which the area of coarse grain is adjacent. Further, the areas of small grain, partial recrystallization and tempering are located. Defects in the structure are absent.

According to the distribution curve (Figure 2), the hardness in the joint grows in the area of coarse grain and reduces in the tempering area. The level of deviation from the hardness of the base metal meets the requirements of the European standard: the maximum hardness should not exceed the hardness of the base metal by 60 *HV* 30, the minimum one should not be lower than the hardness of the base metal by 30 *HV* 30 [7]. Examinations of the joint microstructure showed that the base metal is hardening sorbite with some hypoeutectoid ferrite on the boundaries of primary austenitic grains (Figure 3). The contamination with nonmetallic inclusions is insignificant and corresponds to the grain size number 3–4 according to GOST 1778–70. Nonmetallic inclusions are represented by sulfides of a globular shape or which are elongated along the rolling direction with embeddiments of oxides and carbonitrides. Single globular inclusions of oxides are observed.

In the HAZ, microstructure represents mainly a lamellar pearlite of varying degree of dispersion (Figure 4). The size of the interlamellar distance in pearlite affects the values of hardness: reduction in the interlamellar distance leads to an increase in hardness. The exception is the tempering area. The microstructure of the tempering area is granular sorbite formed as a result of coagulation of carbide plates. Along the joint line in the band with a width of ~ 200 μm, primary austenitic grains are edged by the precipitations of hypoeutectoid ferrite. The size of primary austenitic grains corresponds to the size number 3–4 on the ASTM scale.

A characteristic feature of the joint microstructure is the formation of light areas in the HAZ, which are well distinguished against the background of pearlite.

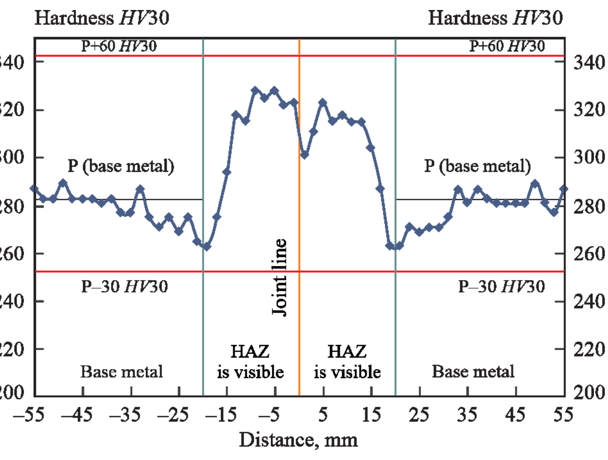

Figure 2. Distribution of hardness in the joint of rails of R260MN grade

Their size varies from tens to hundreds of microns. These structural components are observed along the rolling bands (Figure 5, *b*) and in the form of volumetric formations of arbitrary shape (Figure 5, *c*) at a distance of 1–5 mm from the joint line. Examinations in the electron microscope revealed similar structural components also on the boundaries of primary austenitic grains (Figure 5, *d*). The presence of acicular and lens-like inclusions within these structures with a hardness of 901–928 *HV* 0.1 and 762–776 *HV* 0.1 respectively gave reason to claim that these structural components represent residual austenite with decay products, in particular, acicular martensite, so-called martensitic-austenitic structure.

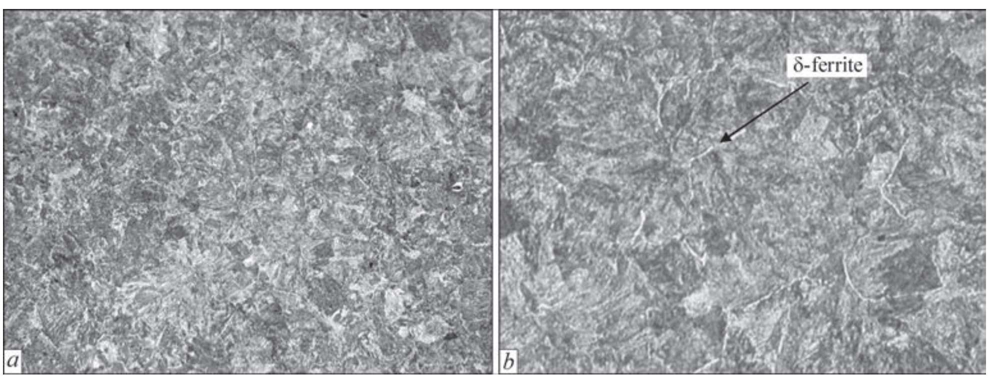

Figure 3. Microstructure of base metal of the rail of R260MN(60E1) grade: *a* — ×100; *b* — ×1000

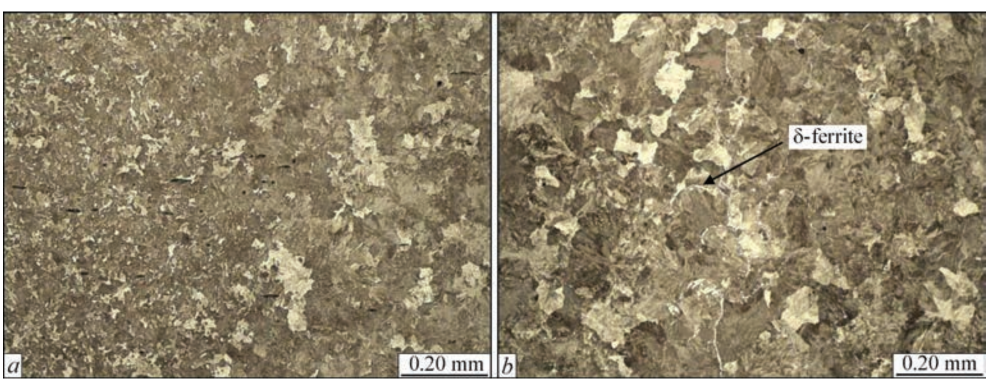

Figure 4. Microstructure of joint of rails of R260MN grade: *a* — transition zone base metal-HAZ; *b* — joint line, ×100

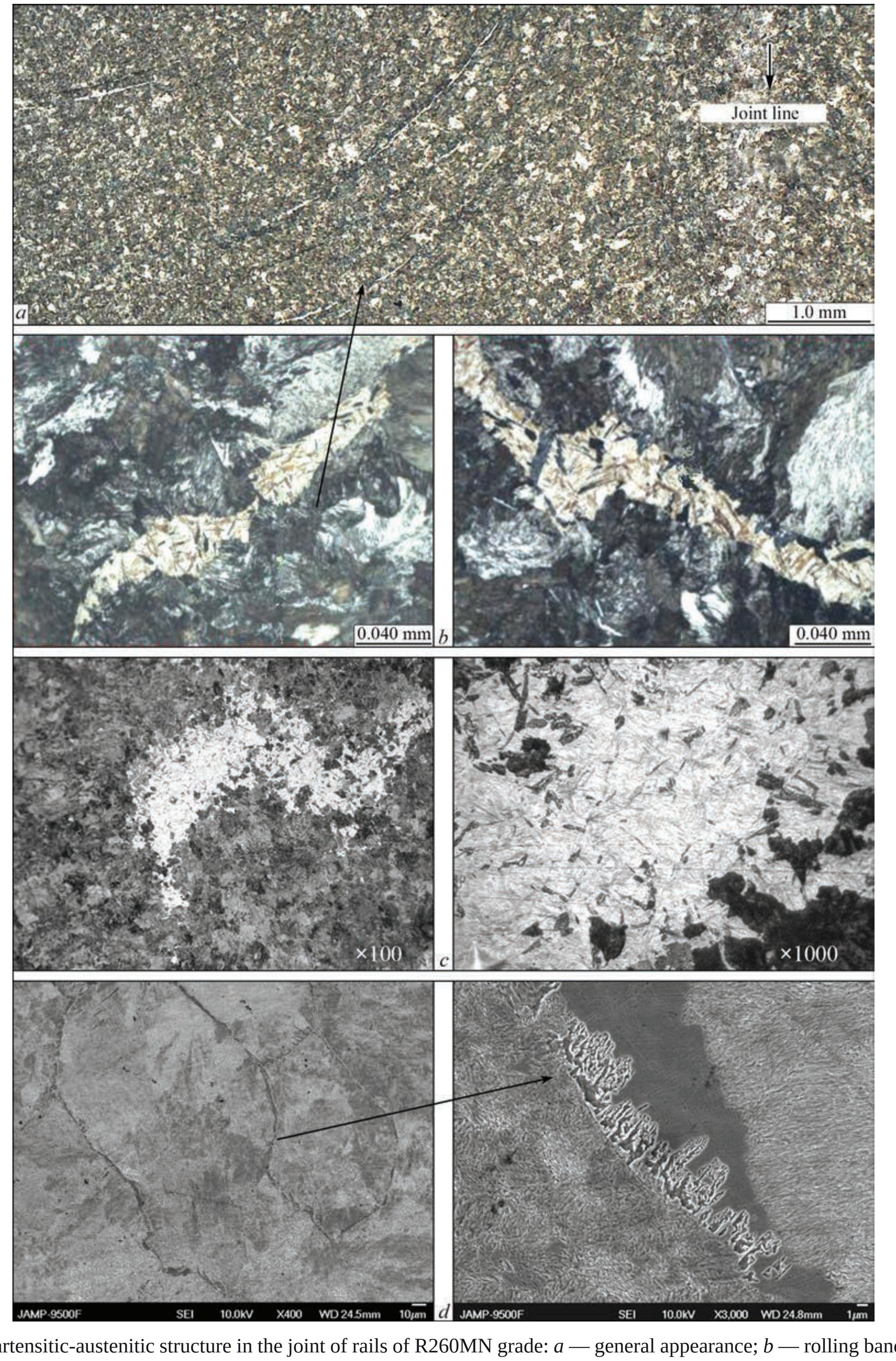

Figure 5. Martensitic-austenitic structure in the joint of rails of R260MN grade: *a* — general appearance; *b* — rolling bands; *c* — volumetric formations; *d* — boundaries of primary austenitic grains

While studying microstructure in the scanning electron microscope, the area presented in Figure 6, *a*, was considered. It was found that lens-like inclusions in residual austenite are bainite (Figure 7). Bainite is formed both in the volume of residual austenite (Figure 7, *a*) as well as on its boundary with the matrix (Figure 7, *b*). The features of bainite morphology and carbon distribution between ferrite, carbides and adjacent residual austenite are presented in Figure 7, *b*. Analysis of the structure parameters showed that the interlamellar distance in the pearlite of the matrix varies within 0.102–0.123 μm (Figure 6, *c*). This is commeasurable with the parameters of the structure of ordinary rail joints — 0.8–0.12 μm [8]. It should be noted that in the microstructure, there are areas with a higher degree of pearlite dispersion, in

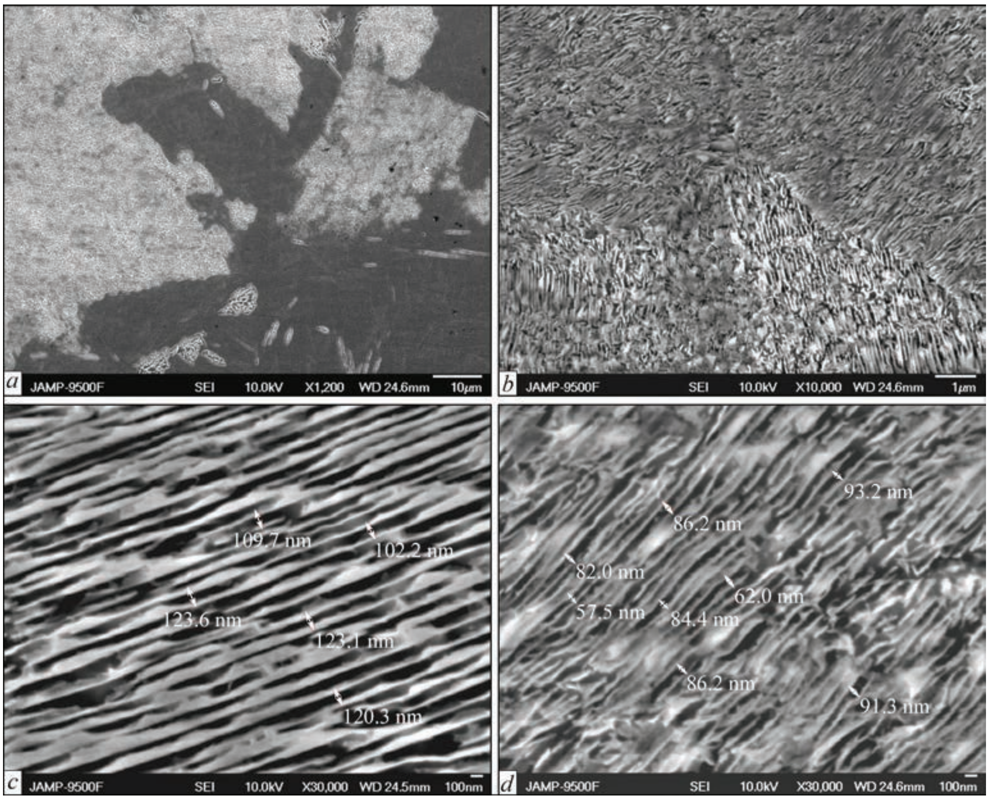

Figure 6. Pearlite in the microstructure of joints of rails of R260MN grade: *a* — area of analysis; *b* — matrix; *c*, *d* — results of measuring interlamellar distance

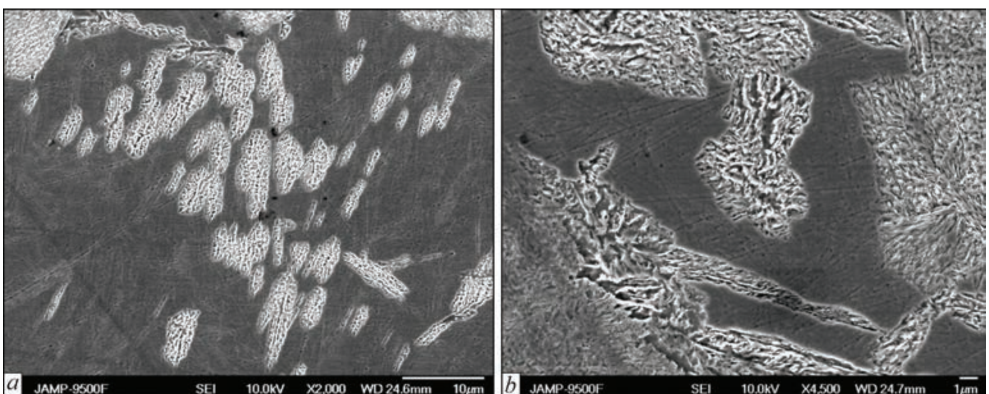

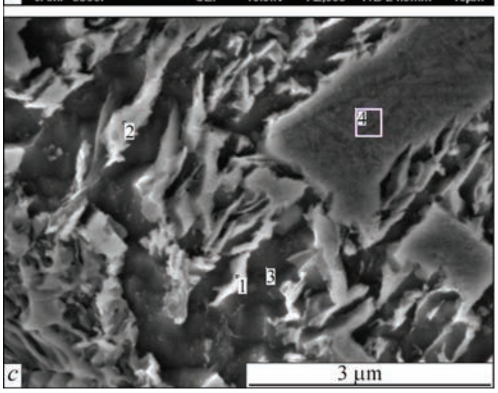

	C	Si	Mn	Fe	
1	12.79	0.58	1.90	84.73	Carbide
2	16.87	0.50	3.08	79.55	Carbide
3	4.98	0.66	2.13	92.23	Ferrite
4	8.45	0.50	2.94	88.11	Austenite

Figure 7. Bainite in the microstructure of joints of rails of R260MN grade: *a* — in the volume of residual austenite; *b* — on the boundary of residual austenite and matrix; *c* — results of X-ray microanalysis of structural components (at.%)

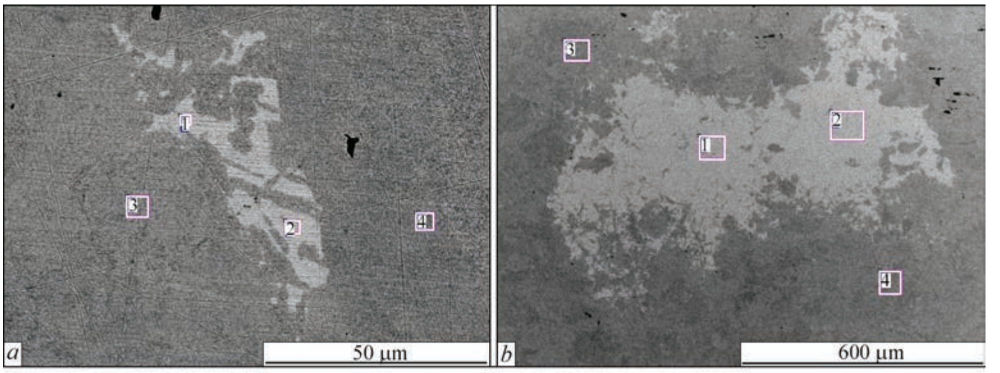

	C	O	Si	Mn	Fe
1	4.98	0.15	0.36	2.63	91.89
2	3.41	0.74	0.55	2.34	92.96
3	4.73	1.06	1.08	1.62	91.50
4	5.74	1.46	0.48	0.76	91.56

	C	O	Si	Mn	Fe
1	5.56	0.69	0.75	2.25	90.75
2	6.51	1.00	0.43	2.22	89.85
3	5.50	0.84	0.43	1.39	91.84
4	6.04	0.34	0.55	1.42	91.65

Figure 8. Results of X-ray microanalysis of chemical inhomogeneity in the region with martensitic-austenitic structures (at.%)

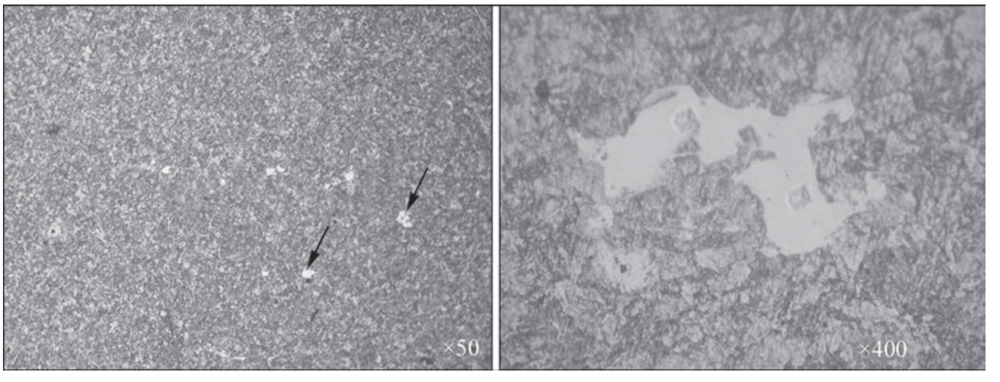

Figure 9. Microstructure of base metal after heat treatment on the mode: $T = 850$ °C, exposure is 4 min, cooling in the air

particular, on the boundary with residual austenite — 0.057–0.093 μm (Figure 6, *d*).

It is known that under other equal conditions, the nature of the decay of austenite during cooling is affected by the chemical composition [9]. The lack of systematic formation of residual austenite areas gives grounds to suggest about the chemical inhomogeneity of the joint metal. In the comparative analysis of the chemical composition of the matrix and residual austenite, an increased content of manganese in the latter was noted: 2.63–2.34 and 1.62–0.76 at.% (Figure 8, *a*) and 2.25–2.22 and 1.42–1.49 at.% (Figure 8, *b*), respectively. This is agreed with the fact that manganese is an austenite stabilizing element. The inhomogeneity of the distribution occurs due to the tendency of manganese to dendritic and zonal segregation during crystallization of steel castings [10]. The initial inhomogeneity is to some extent preserved after rolling and heat treatment, although it is converted. In the metal it is observed near the separate volumes enriched with manganese of the rolling band.

The effect of heat treatment on the possible transformation of martensitic-austenitic structures was studied. The following modes of the specimen heat treatment were used: $T = 850$ °C, $t = 4$ min; $T = 920$ °C, $t = 4$ min; cooling in the air. The comparative analysis of microstructures showed that normalization does not eliminate martensitic-austenitic structures. Moreover, martensitic-austenitic structures were manifested in the base metal (Figure 9). Obviously, the mentioned modes do not affect the inhomogeneity of manganese distribution. The elimination of inhomogeneity requires a homogenization tempering, which is hardly probable in the conditions of rail production.

It is known [11] that the degree of inhomogeneity depends mainly on the rate of cooling of castings in the production of steel. Probably, to eliminate the nonuniform distribution of manganese, it is necessary to control and improve the metallurgical process.

It is interesting to note about the inhomogeneity of the joint microstructure caused by nonmetallic inclusions. Thus, if manganese sulfides and oxides do not affect the structure formation (Figure 10, *a*, *b*), then, around complex nonmetallic inclusions, whose composition includes chromium oxicarbides, an area with a low carbon content is observed (Figure 10, *c*). The linear size of the area corresponds to the size of nonmetallic inclusions and amounts to ~100 μm. Re-

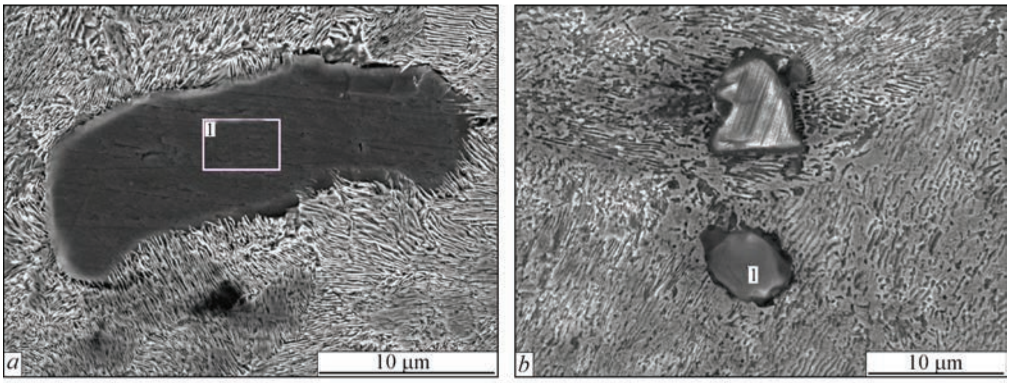

C	Si	S	Mn	Fe
1.01	0.05	46.40	44.87	2. 68

	C	O	Mg	Al	Ti	Mn	Fe
1	6.0	62.07	3.08	23.99	0.41	7.96	1.48

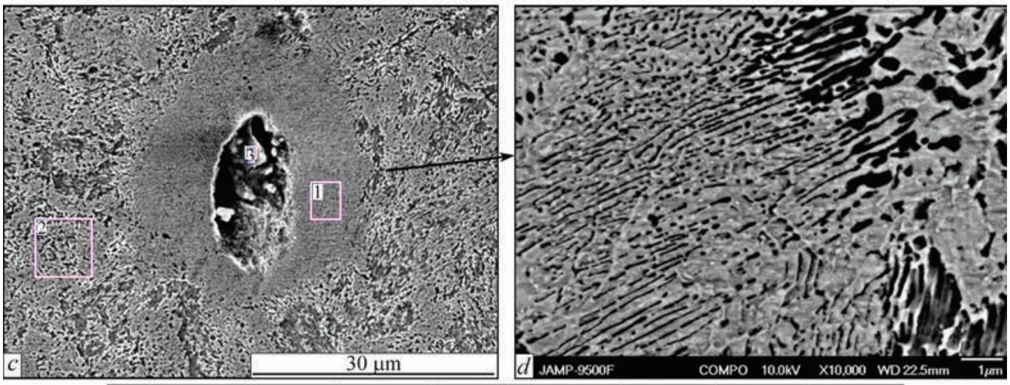

	C	N	O	S	Si	Cr	Mn	Fe
1	7.04	0.12	4.77	0	0.43	0.36	1.26	86.02
2	12.19	0.51	5.05	0.12	0.42	0.18	1.26	80.28
3	18.73	1.77	37.15	30.28	0	7.32	2.74	2.03

Figure 10. Nonmetallic inclusions in the steel of R260MN grade and the results of X-ray microanalysis of chemical composition of structures (at.%): *a* — manganese sulfide; *b* — complex oxides; *c* — complex nonmetallic inclusions with chromium content; *d* — transition zone

duction in carbon content shifts the transformation of austenite into a region of higher temperatures. This finds its reflection in the microstructure (Figure 10, *d*).

CONCLUSIONS

1. Formation of joints of the rails of R260MN grade with an elevated content of manganese in FBW as compared to the rails of R260 grade is satisfactory and similar to that one observed in typical pearlite rails.

2. In the joints of the rails of R260MN grade, there may be the formation of martensitic-austenitic structures along the rolling bands, on the boundaries of the primary austenitic grains, and also in the form of volumetric formations of an arbitrary shape at a distance of 1–5 mm from the joint line. The appearance of martensitic-austenitic structures is caused by the inhomogeneity of the distribution of an austenitic stabilizing manganese in the metal of the rails, which is prone to dendritic and zonal segregation during crystallization of steel castings. The presence of martensitic-austenitic structural components does not meet the requirements of the European standard for microstructure.

3. Normalization does not eliminate the inhomogeneity of manganese distribution in the joints of the rails of R260MN grade. Preventing the inhomogeneity of manganese distribution and the formation of martensitic-austenitic structural components in the microstructure requires the control and improvement of the metallurgical process in steel production.

REFERENCES

1. Shaposhnikov, N.G., Konov, A.A., Mogutnov, B.M. et al. (2004) Conditions of effective actions of nitride and carbonitride phases on structure refinement of structural pearlitic steels. *Stal*, **7**, 84–87 [in Russian].
2. Shipitsyn, S.Ya. (2014) High-carbon steels with dispersion nitride hardening for transport and other types of mechanical engineering. *Metall i Litio Ukrainy*, 256(**9**), 16–21 [in Russian].
3. Shvets, V.I., Didkovskyi, O.V., Antipin, Ye.V. et al. (2022) Features of microstructure of butt joints of hypereutectoid Areal-136HE-X rail steel in flash-butt welding. *The Paton Welding J.*, **3**, 34–40. DOI: https://doi.org/10.37434/tpwj2022.03.04
4. Popov, A.A., Popova, A.E. (1961) *Isothermal and thermokinetic diagrams of overcooled austenite decay*. Moscow, Mashgiz [in Russian].
5. Kuchuk-Yatsenko, S.I., Didkovsky, O.V., Antipin, Ye.V. et al. (2016) Flash-butt welding of high-strength rails. Mining–In-

formatics. *Automation and Electrical Engineering*, 528(**4**), 40–48.

6. Kuchuk-Yatsenko, S.I., Didkovsky, O.V., Antipin, Ye.V., Shvets, V.I. et al. (2017) Real-time operational control in information management system for flash-butt welding rails. Mining–Informatics. *Automation and Electrical Engineering*, 529(**1**), 36–42. DOI: http://dx. doi.org/10.7494/miag.2017.1.529.35
7. EN 14587–2007: *Flash butt welding of rails*. Pt 1 New R220.
8. Shur, E.A. (2012) *Damages of rails*. Moscow, Intekst [in Russian].
9. Sadovsky, V.D., Fokina, E.A. (1986) *Residual austenite in hardened steel*. Moscow, Nauka [in Russian].
10. Golikov, I.N., Maslenkov, S.B. (1977) *Dendritic segregation in steels and alloys*. Moscow, Metallurgiya [in Russian].
11. Babachenko, O.O., Dyomina, K.G., Kononenko, G.A. et al. (2021) Influence of cooling rate of continuous casting billet being solidified on parameters of dendritic structure of carbon steel with 0.54 % C. *Metalofiz. Novitni Tehnol.*, 43(**11**), 1537–1551[in Ukrainian]. DOI: https://doi.org/10.15407/mfint.43.11.1537

ORCID

V.I. Shvets: 0000-0003-4653-7453,
O.V. Didkovskyi: 0000-0001-5268-5599,
I.V. Zyakhor: 0000-0001-7780-0688,
E.V. Antipin: 0000-0003-3297-5382,
L.M. Kapitanchuk: 0000-0002-8624-2590

CONFLICT OF INTEREST

The Authors declare no conflict of interest

CORRESPONDING AUTHOR

I.V. Zyakhor
E.O. Paton Electric Welding Institute of the NASU
11 Kazymyr Malevych Str., 03150, Kyiv, Ukraine.
E-mail: zyakhor2@ukr.net

SUGGESTED CITATION

V.I. Shvets, O.V. Didkovskyi, I.V. Zyakhor, E.V. Antipin, L.M. Kapitanchuk (2022) Studies of structural features of joints of rails of R260MN grade in flash-butt welding. *The Paton Welding J.*, **1**, 3–10.

JOURNAL HOME PAGE

https://patonpublishinghouse.com/eng/journals/tpwj

Received: 27.12.2022
Accepted: 28.02.2023

DOI: https://doi.org/10.37434/tpwj2023.01.02

INFLUENCE OF THE FREQUENCY OF EXTERNAL ELECTROMAGNETIC FIELD ON THE STRUCTURE OF 09G2S STEEL WELDED JOINTS

O.D. Razmyshlyaev, S.Yu. Maksymov, O.M. Berdnikova, O.O. Prylypko, O.S. Kushnaryova, T.O. Alekseyenko

E.O. Paton Electric Welding Institute of the NASU
11 Kazymyr Malevych Str., 03150, Kyiv, Ukraine

ABSTRACT

Features of metal structure in 09G2S steel welded joints were studied in welding with application of a longitudinal external electromagnetic field. The influence of field frequency (f = 2; 12; 50 Hz) on phase composition, microstructure and microhardness of welded joint metal was studied. It was found that significant changes of structural parameters in the weld metal and in the subzones of the heat-affected zone (HAZ) take place in the studied frequency range. The influence of frequency of electromagnetic effect in low-alloyed steel welding is more pronounced in the metal of the weld and HAZ in the overheated subzone (coarse grain). Application of f = 12 Hz ensured a uniform microhardness level both in the weld metal and in the HAZ subzones, as well as grain structure refinement in the overheated subzone (I HAZ) of 09G2S steel welded joint.

KEYWORDS: 09G2S steel, welded joints, external electromagnetic impact, longitudinal magnetic field, frequency, heat-affected zone, phase composition, microstructural parameters, microhardness

INTRODUCTION

To control the processes of melting electrode and base metals, as well as the process of weld pool metal crystallization, it is promising to use external magnetic fields affecting the drop, arc and liquid metal pool [1, 2]. In arc welding, longitudinal magnetic fields (LMF) and transverse magnetic fields (TMF) are used. In the first ones, an induction vector is parallel and in the second ones, it is perpendicular to the electrode and arc axis. Magnetic control has advantages over mechanical methods, because it is carried out without a direct contact of the control devices with the surfacing (welding) zone [3].

The use of LMF and TMF in arc surfacing and welding allows intensifying the process of melting the electrode, regulating the efficiency of the base metal penetration, influencing the process of the weld metal crystallization [4, 5]. There are many studies devoted to the analysis of the physics of the process of metal penetration under the external electromagnetic effect (EEE), distribution of pressure over the radius of the arc, movement of the electrode drop, flows of liquid metal in the welding pool, metal crystallization, as well as mechanisms of refining the structure of welds metal, including cluster theories of liquid metal crystallization [4, 6–8]. Namely, refinement of the metal structure leads to an increase in the level of metal strengthening (according to the Hall–Petch dependence [9]), and also will ensure its crack resistance [4, 10, 11]. Of course, the structural state, which is formed in the metal of welded joints under the impact of thermodeformation conditions of welding, affects their physical and mechanical properties.

As is known, the frequency of current significantly affects the nature of the power action of the electromagnetic field on the liquid metal [8]. With a decrease in the frequency, on the one hand, the electromagnetic interaction of the inductor with the melt deteriorates and on the other — the area of action of volumetric electromagnetic forces in a liquid metal expands.

If we change the polarity of switching windings with a certain frequency, then the direction of flows of molten metal will also change. This movement of a liquid pool in the real process of arc welding (surfacing) promotes refinement of metal grains in the process of its crystallization. When interacting along the *OX* axis with the component of current density in the pool metal, the induction component B_x of TMF generates an electromagnetic force that directs the flow of a liquid metal along the *OY* axis. Additionally, a vertical component of electromagnetic force (F_z) appears from the interaction of current density j_y in the side edges of the pool with the induction component B_x. When the polarity changes, a liquid metal is mixed across the pool axis [7].

The impact of alternating TMF leads to widening of the deposited beads [12, 13]. At a frequency f = 50 Hz, widening of the bead occurred in proportion to induction. However, it should be taken into account that TMF variable with a frequency of up to 1 Hz provides a wavy transverse movement of the bead axis, and to eliminate this drawback, it is necessary to use the TMF frequency from 2 Hz and higher.

In [14], it was studied how in arc welding the action of alternating magnetic fields with low frequencies affects the microhardness, parameters of microstructure of metal of 09G2S steel welded joints and the dimensions of the HAZ. However, the effect of the external electromagnetic field frequency on the structure of welded joints, generated in the welds and HAZ metal, has not been studied so far.

Therefore, the aim of this work was to find the regularities of influence of the frequency of the external electromagnetic field, namely LMF on the structural and phase composition, microhardness and microstructure of welded joints of low-alloy 09G2S steel.

MATERIAL AND PROCEDURES

To generate LMF, the procedure was used described in [9]. As a result of welding structural low-alloy 09G2S steel (4 mm thick) with the use of additive Sv-08A wire (3 mm diameter) (flux AN-348), the welded joints were produced using LMF on the following welding modes: current I = 360 A; arc voltage U = = 30–32 V; welding speed v = 30 m/h; reverse polarity; on a copper flux baching. The joint type is C4 (GOST 8713–78). Magnetic induction in the zone of the welding pool was 20–25 mT. The welded joints of two variants were produced at different frequency: f = 12 and f = 50 Hz. The results of experimental examinations of microstructure of welded joints produced with the use of LMF at the mentioned frequencies were further compared with the experimental data produced at f = 2 Hz [14].

Microstructure examinations were carried out using the methods of light microscopy (microscopes Neophot-32 and Versamet-2, Japan). The Vicker's hardness was measured in the hardness meter M-400 (Leco Company, USA) at a load of 0.1 kg. The morphology of ferrite (F) and perlite (P), grain sizes (D_g), width of crystallites (h_{cr}), thickness of ferritic interlayers (h_i) and microhardness (HV) were studied. In the welded joints, the base metal (BM), the weld metal, the fusion line (FL), the HAZ over the subzones: I — overheating (coarse grain); II — normalization (complete recrystallization); III — partial recrystallization; IV — recrystallization were studied.

RESULTS AND THEIR DISCUSSION

The structure of the base metal of 09G2S steel is ferritic-pearlitic at D_g(F) = 10–20 μm, D_g(P) = 40–80 μm and HV = 1650–1760 (Figure 1, *a*). The structure of weld metal is also ferritic-pearlitic (F–P), Figure 1, *b*–*d*. The width of the crystallites of the P-component at f = 2 and f = 12 Hz is almost the same (Figure 1, *c*, Table 1). However, at f = 50 Hz, h_{cr}(P) increases in average by 48 % (Figure 1, *d*) with a decrease in microhardness by 10 % (as compared to the mode f = 2 Hz) and by 17 % (as compared to the mode f = 12 Hz, Table 1). The F-component is finer with approximately the same size for all modes and lower microhardness than pearlitic one. An

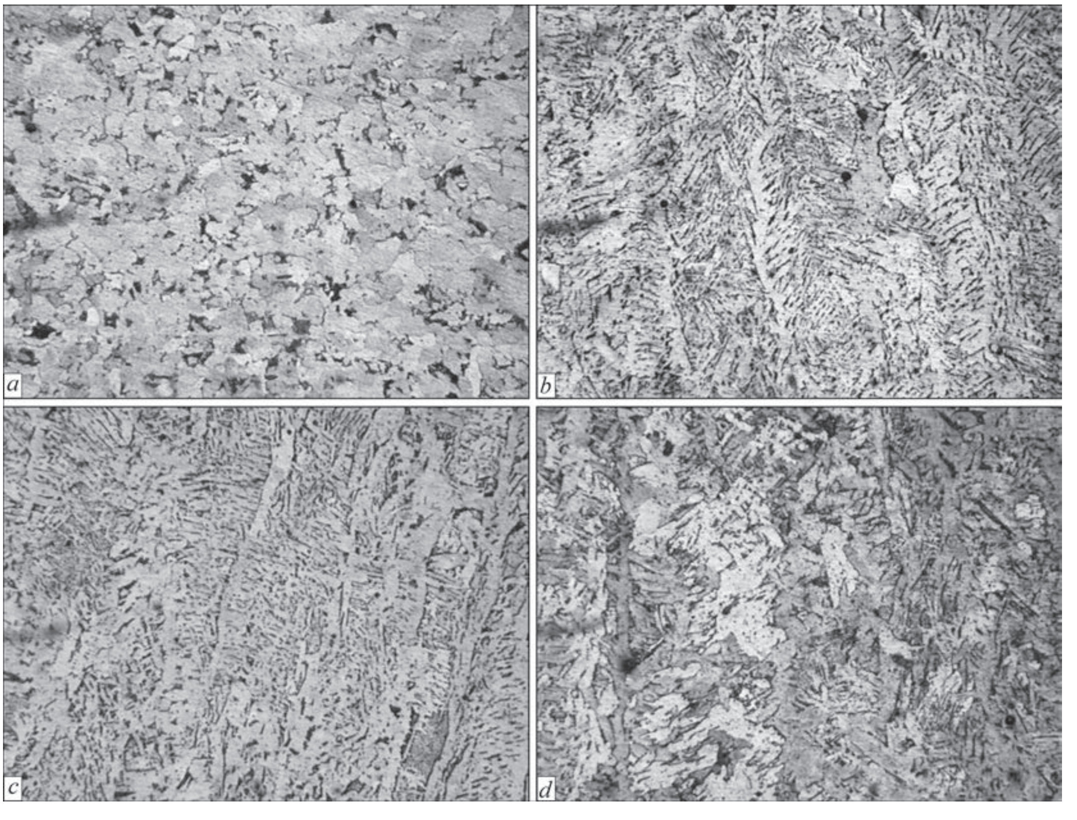

Figure 1. Microstructure (×250) of base metal (*a*) of 09G2S steel and welds (*b*–*d*) produced at different frequency: *b* — f = 2 Hz; *c* — 12; *d* — 50

increase in the width of crystallites at an increase in *f* correlates with the data of [14]. However, at *f* = 50, the structure is finer in average by 17 % as compared to the mode without the use of EEE [14].

Of course, an increase in the width of crystallites occurs at the stage of crystallization. If the axis of adjacent dendrite does not match the direction of a heat flow, it grows faster. In this case, the latent heat of melting, released into the surrounding liquid pool before the growing dendrites reduces the value of overcooling and will help to reduce the growth of adjacent ones [15]. Thus, a slow cooling of metal occurs.

In all cases, near the fusion line (FL), as compared to the weld metal, the width of crystallites is reduced (Figure 2, *a*, Table 1), which is associated with more intensive metal cooling in this subzone. In the specimen produced at *f* = 2 Hz near FL, a slight increase in *HV* (by 5 %, Table 1) is observed. At *f* = 50 Hz, in this zone, an average *HV* does not change, but the most uniform level of *HV* during the transition from the weld metal to LS is observed in the welded joint produced with the use of *f* = 12 Hz. It should be noted, that in all welded joints in the fusion line subzone, i.e., during the transition from the weld metal in I HAZ, single cold cracks are formed.

Studies of HAZ of specimens with the use of LMF at different frequency showed that in I HAZ of specimens on all modes a P-structure with ferrite interlayers is formed (Figure 2, *b*). In I HAZ of specimens at *f* = 12 and 50 Hz as compared to the specimen produced at *f* = 2 Hz, P-structure is refined (Table 2). The maximum grain size and the thickness of ferrite interlayers decrease, respectively, by 17 and 29 %. At the same time, the microstructure is slightly reduced — in average by 5 %. In II–IV HAZ in all modes, the structure is refined with the further uniform reduction in *HV* (Figure 2, *c*–*e*).

The studies of HAZ metal also revealed that during LMF, the frequency of the external electromagnetic field has an effect on the size of HAZ subzones (Table 2). In the studied welded joints at *f* = 12 and *f* = 50 Hz as compared to the welded joint produced at *f* = 2 Hz, the width (δ) of I HAZ increases by 25 and 8 %. This is associated with the more intensive movement of liquid

Table 1. Width of crystallites (h_{cr}, μm) and microhardness (*HV*, MPa) of metal of welded joints at different frequency (*f*) of LMF

Zone	h_{cr}(F)	h_{cr}(P)	*HV*(F)	*HV*(P)
	f = 2 Hz			
Weld	40–100	100–160	1760–1930	1990–2080
FL	20–40	60–140	1680–1990	1990–2280
f = 12 Hz				
Weld	20–100	80–160	1760–1930	2210
FL	20–60	60–140	1860	2060–2280
f = 50 Hz				
Weld	20–100	100–300	1650–1760	1810–1870
FL	50–100	60–200	1560–1700	1870

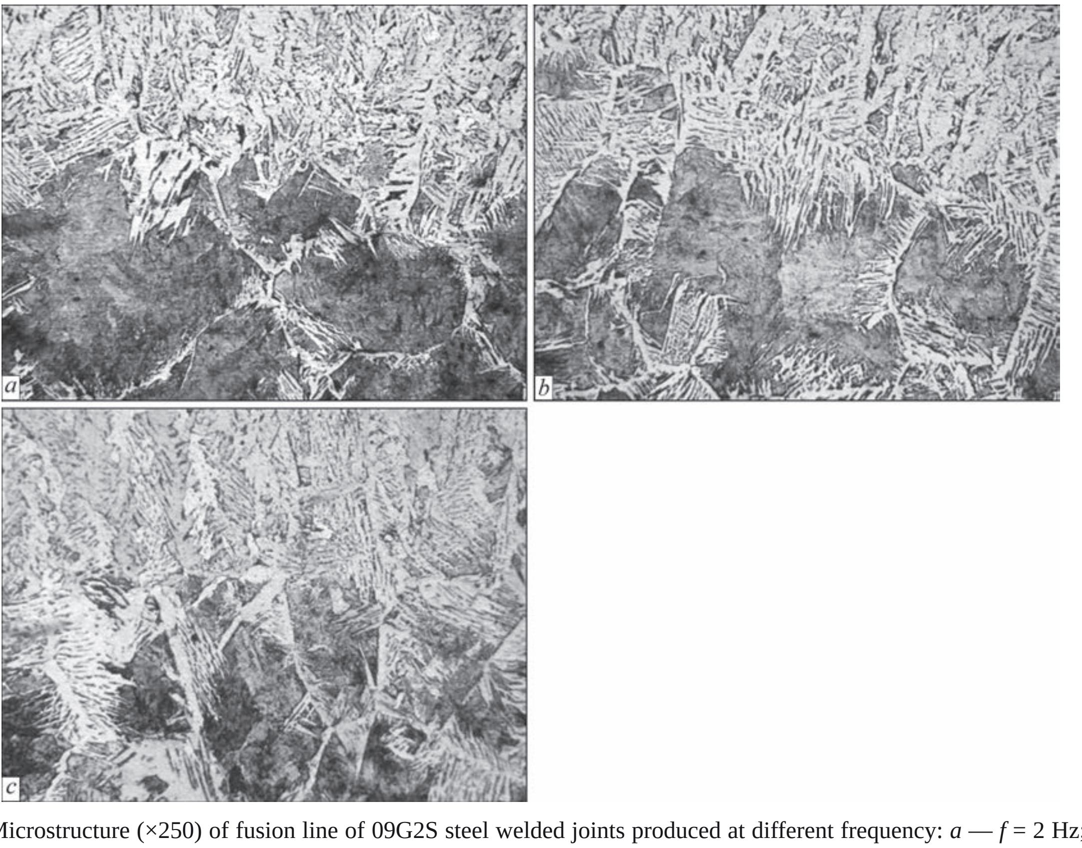

Figure 2. Microstructure (×250) of fusion line of 09G2S steel welded joints produced at different frequency: *a* — *f* = 2 Hz; *b* — 12; *c* — 50

Table 2. Width of HAZ subzones (δ, μm), grain size (D_g, μm) and microhardness (*HV*, MPa) of HAZ metal of welded joints at different frequency (*f*) of LMF

Zone	δ	D_g(F)h_i (F)*	D_g(P)	*HV*(F)	*HV*(P)
f = 2 Hz					
I HAZ	1300	30–70*	100–360	1810–1990*	2130–2210
II HAZ	1200	30–70	30–80	1870–1930	2060
III HAZ	1000	20–30	10–40	1810–1930	
IV HAZ	800	20–50	10–50	1870	
f = 12 Hz					
I HAZ	1650	20–50*	100–300	1760–1860*	2060
II HAZ	1000	50–100	30–100	1860	2060
III HAZ	1250	30–50	20–40	1700–1930	
IV HAZ	950	30–70	20–50	1650–1870	
f = 50 Hz					
I HAZ	1400	20–50*	140–300	1810–1870*	1890–2210
II HAZ	1500	20–80	50–100	1810–1870	2060
III HAZ	800	20–50	10–30	1760–1990	
IV HAZ	800	20–50	10–40	1600–1990	

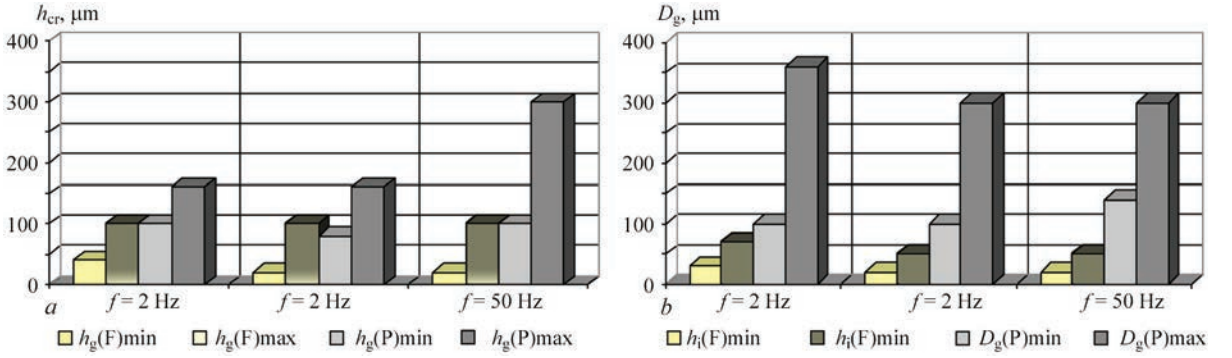

Figure 3. Change in structural parameters in the metal of 09G2S steel welded joints produced: with the use of LMF at different frequency *f*: *a* — width of crystallites (h_{cr}) in the weld metal; *b* — size of pearlite grains (D_g(P)) and thickness of ferrite interlayers (h_i(F)) in I HAZ

metal in the welding pool with an increase in *f* and, accordingly, with the thermal deformation conditions of structure formation in the HAZ metal.

An increase in the parameters of I HAZ, namely, in the overheating subzone can occur by changing the conditions of the process of melting and metal crystallization, namely, increasing the rate of heating liquid metal in the welding pool, as well as the temperature of its heating under the action of current pulses. Accordingly, this has an impact on an increase in the size of the overheating subzone (I HAZ) with an increase in the parameter *f*. The resulting temperature gradient contributes to an increase in the degree of overcooling and the rate of crystallization of the metal of the overheating subzone (I HAZ). This, in turn, leads to grain refinement of the structure in this subzone. In this case, an increase in width of I HAZ, which occurs with an increase in *f* will not negatively affect the properties of welded joints due to the refinement of the structure, as well as almost twice equalization of the gradient (Δδ) across the width of this zone — from Δδ = 600 μm (*f* = 2 Hz) to Δδ = 300 μm (*f* = 12 Hz) and Δδ = 400 μm (*f* = 50 Hz) (Table 2). This will provide a more uniform level of mechanical properties of the welded joint.

The studies revealed that the effect of the magnetic field frequency on structural changes is most noticeable in such subzones of welded joints as weld and I–II HAZ. The highest gradients in size of the grain structure are characteristic to the weld metal at *f* = 50 Hz (Figure 3, *a*) and metal of I HAZ at *f* = 2 Hz (Figure 3, *b*). At *f* = 12 Hz, the refinement of the grain structure is provided both in the weld metal as well as in the overheating subzone (I HAZ).

Thus, it was found how the effect of the external electromagnetic field, in particular, while using LMF, affects the sizes of HAZ, microstructure, microhardness of weld and HAZ metal in the welded joints of low-alloy 09G2S steel. The use of LMF at *f* = 12 Hz ensures refinement of grain structure in the weld metal and overheating subzone (I HAZ) as well as a uniform level of microhardness.

CONCLUSIONS

1. It was found that with an increase in the frequency of the electromagnetic field from *f* = 2 to 12 and

50 Hz, the microhardness and parameters of the microstructure of the weld metal and HAZ of 09G2S steel welded joints change. In this case, the phase composition of the base metal, the weld and HAZ metal is the same — ferritic-pearlitic.

2. At f = 50 Hz, in the weld metal, the width of the crystallites of the perlite component increases in average by 48 % with a decrease in microhardness by 10 % (as compared to the mode f = 2 Hz) and by 17 % (as compared to the mode f = 12 Hz). However, at f = 50, the structure is finer by an average of 17 % as compared to the mode without the use of EEE.

3. In the specimen produced at f = 2 Hz near FL, a slight increase in *HV* (by 5 %) is observed, and in I HAZ the most coarse grained structure is formed.

4. In I HAZ of the specimens at f = 12 and 50 Hz as compared to the mode f = 2 Hz, the structure is refined, respectively, by 17 and 29 %. Moreover, microhardness is reduced slightly — in average by 5 %.

5. Increase from f = 2 to 12 and 50 Hz leads to an increase in width of I HAZ in average by 25 and 8 %, but this will not negatively affect the properties of welded joints due to the structure refinement, as well as equalization of the gradient across the width of this zone from both sides of welds.

6. It was found that the mode at f = 12 Hz provides the most uniform level of microhardness both in the weld metal as well as over the subzones of HAZ and the formation of a fine-grained ferritic-pearlitic structure in the welded joint.

REFERENCES

1. Ryzhov, R.N., Kuznetsov, V.D. (2006) External electromagnetic effects in the processes of arc welding and surfacing (Review). *The Paton Welding J.*, **10**, 29–35.
2. Kuznetsov, V.D., Ryzhov, R.N. (2005) Choice of optimal parameters of external electromagnetic action in arc methods of welding. *The Paton Welding J.*, **6**, 27–31.
3. Grabin, V.F. (1982) *Metals science of fusion welding.* Kyiv, Naukova Dumka [in Russian].
4. Ryzhov, R.N. (2007) Influence of pulse electromagnetic effects on process of formation and crystallization of welds. *Svarochn. Proizvodstvo*, **2**, 56–58 [in Russian].
5. Ahieieva, A.D. (2019) Rational using of the controlling longitudinal and transverse magnetic fields at arc welding and surfacing. *IOP Conference Series: Materials Sci. and Engineering*, 582.
6. Korab, N.G., Kuznetsov, V.D., Chernysh, V.P. (1990) Evaluation of effect of controlling magnetic field on crystallization in arc welding. *Avtomatich. Svarka*, **2**, 33–36 [in Russian].
7. Abralov, M.A., Abdurakhmanov, R.U. (1982) On refinement mechanism of weld metal primary structure under electromagnetic action. *Avtomatich. Svarka*, **2**, 18–21 [in Russian].
8. Razmyshlyaev, A.D., Ageeva, M.V. (2018) On mechanism of weld metal structure refinement in arc welding under action of magnetic fields (Review). *The Paton Welding J.*, **3**, 25–29. DOI: http://dx.doi.org/10.15407/tpwj2018.03.05
9. Razmyshlyaev, A.D., Ageeva, M.V. (2014) On optimality of input devices of transverse magnetic field with regard to processes of arc welding and surfacing. In: *Proc. of Int. Sci.-Pract. Conf. on Innovative Technologies and Economics in Mechanical Engineering, 22–23 May, 2014*, **1**, 83–88.
10. Goldshtein, M.I., Litvinov, B.M., Bronfin, V.S. (1986) *Physics of metals of high-strength alloys.* Moscow, Metallurgiya [in Russian].
11. Romaniv, O.N. (1979) *Fracture toughness of structural steels*. Moscow, Metallurgiya [in Russian].
12. Boldyrev, A.M., Birzhev, V.A., Chernykh, A.V. (1992) To calculation of hydrodynamic parameters of liquid metal on bottom of welding pool in arc welding. *Svarochn. Proizvodstvo*, **2**, 31–33 [in Russian].
13. Boldyrev, A.M., Birzhev, V.A., Martynenko, A.I. (2008) Examination of influence of alternating axial magnetic field on process of electrode wire melting. *Svarochn. Proizvodstvo*, 2(**6–8**), 63, 64 [in Russian].
14. Razmyshlyaev, O.D., Maksymov, S.Yu., Berdnikova, O.M. et al. (2022) Effect of external electromagnetic field configuration on metal structure of welded joints of structural steel. *The Paton Welding J.*, **10**, 13–17.
15. Grabin, V.F., Denisenko, A.V. (1978) *Metals science of welding of low- and medium-alloy steels.* Kyiv, Naukova Dumka [in Russian].

ORCID

S.Yu. Maksymov: 0000-0002-5788-0753,
O.M. Berdnikova: 0000-0001-9754-9478,
O.O. Prylypko: 0000-0001-5244-5624,
O.S. Kushnaryova: 0000-0002-2125-1795,
T.O. Alekseyenko: 0000-0001-8492-753X

CONFLICT OF INTEREST

The Authors declare no conflict of interest

CORRESPONDING AUTHOR

S.Yu. Maksymov
E.O. Paton Electric Welding Institute of the NASU
11 Kazymyr Malevych Str., 03150, Kyiv, Ukraine.
E-mail: maksimov@paton.kiev.ua

SUGGESTED CITATION

O.D. Razmyshlyaev, S.Yu. Maksymov, O.M. Berdnikova, O.O. Prylypko, O.S. Kushnaryova, T.O. Alekseyenko (2022) Influence of the frequency of external electromagnetic field on the structure of 09G2S steel welded joints. *The Paton Welding J.*, **1**, 11–15.

JOURNAL HOME PAGE

https://patonpublishinghouse.com/eng/journals/tpwj

Received: 16.12.2022
Accepted: 28.02.2023

DOI: https://doi.org/10.37434/tpwj2023.01.03

TECHNOLOGIES OF REPAIRING CATHODE UNIT OF ELECTRON BEAM GUN WITH THE USE OF ELECTRON BEAM WELDING

V.I. Zagornikov, V.M. Nesterenkov, Yu.V Orsa, A.M. Ignatenko

E.O. Paton Electric Welding Institute of the NASU
11 Kazymyr Malevych Str., 03150, Kyiv, Ukraine

ABSTRACT

The elements of repair technology of electron beam welding in the manufacture of a metal-ceramic cathode unit of a powerful welding electron beam gun are considered. A low degree of heat generation at the place of weld overlapping inherent in electron beam welding reduces the risk of buckling parts being joined and provides the maximum compliance with the required sizes of the unit. The need in repair of the cathode unit was determined by the cases of supplying imported insulators with defects in the form of deviations of a thickness from 0.5 to 1.0 mm in the wall of the metal flange ("collar") in the brazed joint with the insulator. It was necessary to eliminate the consequences of a violation of the mechanical treatment of the insulator collar after brazing. The possible ways and schemes of repair technologies of such units are shown that allow avoiding the rejection of valuable parts and transferring them to the category of those subjected to restoration. The presented repair technologies involve the use of circumferential inserts-bandages of different configuration for two variants to eliminate welding defects associated both with local repair of the edge as well as with repair of its quite elongated areas. Due to a correct choice of the shape of repair inserts, the use of some technological methods and observance of the accuracy of assembly and the sequence of repair welding, it became possible to preserve geometric dimensions and to ensure the functionality of the welded assembly as a whole.

KEYWORDS: electron beam welding, pulsed mode, nickel alloy, cathode unit, repair circumferential shaped insert, schemes of joints of different welding stages

INTRODUCTION

In electronic devices the types of joints are used inherent in general engineering (butt, overlapped and fillet), but the shape of prepared edges in some cases is significantly different from the conventional one. These are joints with edges flanging instead of overlapped or butt joints. Such joints allow reducing the total heating of welded parts, reducing the total deformation of the assembly and restoring joints after cut out for repair [1, 2]. For joints the tolerances on assembly sizes over edges flanging are less rigid, which makes them more challenging in manufacture and repair of thin-walled joints [3].

In repair works, where it is necessary to provide a minimal heat impact on a product (in our case, cathode unit (CU) of the electron beam gun (EBG), the use of electron beam welding (EBW)) is challenging [4].

Since fusion welding of electronic devices is performed without filler material and the weld is formed from the metal of melting edges of welded products, the accuracy of grooving welded edges (thickness of machined edges around the perimeter of the circumferential joint) becomes essential.

The need to consider the variants of restorative repair of this expensive unit was determined by the cases of import delivery of sets of insulators with different thickness of the flange — "collar" brazed-in to the wall for welding EBG. Taken into account a high cost of EBW equipment, the possibility to avoid rejection of individual EBG units and transfer them to the category of those subjected to restoration by repair, is very relevant.

For repair it is necessary to form a defect-free welded joint without damage to adjacent brazed areas. The repair of such joints was not previously carried out, so the development of elements of repair technologies on the example of assembling the joint of the "leg" (CU) into the brazed "collar" of the ceramic insulator of EBG becomes relevant. Welding on the edges flanging did not cause difficulties until there was a need to produce a vacuum-tight weld on flanging in the presence of different thickness of the wall of the "collar" of the insulator along the perimeter as a result of its machining after brazing with the violation of technological mode. In the process of welding in the places of thinning of the wall of the joint, there was a local burnout with the violation of vacuum tightness of the weld, there were undercuts, loss of weld shape (Figure 1, *a*, *b*). This variant is possible and almost inevitable as a result of a violation of the mode of mechanical treatment of the "collar" of the insulator after brazing and before welding. Repeated, "cosmetic" pass in this case appeared to be ineffective, which required the development of other methods of repair technologies.

The following technological repair methods and rules found a real embodiment in our work:

- prevention of burnout and flashing of thin edges in the weld zone by increasing the intersection of parts by inserts to remove the edge from the welding zone;

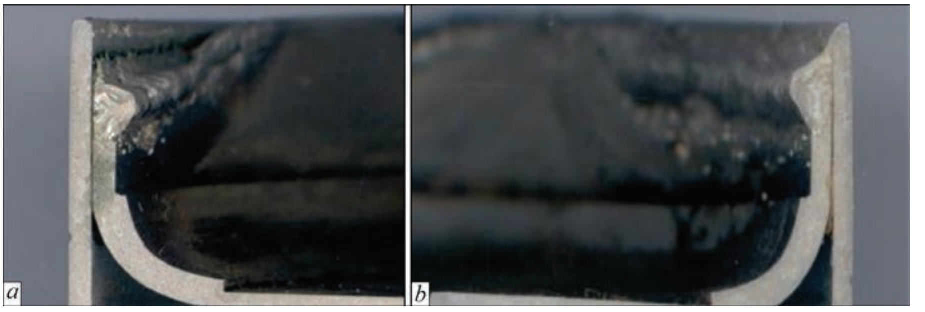

Figure 1. Defects of welded joint formation caused by violation of the technological mode of assembly and welding: *a* — leaking of weld metal down the inner side wall; *b* — loss of weld shape, undercut of the inner edge

- removal of defects by repeated passes with mounting gaskets — circumferential inserts of different configuration;
- pulsed mode that provides minimal specific heat input to the welding zone and accurate power adjustment, minimizes the risk of burn-through and buckling of thin-walled joints (less than 1–2 mm);
- obtaining the required weld shape to eliminate root defects. It is mainly realized by the choice of level of beam focusing and electron beam scanning;
- providing local rigidity of the joint fixation by mounting numerous tacks, i.e. by preliminary welding of edges at several points along the length of the joint.

Development of the tooling with an accurate fixing of parts by the clamp with efforts that do not exclude the possibility of free shrinkage and prevents the development of hot cracks during welds shrinking. I.e., it provides a decrease in rigidity of fixing welded workpieces.

The aim of the work is the development of repair technology of assembly and welding of CU, which is a part of welding EBG, taking into account the need to eliminate the consequences of violation of the mode of mechanical treatment of the “collar” of the insulator after brazing.

The task was to develop a repair technology, which due to the rational designing of welded repair elements, the use of technological EBW methods and the use of modern welding equipment will significantly reduce the cost of manufacture and repair of electronic equipment units.

MATERIALS AND RESEARCH PROCEDURE

The studies were performed in the laboratory installation of UL-112 type for EBW designed by the PWI of the NASU, which has a working chamber with inner sizes of 600×600×600 mm. The installation has a relatively simple design with a stationarily fixed outer welding gun, equipped with a manipulator that provides a linear movement of the table along the coordinates *X*, *Y*. As a structural material for the manufacture of CU, kovar 29NK alloy was used. To work out the technique of welding-in CU in a thin-walled flange (“collar”) of the insulator, the rotator of the installation was provided with a high-precision CNC-controlled electric drive (computer numerical control). A high-voltage power source with a power of 15 kW was used at an accelerating voltage of 60 kV. The emission system of the welding gun provided an electron beam current of up to 250 mA. To combine an electron beam with a welded joint, a coaxial television monitoring system was used. The use of a coaxial television system allows realizing accurate positioning of an electron beam axis with a welded joint [3].

EXPERIMENTAL PART AND DISCUSSION

The influence of preparing welded edges on the quality of welded joints was revealed. To provide the high quality of the weld, the joined surfaces should be obligatory subjected to cleaning from conservation means, contaminants, rust and oxide films. Immediately before welding, the outer surface of welded parts in the joint area can be cleaned with a low-power scanning electron beam, preventing flashing edges to enable the software adjustment of the electron beam position relative to the joint during welding.

When developing the welding technology, simulator specimens for practicing welding modes did not fully reflect the stress-strain state of the real welded joint [5]. However, previous experience in welding parts of such type allowed minimizing the number of adjustable parameters to produce a quality weld. They include the range of admissible specific heat input from the so-called elimination of overheating and violation of vacuum tightness of the weld (welding in the pulsed mode), the minimum value of the gap in the joint, angle and place of guiding of the electron beam into the welded joint. The maximum penetration depth without splashing of metal can be achieved at an optimal combination of increased pulse duration and reduced power density. The coefficient of overlapping of adjacent spots is an important criterion that affects the quality of welds. To produce dense welds, its recommended values are from 50 to 80 % [2, 6]. The choice of welding speed was performed empirically on simulator specimens. For the analyzed thicknesses, the choice of welding speed in the region of 10 mm/s increased the possibility of producing quali-

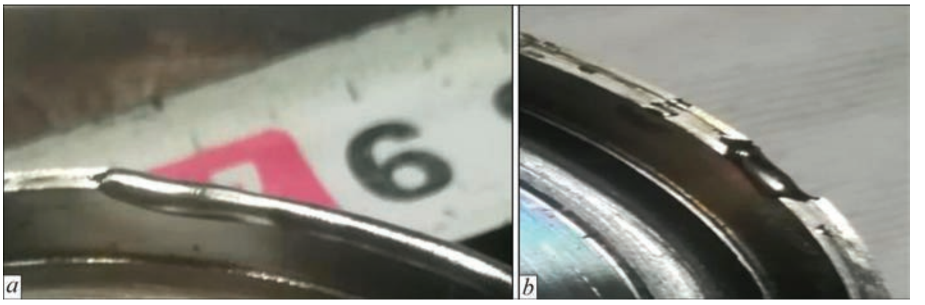

Figure 2. Initial fragment of the weld (*a*) and the tack (*b*)

ty weld formation. On the basis of the carried out calculations and experiments, the following parameters of the pulsed mode of EBW were determined:

Accelerating voltage U_{acc}, kV 60
Beam current, mA. 13.5–15.0
Working distance, mm 70–300
Frequency of passed pulses *f*, Hz 30
Pulse duration τ_{pulse}, ms 16.5
Pause duration τ_{pause}, ms 16.5

For successful welding with full penetration and lack of fusion of the edges, it is necessary to defocus the electron beam so that on the welded surface of edges the focal spot was not less than 0.8 mm and not more than 1.0 mm. The size of the focal spot was set experimentally. The focus of the beam was pulled on 1–2 mm relative to the surface of the welded edge (sharp focusing I_{fo} plus 15–25 mA). Adjusting these values can significantly increase the stability of the welding pool and eliminating metal splashes. The lack of splashing of the welding pool metal significantly improves the aesthetic appearance of the product, and also reduces the probability of surface corrosion appearance.

It is also necessary to consider the fact (related to the features of the EBW method itself), that with an increase in gaps over a certain limit, it is almost impossible to produce satisfactory formation of welds without undercuts and burnouts. The sizes of the gaps are very critical because the thickness itself of the wall of the brazed flange–collar is only 0.5 mm in some places. The developed designs of assembly and welding equipment provided the addition of a butt joint with minimal (not more than 0.08 mm) gaps on the end surfaces and guaranteed tension over cylindrical ones [1, 5]. The negative impact of gaps on the shape of the weld was eliminated. Checking the accuracy of assembly was carried out with templates and probes. In order to provide that in the welding process the set gaps and position of thin-walled parts are not changed, preliminary tacking of the parts is made before welding. The tacks are designed to position the joined elements maintaining their shape and dimensions before the final EBW [4, 5]. In order to avoid overheating of the product and violation of the tightness of the welds, it is necessary to reduce the feeding and removal of the current while producing tacks. The length of each of two linear tacks should be at least 2–5 of the thicknesses of the base metal. The dimensions of the tacks section should be such that they are melted completely during overlay of the main welds (Figure 2).

As the distance between the tacks decreases, the maximum displacement of the joint decreases during the main welding pass with the electron beam [4]. The priority of spot tacks over linear in terms of minimizing heat input into the weld and reducing deformations is emphasized. Therefore, most often at a considerable difference in the thickness of the walls of the parts instead of linear tacks to be welded, numerous spots were used. It is recommended to reduce the heat input of spot tacks, which are placed diametrically opposite (criss-cross) in the amount of 8–16 pcs. The current of the focusing lens corresponded to the sharp focusing at a set working distance — 200 mm (I_{fo} = 600 mA plus 25 mA).

The mode of producing welding tacks is given in Tables 1 and 2.

The formation of the weld of the required shape with a smooth (without undercuts) transition from the weld surface to the base metal was carried out due to the correct distribution of the electron beam concentration. In all cases, the joint is performed by EBW with a requirement (justification) of minimum admis-

Table 1. Parameters of the mode of producing welding spot tacks (without modulation)

Beam current I_b, mA	Current of focusing lens on the surface I_{fo}, mA	Operating current of focusing lens I_f, mA	Working distance, mm
4	600	625	200

Table 2. Parameters of the mode of producing welding spot tacks (with modulation)

Beam current I_b, mA*	Current of focusing lens on the surface I_{fo}, mA	Operating current of focusing lens I_f, mA	Working distance, mm	Welding speed v_w, mm/s
8	600	625	200	10
*Welding in a pulsed mode.				

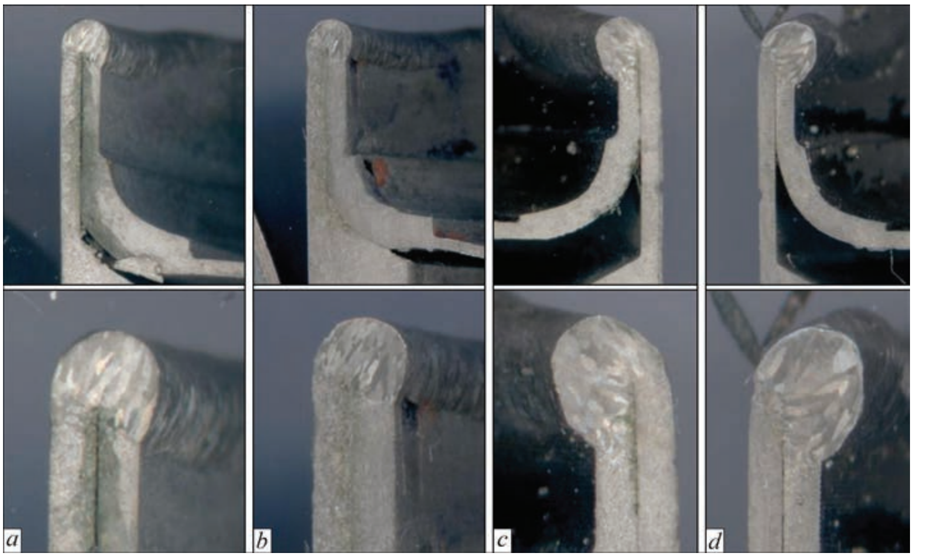

Figure 3. Transverse macrosections on specimens-simulators of different modes of electron beam weld with two-sided edge flanging with one and multiple repair passes: EBW in a standard mode (*a*), pulsed EBW (*b*), double remelting in a pulsed mode (*c*), triple remelting in a pulsed mode (*d*)

sible sizes of welds and limitation of the number of repeated passes (Figure 3). To reduce the probability of pores and cracks formation, edges flashing with the loss of their shape, the number of repeated repair passes should not exceed two.

ASSEMBLY FOR WELDING, APPROPRIATE TECHNOLOGICAL EQUIPMENT, CHOICE OF WELDING MODES BY TWO VARIANTS

Fundamental features of methods of fixing CU elements during its assembly for welding and the main provisions of technology of EBW of CU were developed previously in [3].

For two variants of eliminating welding defects, repair technologies at the final stage of the operation of producing joints of "CU as an assembly" involve the use of circumferential inserts of different configuration and use of them as a bandage to provide the calculated strength and accuracy of the sizes of the assembly.

The similar designs of inserts are simple and advantageous in the fact that they provide sufficient volume of additional metal, fixation and dense contact of the joined parts. A scheme of welded repair joints, fundamentally independent of this was developed irresective of a local or elongated defect.

Before welding CU, it should be mounted into the mandrel and each time the radial beating should be checked, which should not exceed ± 0.05 mm.

Let us consider two repair variants in more detail.

VARIANT No. 1

Welding-in of CU into the brazed flange of the ceramic insulator of EBG in the presence of flange vertical wall thickness different along the perimeter (0.5–1.0 mm) in two stages. Here, it is possible to produce a vacuum-tight weld after a proper preparation of the welding place, butt mounting of a remained shaped circumferential insert with the edges flanging, followed by EBW on both sides in a pulsed mode.

The assembly and welding device represents a support mounted and fixed on the rotator. The insulator for EBW assemblled on it with a shaped circumferential insert is fixed by a flange and studs. Protection of the ceramic surface of the insulator from spraying with metal vapors in EBW at the working power was carried out by aluminium foil outside and by inserts of nonmagnetic material directly in the joint area.

The circumferential insert in the first variant was applied based on the need to give the edges approximately the same cross-sectional size (Figure 4).

Such an insert is intended to reduce the criticality of the failure to keep with the same (1.0 mm) thickness around the perimeter of the wall of the thin-walled "collar" brazed-in to the insulator. The use of this shape of technological insert provides an accurate fixation of welded edges with the minimum gap and provide their parallelism. In the process of welding, the heat source (electron beam) affects mainly on the flange of the shaped substrate, which significantly reduces the overheating of welded parts and makes it possible to avoid the appearance of burnouts in the joint. During welding-in of the "leg" to the repaired insulator, the protection of the ceramic surface of the insulator in the form of a shielding device of nonmagnetic material was used. Atop over the studs, the elastic "rocker" serves as a fixer of the whole structure in the conductor and through it grounding of all elements of CU is performed. The choice of rational (in terms of reduction of residual welding deformations) sequence of overlaying repair welds during welding on the facial and back side of the joint "CU-insulator". Initially, the operation of fixing the

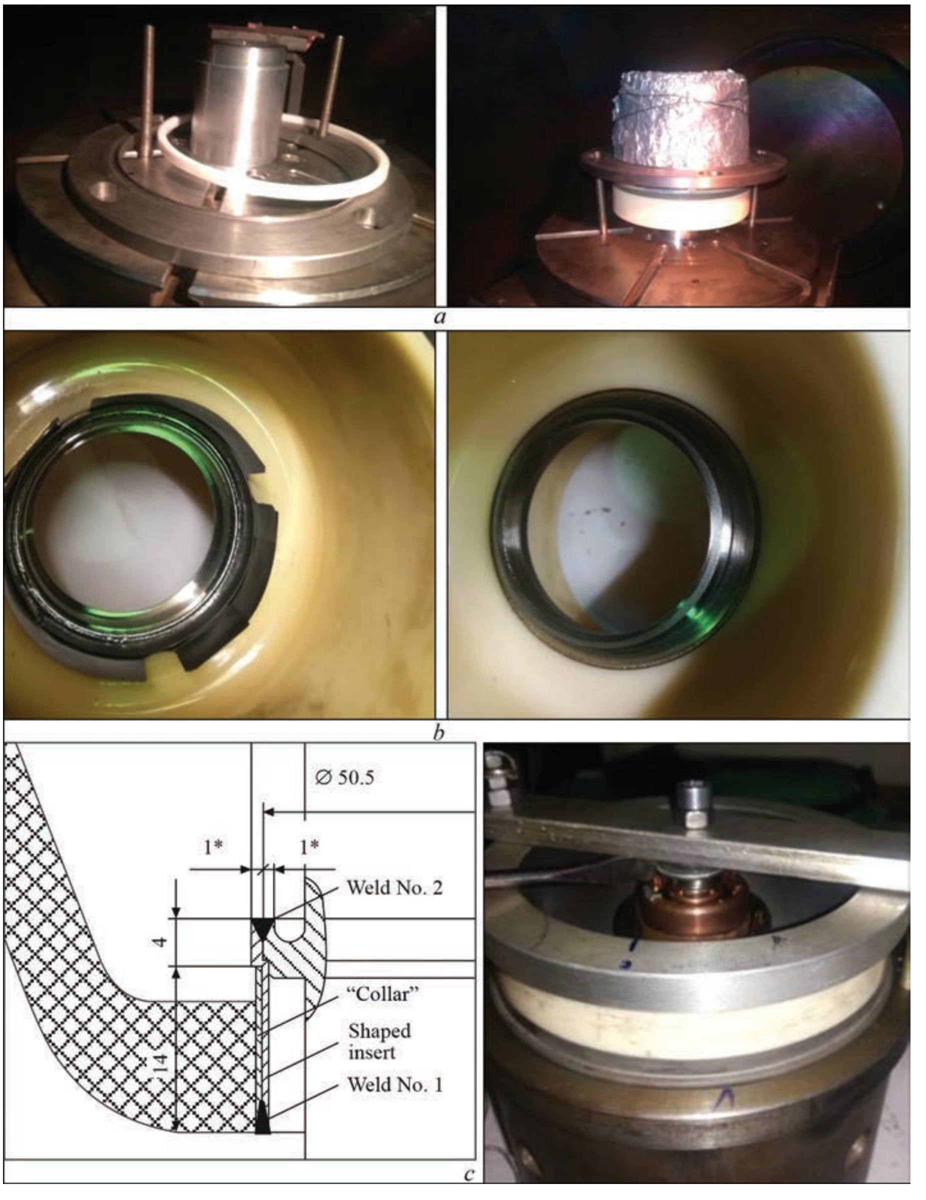

Figure 4. Stages of repair works according to the variant No. 1: *a* — assembly and welding device with a subassembly of insulator with a shaped circumferential insert for EBW according to the variant No. 1; *b* — appearance of the weld with a shaped circumferential insert according to the variant No. 1 after EBW and after machining the weld in size; *c* — fragment of circumferential joint of the "collar" with a shaped insert according to the variant No. 1 and final assembly

shaped circumferential insert to the defective "collar" of the insulator (weld No. 1) was performed. Then, after removing tolerance on mechanical treatment, the operation of final assembly and welding-in was performed using EBW of the "leg" to the insulator (weld No. 2).

The mode of producing the first welding pass (weld No. 1) is presented in Table 3.

The mode of the second welding pass (weld No. 2) is presented in Table 4.

VARIANT No. 2

Restoration of the "leg" after its cutting from the assembly weld with the elongated linear defect. In this case, the restoration was subjected to the "leg", not the "collar" of the insulator. To carry out this repair

Table 3. Parameters of mode of producing welding pass with modulation (weld No. 1)

Beam current I_b, mA*	Current of focusing lens on the surface I_{fo}, mA	Operating current of focusing lens I_f, mA	Working distance, mm	Welding speed v_w, mm/s	Angle of product inclination α°
13.5	600	615	260	10	5
Notes. *Welding in a pulsed mode. I_{fo} = 600 mA corresponds to the sharp focusing of the electron beam on the welded surface. The size of the working distance is 260 mm.					

Table 4. Parameters of mode of producing welding pass with modulation (weld 2)

Beam current I_b, mA*	Current of focusing lens on the surface I_{fo}, mA	Operating current of focusing lens I_f, mA	Working distance, mm	Welding speed v_w, mm/s	Angle of product inclination α°
15	700	715	70	10	10
Note. I_{fo} = 700 mA corresponds to the sharp focusing of the electron beam on the welded surface. The size of the working distance is 70 mm.					

Table 5. Parameters of mode of producing welding pass without modulation

Beam current I_b, mA*	Current of focusing lens on the surface I_{fo}, mA	Operating current of focusing lens I_f, mA	Working distance, mm	Welding speed v_w, mm/s	Angle of product inclination α°
12	635	650	130	10	5–10
Note. I_{fo} = 635 mA corresponds to the sharp focusing of the electron beam on the welded surface. The size of the working distance is 130 mm.					

operation, it is necessary to cut out the "legs" of the insulator and, after welding-in of insert-bandage, repeated assembly-welding should be performed.

The shape of the bandage was different from the variant No. 1 by the absence of a horizontal flange and the presence of rest to the wall of the "leg" for better fixation, preservation of rigidity of the assembly. The center of the heating spot is shifted toward a bandage-insert that has a larger thickness (Figure 5, *a*).

The parameters of the mode of this variant of welding were set on the basis of the conditions of producing a vacuum-tight weld with a good outer formation without undercuts, penetration depth of at least 2.0 mm and the absence of root defects. Choosing the optimal bandage-insert for EBW according to the variant No. 2 and the corresponding parameters of welding mode allowed solving the problem of restoration of geometric dimensions of the "leg" cut out from the insulator.

In welding-in the insert according to the variant No. 2, the angle of inclination of the product from the vertical should be different from zero. The need in inclination is explained by the proximity of the upper vertical wall of the assembly to the welding zone, as a result of which the probability of shielding a part of the electron beam by the wall increases. The weld was located on the end surface of the two-sided flanging with a slight deviation from the vertical. It was experimentally established that the value of the external elimination of the electron beam axis from the inner edge of the end of the bandage in the case of the angle of inclination of the product α within 5–10° from the vertical, should be 0.3 mm. These conditions provide a guaranteed penetration of the required shape. Such negligible values of removing an electron beam are convenient to control with the use of coaxial television monitoring system (Figure 5).

The mode of the "leg" restoration by welding-in a bandage on it without modulation on a normal, not pulsed mode, is shown in Table 5.

FINAL ASSEMBLY OF CU

In the final stage (after welding-in repair inserts and their machining in size), welding was carried out with two-side edges flanging, which eliminates the need in inclination of the product, maintaining all the benefits of this scheme (Figure 6).

The final operation mode of welding-in "leg" (CU) to the brazed "collar" of the ceramic insulator of EBG is shown in Table 6.

The availability of modern welding equipment in combination with a preliminary thought out and veri-

Table 6. Parameters of the mode of welding-in "leg" (CU) to the brazed "collar" of ceramic insulator of EBG

Beam current I_b, mA*	Current of focusing lens I_{fo}, mA	Welding speed v_w, mm/s
12	I_{fo} + 20	10
Notes. *Welding in a pulsed mode. I_{fo} = 600 mA corresponds to the sharp focusing of the electron beam on the welded surface. The size of the working distance is 220 mm.		

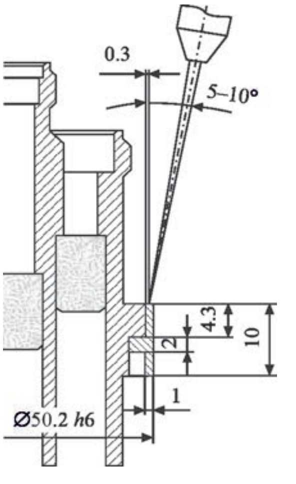

Figure 5. Scheme of welding-in insert according to the variant No. 2 (*a*) and "leg" of CU after EBW and finishing machining of welded-in insert (*b*)

Figure 6. General outside (*a*) and inside (*b*) appearance of repaired CU of EBG

fied design of the welded assembly, a properly selected type of a weld, allowed eliminating deformation of the part and minimizing the percentage of rejection. The geometrical tolerances of CU after completion of all stages of welding were observed. The shapes of the product are preserved.

The technology was checked during the work of standard products in real production conditions. The use of developed EBW technology after repair was proved by a continuous operation of CU for 40 h.

Production and delivery of such assemblies can be carried out by the designing companies, manufacturers of power units and installations for EBW and small business enterprises.

CONCLUSIONS

1. In the work, the method of technological inserts is substantiated, which allows eliminating not only defects of welding the cathode unit, but also producing high-quality vacuum-tight joint on an expensive part, made with violation of geometric dimensions during its mechanical treatment (deviation in the sizes of the vertical wall thickness along the perimeter of the insulator flange).

2. The technology of repair of two types of defects was mastered in the presence of different thickness of the vertical wall of the flange along the perimeter and after its cut out from an assembly weld behind an elongated linear defect. The repair of both types of defects is carried out by means of inserts–rings of a different configuration.

3. The adopted welding technology was successfully applied during repair of CU. Such properties as quality, fatigue life, reliability were confirmed during operation of repaired real products and became the criterion of correctness of the developed technology.

REFERENCES

1. *Technological features of fusion welding*. https://msd.com.ua
2. *Features of fusion welding for electronic mechanical engineering*. https://msd.com.ua › osobennosti-svarki-plavleniem-ma.
3. Nesterenkov, V.M., Zagornikov, V.I., Orsa, Yu.V., Ignatenko, O.M. (2020) Features of applying electron beam welding in manufacture of the cathode assembly of the electron gun. *The Paton Welding J.*, **2**, 30–34. DOI: https://doi.org/10.37434/tpwj2020.02.06
4. Nesterenkov, V.M., Khripko, K.S., Matviichuk, V.A. (2018) Electron beam technologies of welding, surfacing, prototyping: Results and prospects. *The Paton Welding J.*, **11–12**, 126–133. DOI: http://dx.doi.org/10.15407/tpwj2018.11–12.14
5. Makhnenko, O.V., Seyffarth, P. (2008) Calculation prediction of overall distortions in laser welded beams. *The Paton Welding J.*, **3**, 6–12.
6. Slobodyan, M. (2021) Resistance, electron and laser welding of zirconium alloys for nuclear power engineering. *Yadernaya Inzheneriya i Tekhnologii*, 53(**4**), 1049–1078 [in Russian]. DOI: https://doi.org/10.1016/j.net.2020.10.005

ORCID

V.I. Zagornikov: 0000-0003-0456-173X,
V.M. Nesterenkov: 0000-0002-7973-1986,
Yu.V Orsa: 0000-0002-1208-4171

CONFLICT OF INTEREST

The Authors declare no conflict of interest

CORRESPONDING AUTHOR

V.M. Nesterenkov
E.O. Paton Electric Welding Institute of the NASU
11 Kazymyr Malevych Str., 03150, Kyiv, Ukraine.
E-mail: nesterenkov@technobeam.com.ua

SUGGESTED CITATION

V.I. Zagornikov, V.M. Nesterenkov, Yu.V Orsa, A.M. Ignatenko (2022) Technologies of repairing cathode unit of electron beam gun with the use of electron beam welding. *The Paton Welding J.*, **1**, 16–22.

JOURNAL HOME PAGE

https://patonpublishinghouse.com/eng/journals/tpwj

Received: 17.12.2022
Accepted: 28.02.2023

DOI: https://doi.org/10.37434/tpwj2023.01.04

HIGH-FREQUENCY EQUIPMENT FOR LIVE TISSUE WELDING (REVIEW)

G.S. Marynskyy[1], V.A. Tkachenko[1], V.O. Bysko[1], S.E. Podpryatov[1,2], S.S. Podpriatov[1,2], S.D. Grabovskyi[1], S.V. Tkachenko[1]

[1]E.O. Paton Electric Welding Institute of the NASU
11 Kazymyr Malevych Str., 03150, Kyiv, Ukraine
[2]Kyiv City Clinical Hospital No. 1
121 Kharkyvske Hwy, 02091, Kyiv, Ukraine

ABSTRACT

Technology and equipment for high-frequency welding and treatment (coagulation, cutting) of live tissues in surgery is ever wider used in medical practice of many countries of the world. This work, which has been performed on the base of both the materials posted on the Internet and authors' own materials, is a general review of the most typical representatives of such basic equipment, which is proposed by the leading world manufacturers. The main features and advantages of the respective equipment are given as claimed by its developers. The work is designed both for users and for developers of new equipment.

KEYWORDS: electric welding surgery, high-frequency welding of live tissues, equipment, world manufacturers

INTRODUCTION

Technology and equipment for high-frequency (HF) welding and treatment (coagulation, cutting) of live tissues in surgery is ever wider applied in medical practice in many countries of the world. It should be noted that although the "welding" term initially applied for joining live tissues in medicine in Ukraine is more and more often used in foreign publications, in this or that form, there it mostly pertains to vessel closure. In Ukraine the term "welding" of live tissues has a broader meaning. Ukraine certainly is the world leader by the diversity of electrosurgical welding procedures [1–4].

At present a large number of high-quality electrosurgical equipment is manufactured in the world, including welding equipment, which is continuously evolving and is being improved. The actual need for such equipment is constantly growing, and the world market volume reaches billions of US dollars [5]. By our approximate estimatation, the potential volume of the Ukrainian market of welding electrocoagulators is equal to approximately 1.5–2.0 thou pcs.

GENERAL CHARACTERISTICS AND REQUIREMENTS. DESIGN FEATURES AND COMPONENTS

In the general case, the equipment for live tissue welding is an HF generator, usually of output power of 15–300 W, with the necessary tools connected it, through which the HF current directly influences the biological tissues at monopolar (Figure 1, *a*) or bipolar (Figure 1, *b*) connection circuits [6].

A fundamental difference in the connection circuits in case of application of a monopolar variant, in the fact that just one generator output (one electrode) is connected to the organ being operated on, while the second electrode is placed under the patient's body. In case of application of a bipolar variant, both the generator outputs (both the electrodes) are connected directly to the tool. Accordingly, the current runs between the tool electrodes in a very limited zone, where surgery is performed (Figure 2).

Both the circuits have their advantages and disadvantages and are widely used in practice, complementing each other. The working frequency of current at generator output is in the range from 300 KHz and higher, and it is usually equal to 400–500 kHz. The lower frequency threshold and other restrictions on the use of frequency ranges are due to limitations imposed by the respective norms and standards [6]. It should be noted, however, that there is positive practical experience of application of 66 kHz working frequency at bipolar circuit of tool connection that is due, among other things, to reduction of losses in the tool connection cables with lowering of current frequency. It is especially noticeable when working with high power. The working voltage and current, supplied into the zone of impact, are selected, proceeding from the nature of the live tissue being operated on, connection circuit, etc.

MAIN MANUFACTURERS

Nowadays the electrosurgical equipment which is used or can be used for live tissue welding is manufactured by many leading companies in different countries of the world. These are, first of all, Medtronic and Johnson-and-Johnson (USA), ERBE, Martin and BOWA (Germany), etc. [7]. Among them there

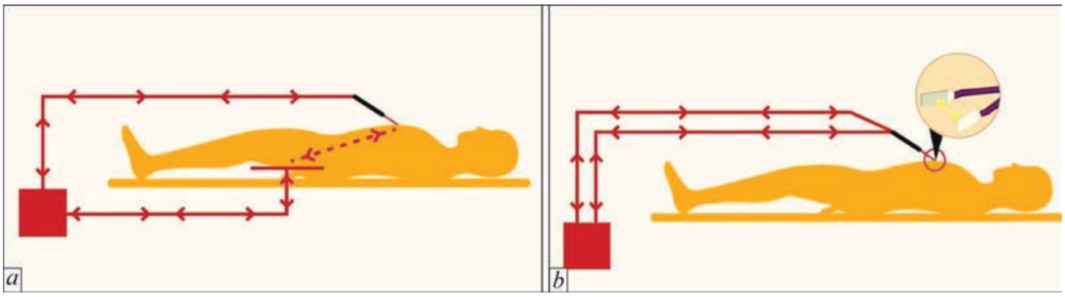

Figure 1. HF generator: *a* — monopolar circuit; *b* — bipolar circuit

are also Ukrainian manufacturers such as “Contact” Company and ISPC “Scientific-Research Institute of Applied Electronics Soc.” (Ukraine), “Patonmed” (Ukraine) and some others.

American Corporation Medtronic plc is one of the world’s largest manufacturers of medical equipment, having its operational and executive headquarters in Minneapolis, Minnesota (USA). In 2015 Medtronic announced a successful completion of acquisition of Covidien plc Company. In keeping with the terms of acquisition agreement, Medtronic Inc. and Covidien plc are merged into Medtronic plc Company. Today, according to published data, the Company has about 90 thou employees, including more than 11 thou of scientists and engineers. It is present in the market of more than 150 countries. Last year its income was equal to 31.69 bln USD [8].

Covidien Company, and now Medtronic plc proposes ValiLab™ units, which realize the LigaSure™ technology [9]. LigaSure technology is that of bipolar closure of vessels by HF current. The feedback program used for controlling the applied amount of energy depends on the scope of the tissue, vessel density and it realizes the limitation of heat evolving in the target tissue. As stated by the developers [10], LigaSure™ technology, which is based on ValeyLab™ energy platforms, still remains the most advanced technology of vessel welding and dissection in the world.

The developers guarantee that:

- in one second LigaSure™ measures the tissue impedance 434000 times, calculates and regulates the level of applied energy by a unique algorithm;
- in two seconds LigaSure™ reliably and stably closes vessels of up to 7 mm diameter, which can stand 3 times the normal systolic pressure;
- in three seconds the surgeon, using LigaSure™ technology, can close the vessel, dissect it and safely go over to the next part of the procedure, due to a short cooling time (to < 60° in less than one second), which is achieved, among other things, also by application of a unique nanocoating.

Note that comparative testing, conducted in March, 2018 with the authors’ participation in Medtronic Center in Shanghai, showed that the local vessel closure technology, realized in EKVZ-300 “Patonmed-™” units is not inferior to LigaSure™ technology.

As an example of this company equipment, we can mention ValleyLab™ FT10 unit (Figure 3), which realizes LigaSure™ technologies [12].

As claimed by the developers [11], this device provides:

- improved efficiency of LigaSure™ electroligation system;
- TissueFect™ system scans the tissue resistance and adapts the characteristics of energy applied with the frequency of 434 kHz;

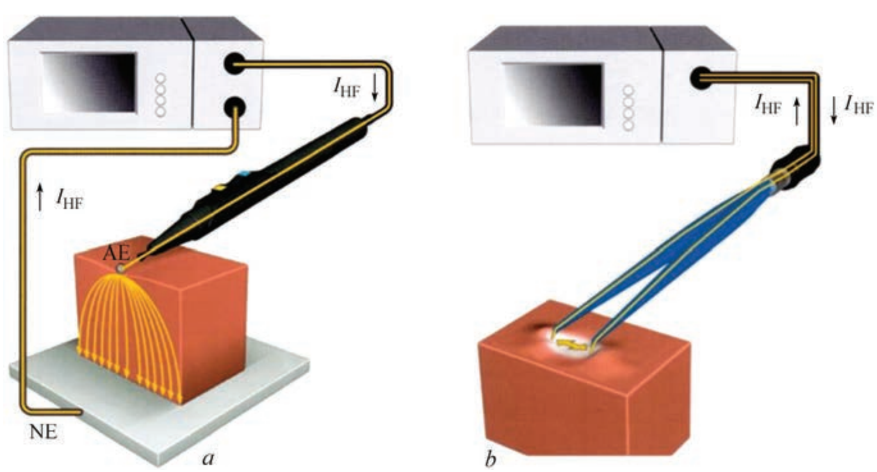

Figure 2. Current flowing in monopolar (*a*) and bipolar (*b*) circuits

Figure 3. Appearance of ValleyLab^{TV} FT10 unit

- automatic identification of the tool and automatic adaptation of power minimizes the time of the unit adjustment before and during surgery;
- one sensory screen with simplified control;
- internet connection and exclusive ValeyLab™ Exchange system of updating the software;
- unique ValeyLab™ mode for improvement of dissection with hemostasis;
- REM™ adaptive system (system of following the patient's neutral electrode);
- Autobipolar mode, Soft coagulation mode;
- 10.1 kg weight;
- 368×462×178 mm dimensions.

An example of a more accessible and compact instrument of this Company is ValleyLab™ LS10 unit (Figure 4) [12], designed for vessel closure. With a weight of 5.5 kg, its overall dimensions are 300×377×105 mm, and it is easy to transport. It ensures fast (in 2–4 s) welding of up to 7 mm vessels. It uses optimal energy characteristics to achieve welding up of vessels and tissue masses with minimal heat propagation. The unit has a simplified control panel with one on/off button and one socket for tool connection by the "plug in and work" principle. The unit identifies, which tool is connected at this moment, and automatically adjusts the instrument operational parameters for fast and stable result of vessel closure.

A more complex multifunctional instrument of the Company is the ForceTriad™ device (energy platform) (Figure 5) [13, 14].

This is a fully functional electric surgery system, which ensures electrosurgical cutting, coagulation and bipolar sealing of vessels in one LigaSure™ generator.

The energy platform of this device is designed for open and laparoscopic surgical procedures and it includes:

- TissueFect™ sensing technology for all tissue types;
- ValleyLab™ mode for electric surgery;
- LigaSure™ closure technology for vessel sealing.

Figure 4. Appearance of ValleyLab™ LS10 unit

As claimed by the developers [14, 15], Force Triad™ energy platform is the only fully functional energy platform in the field, with the capabilities of remote updating of the software. Using the software updating system ValleyLab™ Exchange, the device can be readily updated in site, opening up the most advanced technology capabilities for surgeons, medical nurses and patients.

TissueFect™ sensing technology is a Covidien control system, designed for accurate control of energy supply, creating a range of variants to achieve the desired effect on the tissue.

The improved LigaSure™ tissue welding technology can join up to 7 mm diameter vessels inclusive and tissue bundles.

Bipolar resection with programmed addition of physiological solution allows the surgeons performing various urological and gynecological procedures in a saline environment.

Automatic tool identification is realized in the unit. The device, designed by all-in-one principle, is compatible with the regular electrosurgical tools and all the currently available and new Liga Sure™ tools.

Welding cycles are faster, than those in the original generator at LigaSure™ vessel sealing. ValleyLab™ mode ensures a unique combination of monopolar hemostasis and dissection.

Ethicon Company, which is part of such a giant as Johnson&Johnson Corporation [15], whose products are known all over the world, is represented on the market of welding electrocoagulators by MEGADYNE™ unit [16] (Figure 6). As claimed by its developers, owing to optimized convenient design and

Figure 5. Appearance of ForceTriad™ unit

Figure 6. METADYNE™ electrosurgical generator

optimized energy supply, MEGADYNE™ electrosurgical generator is a simple, but smart choice among the monopolar and bipolar power sources for performance of diverse medical procedures.

This device, which envisages operation in the monopolar and bipolar modes, has large displays, which are easy to read, and an intuitive power setting mode. It provides visual indication of the working current. There is also the function of calling the last used mode. The display is large and bright. The generator weight is 7.7 kg with overall dimensions of 368×439×179 mm.

KLS Martin Group Corporation (Germany, USA), has its branches and representative offices all over the world, and offers numerous equipment and tools on the market, including electrosurgical units for hemostasis and closing of vessels [17–21]. Among such equipment we will focus on their most recent development — maXium® Smart C unit (Figure 7).

As claimed by the developers [21], maXium® Smart C unit combines a proven maXium® user interface with maXium® power adjustment effect, used at coagulation, thus ensuring maximum efficiency in all the power ranges.

SealSafe® IQ bipolar system of vessel sealing, used in this device, allows efficiently sealing vessels or tissue bundles without any required prior preparation or detailed exposure of the tissue to be sealed. Owing to SealSafe® IQ program of providing precise current, specially adapted to such a type of application and special tools, just the tissue located between the tool jaws is sealed. It results in lower side thermal damage to the adjacent tissues.

Figure 7. Appearance of maXium® Smart unit [21]

maXium® Smart C unit is available in three versions and it offers: informative screen, memory of previous settings (up to 500 words of memory), continuous displaying of the main parameters of the instrument.

In addition to the high-frequency part, maXium® Smart C units can be combined with argon feed system to solve the problems associated with extended superficial bleeding in parenchymatous tissues, which is difficult to cope with using classical coagulation. Thus, in the opinion of the authors, argon-plasma coagulation is an ideal complement to usual HF methods.

In combination with maXium® Smart Line series, it additionally incorporates the following elements: a system to provide efficient hemostasis, and it can be used in several ways; maXium® Beamer system, which reduces tissue carbonization during surgery, thus accelerating the wound healing process. The risk of perforation is also greatly reduced, owing to a small depth of HF current penetration.

BOWA MEDICAL Company [22] is a leading supplier of the entire spectrum of innovative energy-based surgical systems, produced in Germany. As claimed by the developers [22], the products and systems are ideally adapted to the requirements of daily medical care in hospitals, and they impress with their high frexibility and safety. Unlike the global market leaders, the BOWA Company product line is not large, but it is focused on electrosurgery. And their target markets are the European Union (mostly Germany), East European, Asian and CIS countries and Ukraine.

Among the instruments produced by BOWA Company, we will consider the ARC series units (Figure 8). This series consists of several modifications, which differ by their maximal output power (from 100 to 400 W) and functionality.

So, ARC100 unit has maximal power of 100 W, and it is fitted with medical tools designed for this power (pincers and monopolar scalpels).

Higher power units, for instance ARC400, have greater functionality and they are fitted with tools, designed for 400 W power (up to 280 mm clamps, ERG310, Night NIFF, LIGATOR special tools, bipolar scissors, etc.). Output powers and software allows these units to be applied in surgery, gynecology and urology [22].

The following convenient functions are realized in ARC series units: dialogue control and adaptive dis-

Figure 8. Unit of ARC series

Figure 9. Front panel of ARC unit with different number of connectors

play; reading information from the unit and software updating using programs, saved on USB-carriers. It greatly simplifies the daily work of the hospital staff. ARC new generation is easy to operate. Five configuration options are available, depending on the requirements to surgical intervention. The number of connectors (monopolar or bipolar) varies from one to two of each (Figure 9).

The unit has COMFORT function for automatic identification of tools and controlling the application cycles. “Setting up Master” program helps creating and optimizing the ARC unit configuration in the dialogue mode.

Power is maximal in MONOPOLAR mode at 400 W (for 200 Ohms), and in BIPOLAR mode it is 200 W (for 75 Ohms). Unit weight is 12.5 kg, its overall dimensions are 430×140×470 mm.

UKRAINIAN COMPANIES

“Contact” Company, based in Kiev, has been on the market of high tech endoscopic equipment for minimally invasive surgery since 2001 [23]. The Company is developing and manufacturing endoscopic units and systems for laparoscopy, arthroscopy, rhinoscopy, thoracoscopy, gynecology and urology. The company now has the following units in its arsenal: electrosurgical units EKONT-0201.1, EKONT-0201.2 (Figure 10) and EKONT-0201.3 (Figure 11), which is positioned by the developers as expert-class modern electrosurgical system [23].

These multifunctional units have maximal output power of up to 300 W.

Here are some of the features and advantages of EKONT-0201.3 system, claimed by the developers.

Special features of EKONT-0201.3 system are as follows: two monopolar channels; one bipolar channel; colour TFT display; neutral electrode circuit control system (ANECS); wide range of modern electrosurgical modes; interactive visual system of help during operation (InViNS help); continuous self-control of critical systems (ART-SCS); 100 sets of modes (programs), which are saved.

Figure 10. Appearance of ECONT-0201.2 unit

Advantages of EKONT-0201.3 system are as follows: special modes of argon-plasma coagulation (APC) for general surgery, laparoscopy and flexible endoscopy with maintenance of argon-plasma discharge starting from 5 W and up to 15 mm distances to the treated tissue; special mono- and bipolar modes for arthroscopy; special mono- and bipolar modes for urology and gynecology; fully automated system of vessel welding; special modes of polypectomy/papillotomy.

By the information of the developers [23], among its advantages are special APC modes for general surgery, laparoscopy and endoscopy with maintenance of argon-plasma discharge. It has special mono- and bipolar modes for arthroscopy, urology and gynecology.

Given below are some main modes for bipolar cutting, coagulation and welding.

Bipolar cutting/(hemostasis of 0–7 mm), 100 W. Bipolar coagulation: micro — 60 W, 100 Ohms; standard — 100 W, 100 Ohms; auto — 300 W, 20 Ohms. Vessel welding: 5 mm laparoscopic tool — 100 W, 20 Ohms; 10 mm laparoscopic tool — 300 W, 20 Ohms; general surgery — 300 W, 20 Ohms.

General characteristics are as follows: working frequency of 440 kHz, supply voltage of 220 V, consumed power of 690 W, weight of 8.0 kg, and overall dimensions of 350×140×350 mm.

ISPC “Scientific-Research Institute of Applied Electronics” Soc., Kyiv, is represented in the local market by electrosurgical units called “Nadiya-4” [24]. At present it is a whole line of units, differing both by their power and technological capabilities given in the Table 1. As one can see from the pre-

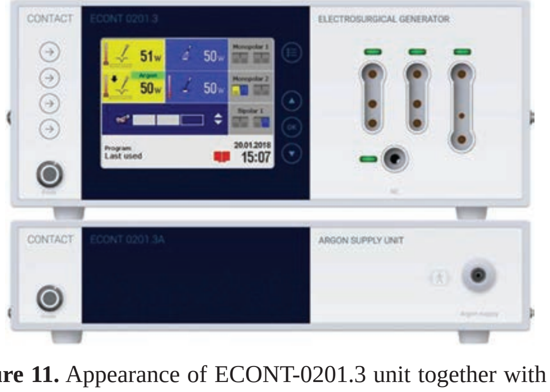

Figure 11. Appearance of ECONT-0201.3 unit together with the argon station

Figure 12. Appearance of "Nadiya-4" EKhVCh unit

sented materials, although the developers do not position these units as welding equipment, they largely meet the requirements made, which was the base for inclusion of this equipment into this review. Note, that units operating at the frequency of 1.76 MHz and even 3.5 MHz, are presented, alongside units with working frequency of 440 kHz, which can be regarded as a standard one for this type of equipment. Figure 12 gives the appearance of "Nadya-4" unit.

PWI, Kyiv, offers in the local market electrosurgical tools under "Patonmed™" trade name. Today PWI is represented by EKVZ-300 unit (high-frequency welding electrocoagulator). This device, the design of which was developed in 2010–2011, has been used with success in practical medicine in Ukraine, starting from 2012 in many specialities: from abdominal surgery to ophthalmology.

Its design features are multifunctionality, which is ensured by the capability of programming to accommodate the peculiarities of application in medical or veterinary science, as well as the needs of an individual user (surgeon).

EKVZ-300 functional diagram ensures operation in the following modes: bipolar cutting, manual welding — pulsed coagulation, controlled by the surgeon, and automatic welding.

A capability of simultaneous connection of two tools is envisaged with their switching and their one-time operation in the mode of one control pedal.

Working frequency of EKVZ-300 "Patonmed" unit is 440 kHz, its maximum output power is 300 W.

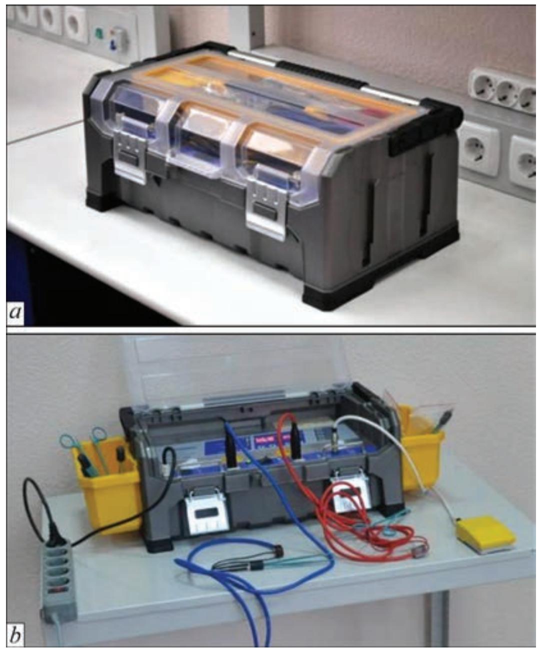

Figure 14. Appearance of mobile variant of EKVZ-300 unit in transportation (*a*) and working (*b*) position

Its weight is 7.5 kg, and overall dimensions are 410×400×130 mm.

From the time of its development, the unit has been continuously improved (Figure 13) [25]. At present, it has a great diversity of operating algorithms and parameters, depending on the type of surgical to be performed. This unit allows adaptation, correction and loading of additional programs by user preference. The capability of saving and using "favourite" programs and algorithms is envisaged. Other manufacturers' tools can be applied.

The operating algorithm of modern EKVZ-300 units, which is described in sufficient detail in the patent [25, 26], and the respective proprietary software guarantee a reliable performance of the necessary tasks in live tissue welding.

In addition to the stationary variant, its mobile variant (Figure 14) and other modifications were developed. The mobile variant, having the same technical characteristics as the stationary one, is convenient in case of the need to frequently transport the unit and

Figure 13. Appearance of EKVZ-300 unit

Figure 15. Appearance of EKVZ-300-2 unit

Table 1. Comparative characteristics of “Nadiya-4” electrosurgical units

Maximal power in modes	EKhVCh-3000RK	EKhVCh-300 Model-200	EKhVCh-200			EKhVCh-120	
			Model-200RKh	Model-120	Model-120RKh/1.76	Model 120RKh/3.5	
Monopolar cutting-1	300 W	300 W	200 W	200 W	120 W	120 W	120 W
Monopolar cutting-2 (mixed)	200 W	200 W	200 W	200 W	120 W	120 W	120 W
Bipolar cutting-1	300 W	–	–	–	–	–	–
Bipolar cutting-2 (closure)	300 W	–	–	–	–	–	–
Monopolar coagulation-M	–	200 W	120 W	120 W	120 W	120 W	120 W
Monopolar coagulation-M1	250 W	–	–	–	–	–	–
Monopolar coagulation-M (forced)	120 W	–	–	–	–	–	–
Bipolar coagulation B	–	120 W	120 W	120 W	120 W	120 W	120 W
Bipolar coagulation B1	120 W	–	–	–	–	–	–
Bipolar coagulation B2 (with higher tissue resistance)	120 W	–	–	–	–	–	–
Consumed power	600 W	600 W	450 W	450 W	450 W	300 W	300 W
Working frequency	440 kHz	440 kHz	440 kHz	1.76 MHz	440 kHz	1.76 MHz	3.5 MHz
Overall dimensions							
Electronic module	–			(290×215×125) mm		–	
Control pedal	–			(230×195×45) mm		–	
Complex weight	<6 kg	<4.5 kg					

at operation outside a stationary operating room, for instance, in veterinary medicine.

A further development of this series is EKVZ-300-2 “Patonmed™” unit, which realizes novel welding algorithms, based on multilevel feedbacks. It provides a stage-by-stage assessment of the quality of the tissue being welded and power feed regulation (Figure 15). It ensures improved functional performance of the tissue joint. This instrument has a large LC display. In this unit a function of the connected tool identification is realized, as well as automatic change of operating parameters and algorithms, in keeping with the peculiarities of the connected tool. It has a built-in system of self-control and activation of prompts for the surgeon, and controls the condition of the connected tool. It enables visualization of the changes in tissue parameters during joining, which allows conducting research and having the joint quality feedback.

Note that within one article it is impossible to describe the entire range of equipment for such a promising field as live tissue welding in medical and veterinary science. The authors presented the most characteristic samples.

CONCLUSIONS

1. The large number of models is indicative of intense competition in the market of electrosurgical equipment, which has already become habitual.

2. All the considered units without exception have similar claimed technical characteristics, which are due to the requirements to technical parameters of medical radiofrequency equipment, and they differ mainly by ergonomics, design and their inherent functions.

3. Most of the units combine the possibility of operating both by bipolar and monopolar circuit. Application of a monopolar tool is due to popularity and familiarity for the surgeon of a fine fast cutting impact of such a tool.

4. In some units, the high-frequency module is combined with other technological modules, for instance, argon-plasma or module for convection-infrared treatment of the tissue, targeting special branches of surgery, which require a powerful impact over an area to a small depth (for instance, liver surgery).

5. All the manufacturers are trying to achieve maximal automation of the process, minimizing the performer impact on evaluation of the tissue internal characteristics. The application principle consists in involving the surgeon into correct selection of the mode and tool, in accordance with the conditions of using the units in surgery, specified by the manufacturer. At the same time, evaluation of the tissue condition during its treatment and dosing of the impact on it are assigned to the unit algorithms.

6. The EKVZ-300 series units developed at PWI meet the highest world standards by their technical characteristics.

7. The functional of PWI electric welding units of EKVZ-300 series incorporates programs based of the results of developments by Ukrainian researchers and doctors in the fields of abdominal surgery, thoracic surgery, proctology, ophthalmology, neurosurgery, oncology and gynecology.

REFERENCES

1. Paton, B.E., Ivanova, O.N. (2009) Tissue-saving high-frequency electric welding surgery: Atlas. Kyiv, IAW [in Russian].
2. Paton, B.E., Krivtsun, I.V., Marinsky, G.S., et al. (2013) Welding, cutting and heat treatment on live tissues. *The Paton Welding J.*, **10–11**, 142–153.
3. Podpriatov, S.S., Podpryatov, S.E., Marynsky, G.S. et al. (2022) The experimental biologic and structural grounds of clinical advantages for next-generation, sutureless, bio-welded gut anastomosis. In: *Proc. 17th Int. Conf. of Colonoproctologists ESC22ABS-1742 (Dublin, Ireland, 21–23 September 2022)*.
4. Pasechnikova, N.V., Naumenko, V.A., Umanets, N.N. (2011) Our experience of application of high-frequency electric welding of live tissues during endovitreal interventions. In: *Proc. of 6th Int. Seminar on Welding of Soft Live Tissues. State-of-the-Art and Prospects of Development (Ukraine, Kyiv, 2–3 December 2011)*.
5. Messenger, D., Carter, F., Noble, E. et al. (2020) Electrosurgery and energized dissection. *Surgery (Oxford)*, 38(**3**), 133–138. DOI: http://doi.org/10.1016/j.mpsur.2020.01.006
6. *Electrosurgical Generators Market Share 2025. Growth Analysis. Global Market Insights Inc.* https://www.gminsights.com/industry-analysis/electrosurgical-generators-market
7. *Electrosurgical device market share by company globally 2016. Statista.* https://www.statista.com/statistics/909626/electrosurgical-devices-market-share-by-top-company
8. *Engineering the Extraordinary. Medtronic.* https://www.medtronic.com/uk-en/index.html
9. *LigaSure™ Technology. Medtronic.* https://www.medtronic.com/covidien/en-us/products/vessel-sealing/ligasure-technology.html
10. *LigaSure™ 123. Medtronic.* https://www.medtronic.com/covidien/en-gb/products/vessel-sealing/ligasure-123.html?cid=PPC:GOOG:branded:UK_EN_SI_LigaSureTechnology12
11. *Energy product catalogue.* https://asiapac.medtronic.com/content/dam/covidien/library/emea/en/product/electrosurgical-hardware-and-accessories/weu-energy-catalogue-2020.pdf
12. *Valleylab™ LS10 Generator. Medtronic (UK). Medtronic.* https://www.medtronic.com/covidien/en-gb/products/electrosurgical-hardware/valleylab-ls10-generator.html
13. *ForceTriad™ Energy Platform. Medtronic Animal Health.* https://www.medtronic.com/animal-health/en-us/products/electrosurgical-hardware/forcetriad-energy-platform.html
14. *Coagulator Medtronic Force Triad. Medicalstore.* https://medicalstore.com.ua/product/medtronic-force-triad
15. *Johnson & Johnson. Content Lab U.S.* https://www.jnj.com
16. *MEGADYNE™ Electrosurgical Generator. Ethicon, a Johnson & Johnson MedTech Company.* https://www.jnjmedtech.com/en-US/product/megadyne-mega-power-electrosurgical-generator
17. *Electrosurgery. KLS Martin. Surgical Innovation is our Passion.* https://www.klsmartin.com/en/products/electrosurgery/
18. *Electrosurgery. KLS Martin. Surgical Innovation is our Passion.* https://www.klsmartin.com/en/products/electrosurgery/#c4014
19. *Electrosurgery. KLS Martin. Surgical Innovation is our Passion.* https://www.klsmartin.com/en/products/electrosurgery/#c4009
20. *Electrosurgery unit maXium®. KLS Martin. Surgical Innovation is our Passion.* https://www.klsmartin.com/en/products/electrosurgery/electrosurgery-units/major-electrosurgery-units/maXium®/
21. *BOWA MEDICAL Electrosurgery.* https://www.bowa-medical.com/?lang=en#gref
22. *The new ARC generation BOWA MEDICAL.* https://www.arc-electrosurgery.com/en/
23. *Electrosurgical system, advanced model* [in Russian]. Contact Co. https://contact-endoscopy.com/ru/electrosurgical-system/
24. *Nadiya-4. High-frequency electrosurgical unit* [in Ukrainian]. http://www.xn-4-6kcq7b0g0b.com.ua
25. Tkachenko, V.A., Marynskyi, G.S., Podpryatov, S.Ie. et al. (2022) *High-frequency welding electrocoagulator EKVZ "Patonmed"*. Pat. Ukraine on utility model 151770, Int. Cl. A61B18/12(2006.01), Publ. 14.09.2022 [in Ukrainian].
26. Paton, B.E., Tkachenko, V.A., Marynsky, G.S. et al. (2014) *Method of joining by welding of human and animal biological tissues using high-frequency current.* Pat. Ukraine 106513, Publ. 10.09.2014 [in Ukrainian].

ORCID

G.S. Marynskyy: 0000-0003-0753-0154,
V.A. Tkachenko: 0000-0003-2983-778X,
V.O. Bysko: 0000-0003-1574-5630,
S.E. Podpryatov: 0000-0003-1350-7532,
S.S. Podpriatov: 0000-0001-5942-6311,
S.D. Grabovskyi: 0000-0002-9082-4059,
S.V. Tkachenko: 0000-0002-5524-6273

CONFLICT OF INTEREST

The Authors declare no conflict of interest

CORRESPONDING AUTHOR

G.S. Marynskyy
E.O. Paton Electric Welding Institute of the NASU
11 Kazymyr Malevych Str., 03150, Kyiv, Ukraine.
E-mail: g.marynsky@gmail.com

SUGGESTED CITATION

G.S. Marynskyy, V.A. Tkachenko, V.O. Bysko, S.E. Podpryatov, S.S. Podpriatov, S.D. Grabovskyi, S.V. Tkachenko (2022) High-frequency equipment for live tissue welding (Review). *The Paton Welding J.*, **1**, 23–30.

JOURNAL HOME PAGE

https://patonpublishinghouse.com/eng/journals/tpwj

Received: 12.12.2022
Accepted: 28.02.2023

DOI: https://doi.org/10.37434/tpwj2023.01.05

METHODS TO PREVENT THE STRESS SHIELDING EFFECT IN IMPLANT–BONE SYSTEM (REVIEW)

A.V. Moltasov[1], S.G. Voinarovych[1], M.M. Dyman[1], S.M. Kalyuzhnyi[1], S.V. Burburska[2]

[1]E.O. Paton Electric Welding Institute of the NASU
11 Kazymyr Malevych Str., 03150, Kyiv, Ukraine
[2]OSTEONIKA Limited Liability Company
98 Striiska Str., 79026, Lviv, Ukraine

ABSTRACT

Statistical data of many national registers and medical societies show that aseptic instability of the hip joint prosthesis is one of the main obstacles in the path to application of orthopedic implants. One of the causes for aseptic instability is manifestation of stress shielding effect, which is due to mismatch of the moduli of elasticity of the implant and bone tissue. Methods are considered, which allow lowering the modulus of elasticity of the metal implant, bringing it closer to the respective modulus of elasticity of bone tissue. It is found that reaching the posed goal by replacement of the traditional metals, which are used for implant manufacture, by alloys with much lower modulus of elasticity, is a task, which has not been solved technologically in their mass production. The currently most common methods of lowering the modulus of elasticity of orthopedic implants were analyzed, and their advantages and short-comings are indicated. The most serious problem in mass application of advanced additive technologies in implant manufacture is their labour- and material consumption. It is found that application of surface modification technologies, in particular plasma methods of porous coating deposition is the most affordable and effective method of lowering the modulus of elasticity of the implant surface, contacting the bone, with a high probability of reduction of the stress shielding effect manifestation.

KEYWORDS: orthopedic implant, titanium alloys, modulus of elasticity, porous coatings, surface modification

INTRODUCTION

Mass commercialization and technological achievements of the several recent decades shifted dynamics of the society to the side of more sedentary life style that is related with increased index of body weight which has a detrimental effect on a state of locomotor apparatus [1] and results in many diseases, including osteoarthritis of hip and knee joints [2]. As for 2014 up to 15 % of planet's population [3] suffered from osteoarthritis [3]. In view of global aging of the population and change of the life style the scientists predict that more and more people will suffer from orthopedic diseases [4] in future.

However, when physiotherapy and therapeutic treatment can not improve patient's state an endoprosthesis replacement, i.e. replacement of a joint with orthopedic implant by means of surgical intervention, is used in order to reduce painful sensation and restore joint functionality. This allows patients to come back to normal quality of life and demand for orthopedic implants rises together with intensive development of implantation technologies [5].

Current technologies of endoprostheses manufacture allow producing standard implants (Figure 1, *c*) as well as individual ones, i.e. formed with consideration of all defects of a bone of a specific patient (Figure 1, *d*) [6] providing porous or trabecular surface structure. Nevertheless, increase of the cases of disease among young people provokes a need of noticeable increase of endoprostheses life. Virtually, most of the young patients with overweight, which require replacement of a hip joint, will need that their prosthesis operates for 50 and more years [7]. At that, the work [8] had an assumption that only 58 % of the patients could count on trouble-free operation of an artificial hip joint for at least 25 years.

One of the main reasons of implant reject is its aseptic loosening due to decrease of density of a bone tissue that is caused by insufficient loading, which affects the bone surrounding the endoprosthesis, since the bone tissue is formed and fixed in a direction of mechanical stress effect [9]. In the literature such a phenomenon is called "stress shielding". It is caused by the fact that the implants are made of the metals and alloys the elasticity modulus of which is significantly higher the corresponding characteristic of the bone tissue that results in appearance of the tangential stresses in a zone of contact between the bone and its substitute [10].

Among the metallic materials of biomedical designation the most widespread are titanium and its alloys due to exceptional biocompatibility, excellent corrosion resistance and low specific weight in combination with high mechanical characteristics [11]. One of the most widespread materials being used in manufacture of the substitutes of highly-loaded joints such as hip, knee and shoulder is the ($\alpha+\beta$)-titanium alloy Ti–6Al–4V (VT6) [13]. It has high indices of mechanical properties due to such alloying components as aluminum which greatly strengths α-phase and decreases alloy density as well as allows reaching significant strengthening with preserva-

Figure 1. General view of endoprosthesis replacement: *a* — proximal part of femoral bone (*1* — whirlbone; *2*, *3* — head and stem of endoprosthesis respectively); *b* — femoral bone – endoprosthesis – hip bone system; *c* — standard endoprostheses; *d* — mock-up and X-ray picture of individual endoprosthesis after implanting

tion of sufficient ductility [14]. However, regardless high indices of mechanical strength and wear-resistance the service life of any metallic implants rigidly fixed in the bone tissue is greatly limited due to unconformity of the elasticity moduli of the bone tissue and implant material.

The phenomenon of stress shielding slows down the processes of shape restoration and healing of the bone that decreases density of the bone tissue with increase of its porosity [11]. This can provoke reject in implant operation, namely instability of fixation of the implant in a bone due its structural changes. The instability of endoprosthesis results in increase of defectiveness of a bone and requires repeated, i.e. revision surgery. At that the revision surgeries are undesirable since they have high cost and higher risk of the postoperative complications. Therefore, search of the ways of increase of service life for the endoprosthesis is a relevant task for today not only in the field of medicine, but materials science and mechanical bioengineering as well.

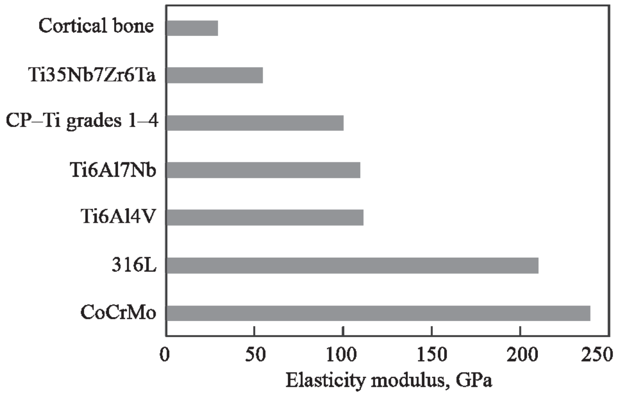

Figure 2. Moduli of elasticity of metallic materials for implants in comparison with cortical bone tissue [15]

MATERIALS AND METHODS

The most widespread methods for shielding stress prevention are application of low modulus alloys, providing a porous structure to the implants and application of the implants with functionally-gradient coatings of different porosity.

The current trends towards low-modulus materials resulted in development of new alloys with better relationship of bone-implant elasticity moduli. Thus, there are attempts to replace the main and the most widespread ($\alpha+\beta$)-titanium alloy Ti6Al4V by β-titanium alloys, doped with niobium, zirconium and tantalum (Ti13Nb13Zr, Ti29Nb13Ta4.6Zr), the modulus of elasticity of which can be lower than 50 GPa[16]. At that the values of elasticity modulus of a cortical bone tissue is changed from 5 to 23 GPa. This characteristic makes approximately from 112 to 240 GPa, respectively (Figure 2), for such most widespread materials being used for implants' manufacture as titanium alloy Ti6A14V, stainless steel 316L and cobalt-chromium alloy CoCrMo.

Recent results of development of alloy Ti35Nb7Zr6Ta, the modulus of elasticity of which was approximated to the modulus of elasticity of the cortical bone tissue for the purpose of prevention of its resorption, turned to be successful [17]. However, β-phase alloys have lower strength than alloys with α- and $\alpha+\beta$ phases and their synthesis today is much more expensive in comparison with traditional (α+β) alloys [18]. Therefore, solution of the indicated problem in short-term perspective by means of mass application of these low modulus alloys is impossible.

The simplest technological solution for suppression of the effect of stress shielding and acquiring the positive results as for extension of their service life is a provision of a porous structure [19] to the metallic implants, including using porous coatings [20]. Besides, it is known that [21] roughness of the implant surface promotes its osseointegration. Thus, the investigations [22] showed improved attachment of the bone to the implant due to reproduction of a bone inner porosity on its surface. The implant is fixed by means of a joining between the bone and its porous matrix as a result of bone growth in the implant pores and provides not only fixation, but also a system that allows transfer of loading from the implant to the bone [23].

Current tendencies of automation development and computerization initiated the direction of additive manufacturing technologies (AT) known as 3D-printing technologies. They are also used for decrease of effect of stress shielding by means of production of structures with a gradient of size and shape of the pores from the surface to the center of the part [24]. Such implants have a series of unique advantages such as high biocompatibility, open interconnected structure of the pores, which promotes growth of the bone tissue, and elasticity modulus close to bone one [25].

The most widespread methods of AT for manufacture of metallic structures with functional gradient are the methods of selective laser and electron-beam melting [26]. The gradient structures obtained by AT methods allow decreasing the elasticity modulus due to the presence in them of significant volume of pores [27]. There is a wide assortment of the implants with through porosity as well as solid base with present porous structure on their surface. They are produced by such well-known manufacturers as Zimmer Biomet Trabecular Metal™, Lima Corporate Trabecular Titanium, Gruppo Bioimpiant Fin System, Permedica Orthopedics Trabecular Titanium TRASER (Figure 3).

The most significant obstacle on a way of mass application of AT in manufacture of implants is their labor intensity and material consumption. At that all the manufacture stages should be agreed from the side of doctors as well as engineers.

In turn there is a problem of high cost of consumables for manufacture of 3D-implants and their limited by chemical composition assortment in the market. Current state of development of AT does not allow printing using different materials in one stage, and their replacement takes place only after complete termination of the process and performance of operations on cleaning from previously used material. Therefore, today these technologies are profitable only in those cases when other methods can not be used or complexity of open surgical treatment requires production of individual implants [29].

The powder sintering technologies have also found their application for manufacture of implants in orthopedics. These implant production technologies include the most widespread processes of pressing, spark plasma sintering and stamping of powder billets. The advantage of these methods lies in the fact that the raw

Fiugre 3. Implants of known manufacturers produced using AT [25]: *a* — Zimmer Biomet Trabecular Metal ™; *b* — Lima Corporate Trabecular Titanium; *c* — Gruppo Bioimpiant Fin System; *d* — Permedica Orthopedics Trabecular Titanium TRASER®

materials are the powders of metals, alloys, ceramics and other materials [30]. Using them it is possible to obtain the products with set characteristics and sizes since a wide spectrum of metal powders allows selecting the properties of these powders and predict them in finished products. Powder metallurgy technologies can provide production of high-porosity materials that affects the decrease of stress shielding effect. The review [31] shows the positive aspects of application of high-voltage current discharge for production of porous materials from powders of titanium, niobium and tantalum, which can be successfully used in medicine.

Work [32] demonstrates application of a method of spark plasma sintering of titanium powders with 110 μm average diameter of particles of compacts which had porosity at a level of 28 % and compression elasticity modulus of 7.9 GPa. Such indices of elasticity modulus lie in a range of change of a corresponding characteristic of the cortical bone tissue, thus, application of such coatings allows obtaining the significant success in suppression of the effect of stress shielding.

In work [33] the specimens with open porosity in 70–80 % range were made from spherical particles of titanium alloy of 0.5–1.0 mm diameter and demonstrated the value of elasticity modulus of 0.86 GPa, close to the indices of a corresponding characteristic of the trabecular bone tissue.

The main disadvantage of the methods of powder metallurgy lies in the fact that the technological process requires long-term holding of the specimens at high temperature and the indices of implants' strength often appear to be insufficient. One of the methods for solving the problem of increase of mechanical characteristics is application of double sintering. This allows increasing

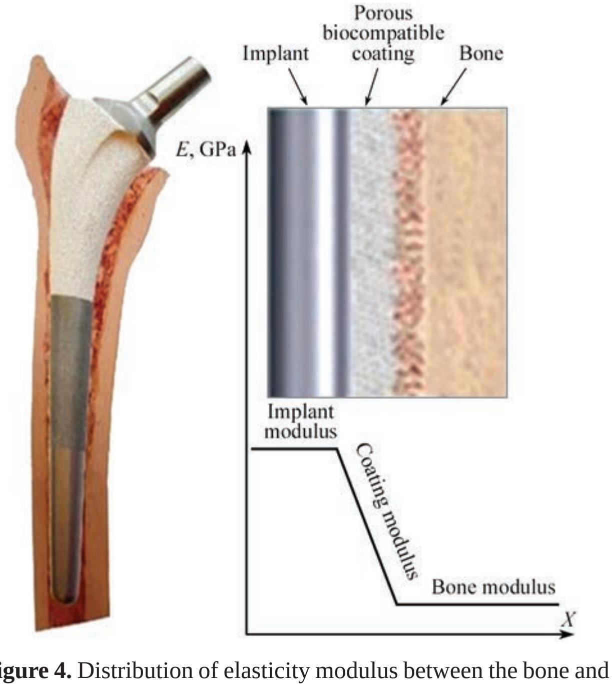

Figure 4. Distribution of elasticity modulus between the bone and the implant

the strength of porous specimens for more than 2 times without noticeable decrease of porosity part [34]. However, additional technological operations of holding at high temperatures for a sufficiently long time rise energy capacity of the production process and, as a result, its cost and can change structure of the output material.

Application of functionally-gradient coatings with different volume porosity provides a progressive approximation of the elasticity modulus from the implant to the bone as a result of multilayer coating (Figure 4). This permits prevention of appearance of the stresses which result in its delamination from a core in a zone of contact of the first layer with the maximum elasticity modulus as well as suppress the effect of stress shielding in a zone of contact of the last layer, which has the lowest elasticity modulus, with the cortical bone tissue [35].

The high efficiency of application as the implants of combined structure is shown by intraosseous plates with compact part from VT1-0 alloy. They were coated using the method of vacuum sintering by porous coating from titanium powder made by the technology of cold double sided pressing. As a result the bone tissue being formed around the implant actively penetrates inside it, providing, thus, its secondary fixing, and presence of porosity in the coating leads to decrease of elasticity modulus [36].

In work [34] a double-layer coating with pore sizes of 800–900 and 600–700 μm, respectively (Figure 5) was formed by means of burning of titanium powders on a surface of dental implant at 1233 and 1623 K temperatures.

Spark plasma sintering [37] is also used among the methods of powder metallurgy for modification of the surface of implants by means of deposition of the porous layers. Bending strength and elasticity modulus of the coatings from alloy Ti6A14V, produced by this method, made 128–178 MPa and 16–18 GPa, respectively, that corresponds to a range of changes of respective characteristics of the cortical bone tissue [38].

The main disadvantage of the burning methods for production of porous structures from powder materials on the implant surface, as in the case with the processes of volume pressing and sintering, is the indices of coating strength and the high temperatures of treatment in course of a long interval of time. For example, in order to obtain the powder coatings from titanium alloy Grade 4 (ASME standard alloy) with a level of volume porosity in 30–50 % range, which provides the elasticity modulus close to corresponding value of the cortical bone tissue, it is necessary to sinter them at 1000–1100 °C temperatures during 2 h [39].

A technology of laser modification of a surface of metallic materials became popular in recent time. In it the laser is used as a heat source (Figure 6). This technology of deposition of gradient coatings on the products from

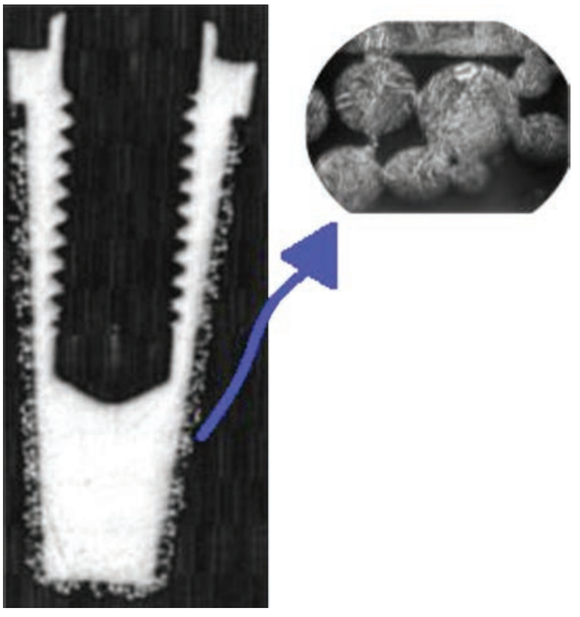

Figure 5. Porous coating on dental implant produced by burning of layers of titanium powder [34]

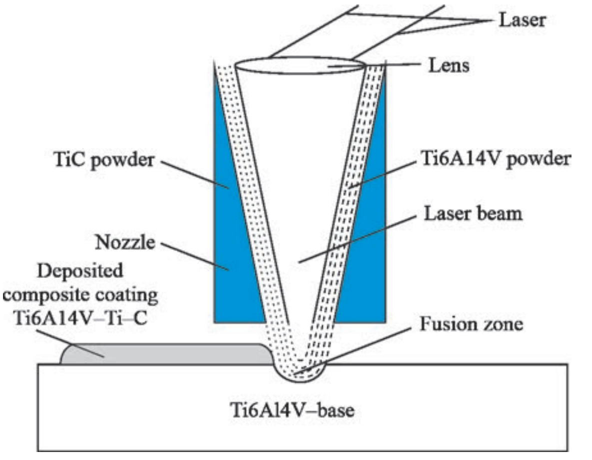

Figure 6. Scheme of the process of laser burning of powder

titanium alloys is considered as a competitive method. It allows controlling an accuracy and features of the implant surface being at that high-efficient, eco-friendly and economic from point of view of consumables [40]. However, adhesion strength of the coatings, deposited by laser burning of powder, to the base sometimes is not sufficient and applied stresses can exceed it that promotes delamination of the coating from the prosthesis surface, thus violating its function [41].

The implants with low elasticity modulus are manufacture by a known company Zimmer Biomet, a founder of patented technology of production of trabecular structure Trabecular Metal™. This structure is similar to bone tissue and consists of porous glass-like carbon coated by tantalum with the help of vacuum spraying [42, 43]. The produced implants have 80.9 % porosity, 527±27 μm size pores and elasticity modulus 3 GPa.

Current implants made using AT also simulate the surfaces with trabecular structure (Figure 7). Nevertheless, presence of the pores in their volume results in decrease of strength of such structures. This is the reason of their limited application only by those implantation places where they do not bear the main service loading. A contraindication to application of these implants in a practical aspect is the presence of a septic process at intervention since the main disadvantage of the trabecular components is the problems with their explantation [25].

In literature there are other approaches to reduction of elasticity modulus using current polymer materials such as PEEK. Thus, work [44] describes an innovative approach to decrease of the elasticity modulus of metallic implant due to application of composite carbon/polymer material (PEEK), which is formed on the surface of hip joints. Performed model experiments and numerical results indicate that a composite carbon/polymer material significantly rises the characteristics of fatigue resistance of the surface layers with distribution of applied load and its transfer to the bone. This decreases the effect of stress shielding and provides better stability of the implant during the long service life.

However, this idea of application of the coating was only modeled and was not proved by practical results which can significantly differ from the calculation ones and their application can reveal a series of other problems such as fixation of osteoblasts on the surfaces of PEEK material.

In contrast to methods mentioned above today a method of plasma spraying (Figure 8) is the most

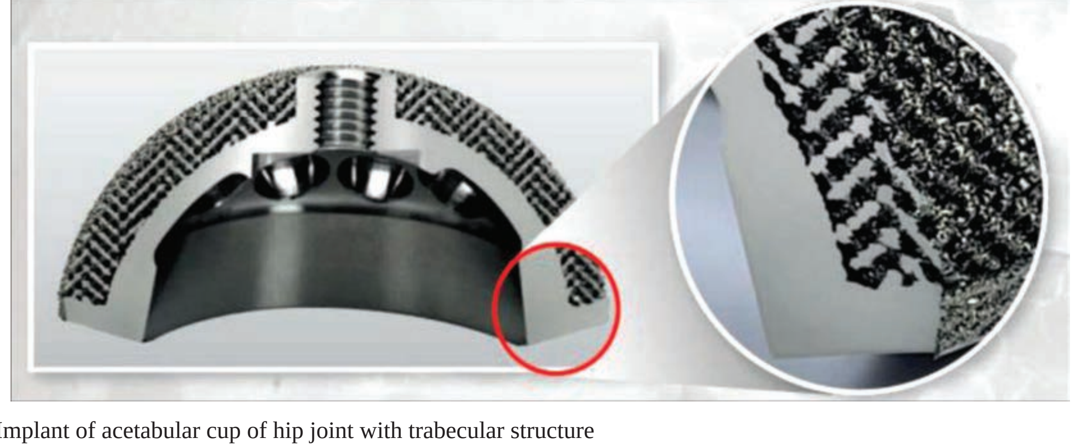

Figure 7. Implant of acetabular cup of hip joint with trabecular structure

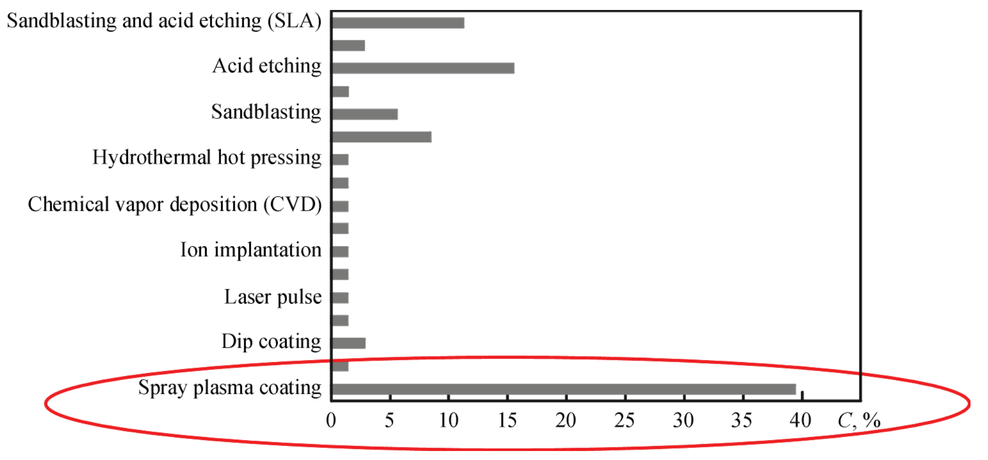

Figure 8. Distribution of technology of production of porous structures on implant surface [45]

available and technologically simple in realization of production of porous structures on the surfaces of implants with verified numerous successful results of practical application. This method attracted a lot of attention in biomedicine due to low cost, high efficiency and wide regulation of coating thickness with possibility of application of different spraying materials on the same equipment [46, 47]. Successful application of the plasma spraying for coating production is promoted by several factors, namely high efficiency of spraying process; relatively insignificant heating of a base (to > 200 °C) that decreases possibility of change of its properties; simplicity of regulation of coating production process (power characteristics of plasma can be changed technologically depending on the requirements in the process of coating production); possibility of application of automated manipulator in the process of coating deposition that promotes uniform distribution of a sprayed layer over a part surface.

Versatile and flexibility of the technology of plasma spraying allows adjusting it to almost any spectrum of materials being sprayed such as metals and their oxides, apatites and other materials [48].

There was accumulated a significant experience of application of plasma spraying for improvement of the surface of dental implants due to a plasma-sprayed layer of titanium and hydroxyapatite powder which influences the acceleration of osseointegration [49]. Among the disadvantages of given method of coating deposition are relatively not high strength of adhesion of the coating with the base as well as low coefficient of material application. Particularly, substantial losses of material will take place at spraying of implants of small size (intervertebral cages, dental implants). At that overheating of a small-size part is also possible as a result of effect of a high-temperature plasma jet. In order to reduce losses of the material provoked by the fact that part size is smaller than the spaying spot it is necessary to try to decrease the diameter of the latter.

Solution of some of the issues mentioned above is possible with the help of application of a technology of microplasma spraying developed at the PWI of the NASU. It provides formation of a plasma jet with reduced heat power and a spraying spot of small size [50]. Structural peculiarity of the equipment, namely microplasmatron in combination with technological approaches allow spraying powder as well as wire materials with formation of structures with high level of porosity and pore size to 300 μm. Such structures increase osseointegration with the bone and provide necessary indices of mechanical strength of the coating-base system [51] that permits to use them on the surfaces of endoprostheses for cementless fixation [52]. Therefore, the technology of microplasma spraying is perspective for modification of the surfaces of implants since formed by such method coatings from alloys based on titanium or zirconium with maximum possible level of porosity (25 % for titanium and 20.3 % for zirconium alloy) and elasticity modulus 12 and 5 GPa, respectively [53], allow significantly approaching them to the corresponding characteristic of the cortical bone tissue. This will promote more uniform distribution of stresses during operation of the implants.

CONCLUSIONS

1. The analysis of the modern references as for appearance of aseptic instability was carried out and it was determined that one of the reasons of its appearance is the effect of stress shielding caused by nonconformity of the elasticity moduli of the implant and the bone.

2. Such methods as application of low modulus alloys, additive manufacturing technologies, powder sintering and plasma spraying were analyzed for reduction of the elasticity modulus of the orthopedic implants for the purpose of prevention of the effect of stress shielding.

3. It was determined that today the technologies of plasma spraying are the most effective and economically feasible methods of production of porous structures on the implant surfaces. In particular, it was shown that application of the technology of microplasma spraying of the coatings on the implants'

surface removes the disadvantages typical for conventional plasma spraying as well as promotes suppression of the stress shielding effect.

REFERENCES

1. Malnick, S.D.H., Knobler, H. (2006) The medical complications of obesity. *QJM*: *An Int. J. of Medicine*, 99(**9**), 565–579. DOI: https://doi.org/10.1093/qjmed/hcl085
2. Musumeci, G., Aiello, F.C., Szychlinska, M.A. et al. (2015) Osteoarthritis in the XXIst century: Risk factors and behaviours that influence disease onset and progression. *Int. J. of Molecular Sci.*, 16(**3**), 6093–6112. DOI: https://doi.org/10.3390/ijms16036093
3. Johnson, V.L., Hunter, D.J. (2014) The epidemiology of osteoarthritis. *Best Practice & Research Clinical Rheumatology*, 28(**1**), 5–15. DOI: https://doi.org/10.1016/j.berh.2014.01.004
4. Zethraeus, N., Borgström, F., Ström, O. et al. (2007) Cost-effectiveness of the treatment and prevention of osteoporosis: A review of the literature and a reference model. *Osteoporosis Int.*, 18(**1**), 9–23. DOI: https://doi.org/10.1007/s00198-006-0257-0
5. Barrère, F., Mahmood, T.A., de Groot, K., van Blitterswijk, C.A. (2008) Advanced biomaterials for skeletal tissue regeneration: Instructive and smart functions. *Materials Sci. and Engin. R: Reports*, 59(**1–6**), 38–71. DOI: https://doi.org/10.1016/j.mser.2007.12.001
6. Kosyakov, A.N., Grebennikov, K.A., Miloserdov, A.V. et al. (2019) 3D-planning and prototyping at complex primary endoprosthetics of hip joint. *Travma*, 20(**5**), 53–61 [in Russian]. DOI: https://doi.org/10.22141/1608-1706.5.20.2019.185557
7. Quinn, J., McFadden, R., Chan, C.-W., Carson, L. (2020) Titanium for orthopedic applications: An overview of surface modification to improve biocompatibility and prevent bacterial biofilm formation. *Science*, 23(**11**), Article number 101745. DOI: https://doi.org/10.1016/j.isci.2020.101745
8. Evans, J.T., Evans, J.P., Walker, R.W. et al. (2019) How long does a hip replacement last? A systematic review and meta-analysis of case series and national registry reports with more than 15 years of follow-up. *The Lancet*, 10172(**393**), 647–654. DOI: https://doi.org/10.1016/S0140-6736(18)31665-9
9. *Kuibida V.*, Kokhanets P. and Lopatynska V. (2021) Mechanism of strengthening the skeleton using plyometrics. *J. of Physical Education and Sport*, 21(**3**), 1309–1316. DOI: https://doi.org/10.7752/jpes.2021.03166
10. Arabnejad, S., Johnston, B., Tanzer, M., Pasini, D. (2017) Fully porous 3D printed titanium femoral stem to reduce stress-shielding following total hip arthroplasty. *J. of Orthopaedic Research*, 35(**8**), 1774–1783. DOI: https://doi.org/10.1002/jor.23445
11. Zhang, B., Pei, X., Zhou, C. et al. (2018) The biomimetic design and 3D printing of customized mechanical properties porous Ti6Al4V scaffold for load-bearing bone reconstruction. *Materials and Design*, **152**, 30–39. DOI: https://doi.org/10.1016/j.matdes.2018.04.065
12. Attarilar, Sh., Djavanroodi, F., Irfan, O.M. et al. (2020) Strain uniformity footprint on mechanical performance and erosion-corrosion behavior of equal channel angular pressed pure titanium. *Results in Physics*, **17**, Article number 103141. DOI: https://doi.org/10.1016/j.rinp.2020.103141
13. Apostu, D., Lucaciu, O., Lucaciu, G.D.O. et al. (2017) Systemic drugs that influence titanium implant osseointegration. *Drug Metabolism Reviews*, 49(**1**), 92–104. DOI: https://doi.org/10.1080/03602532.2016.1277737
14. Arzamasov, B.N., Brostrem, V.A., Bushe, N.A. et al. (1990) *Structural materials*. Ed. by B.N. Arzamasov. Moscow, Mashinostroenie [in Russian].
15. Geetha, M., Singh, A.K., Asokamani, R., Gogia, A.K. (2009) Ti based biomaterials, the ultimate choice for orthopaedic implants: A review. *Progress in Mater. Sci.*, 54(**3**), 397–425. DOI: https://doi.org/10.1016/j.pmatsci.2008.06.004
16. Niinomi, M., Nakai, M., Hieda, J. (2012) Development of new metallic alloys for biomedical applications. *Acta Biomaterialia*, 11(**8**), 3888–3903. DOI: https://doi.org/10.1016/j.actbio.2012.06.037
17. *Lubov* Donaghy, C., McFadden, R., Kelaini, S. et al. (2020) Creating an antibacterial surface on beta TNZT alloys for hip implant applications by laser nitriding. *Optics and Laser Technology*, **121**, Article number 105793. DOI: https://doi.org/10.1016/j.optlastec.2019.105793
18. Liu, J., Chang, L., Liu, H. et al. (2017) Microstructure, mechanical behavior and biocompatibility of powder metallurgy Nb–Ti–Ta alloys as biomedical material. *Mater. Sci. and Engin. C: Materials for Biological Applications*, **71**, 512–519. DOI: https://doi.org/10.1016/j.msec.2016.10.043
19. Wen, C.E., Mabuchi, M., Yamada, Y. et al. (2001) Processing of biocompatible porous Ti and Mg. *Scripta Materialia*, 45(**10**), 1147–1153. DOI: https://doi.org/10.1016/S1359-6462(01)01132-0
20. Mahmoud, D., Elbestawi, M.A. (2017) Lattice structures and functionally graded materials applications in additive manufacturing of orthopedic implants: A review. *J. of Manufacturing and Materials Processing 1*, 13(**2**), Article number jmmp1020013. DOI: https://doi.org/10.3390/jmmp1020013
21. Kane, R., Ma, P.X. (2013) Mimicking the nanostructure of bone matrix to regenerate bone. *Materials Today*, 16(**11**), 418–423. DOI: https://doi.org/10.1016/j.mattod.2013.11.001
22. Pałka, K., Pokrowiecki, R. (2018) Porous titanium implants: A review. *Advanced Engineering Materials*, 20(**5**), Article number 1700648. DOI: https://doi.org/10.1002/adem.201700648
23. Schneider, E., Kinast, C., Eulenberger, J. et al. (1989) A comparitive study of the initial stability of cementless hip prostheses. *Clinical Orthopaedics and Related Research*, **248**, 200–209. DOI: https://doi.org/10.1097/00003086-198911000-00032
24. Yuan, L., Ding, S., Wen, C. (2019) Additive manufacturing technology for porous metal implant applications and triple minimal surface structures: A review. *Bioactive Materials*, 4(**1**), 56–70. DOI: https://doi.org/10.1016/j.bioactmat.2018.12.003
25. Kosyakov, A.N., Grebennikov, K.A., Miloserdov, A.V. et al. (2019) Applications of trabecular components during endoprosthetics of hip joint (Review). *Visnyk Ortopedii, Travmatologii ta Protezuvanniya,* 103(**4**), 116–123 [in Russian]. DOI: https://doi.org/10.37647/0132-2486-2019-103-4-110-117
26. Bikas, H., Stavropoulos, P., Chryssolouris, G. (2016) Additive manufacturing methods and modeling approaches: A critical review. *Int. J. Adv. Manuf. Technol.*, 83(**1–4**), 389–405. DOI: https://doi.org/10.1007/s00170-015-7576-2
27. Chashmi, M.J., Fathi, A., Shirzad, M. et al. (2020) Design and analysis of porous functionally graded femoral prostheses with improved stress shielding. *Designs*, 4(**2**), 1–15, Article number 12. DOI: https://doi.org/10.3390/designs4020012
28. Kosyakov, A.N., Grebennikov, K.A., Miloserdov, A.V. et al. (2018) Compensation of bone defects of cotyloid cavity using the additive technologies. *Visnyk Ortopedii, Travmatologii ta Protezuvanniya,* 99(**4**), 64–74 [in Russian]. DOI: https://doi.org/10.37647/0132-2486-2018-99-4-64-74
29. Shi, H., Zhou, P., Li, J. et al. (2021) Functional gradient metallic biomaterials: Techniques, current scenery, and future prospects in the biomedical field. *Frontiers in Bioengineering and Biotechnology*, **8**, Article number 616845. DOI: https://doi.org/10.3389/fbioe.2020.616845
30. Goodall, R. (2013) *Advances in Powder Metallurgy*. Elsevier.
31. Minko, D., Belyavin, K. (2016) A porous materials production with an electric discharge sintering. *Int. J. of Refracto-*

ry Metals and Hard Materials, **59**, 67–77. DOI: https://doi.org/10.1016/j.ijrmhm.2016.05.015
32. Sakamoto, Y., Asaoka, K., Kon, M. et al. (2006) Chemical surface modification of high-strength porous Ti compacts by spark plasma sintering. *Bio-Medical Materials and Engineering*, 16(**2**), 83–91. PubMed ID: https://pubmed.ncbi.nlm.nih.gov/16477117
33. Jia, J., Siddiq, A.R., Kennedy, A.R. (2015) Porous titanium manufactured by a novel powder tapping method using spherical salt bead space holders: Characterization and mechanical properties. *J. of the Mechanical Behavior of Biomedical Materials*, **48**, 229–240 DOI: https://doi.org/10.1016/j.jmbbm.2015.04.018
34. Itin, V.I., Ponter, V.É., Khodorenko, V.N. et al. (1997) Strength properties of porous permeable stomatological materials based on titanium. *Powder Metallurgy and Metal Ceramics*, 36(**9–10**), 479–482. DOI: https://doi.org/10.1007/BF02680496
35. Helsen, J.A., Breme, H.J. (1998) *Metals as biomaterial*. Chichester, John Wiley & Sons Ltd.
36. Smetkin, A.A., Konyukhova, S.G., Yarmonov, A.N. (2003) Application of porous permeable materials in dental implant technique. *Izvestiya Vysshikh Uchebnykh Zavedenij. Tsvetnaya Metallurgiya*, **5**, 65–67 [in Russian].
37. Kon, M., Hirakata, L.M., Asaoka, K. (2004) Porous Ti–6Al–4V alloy fabricated by spark plasma sintering for biomimetic surface modification. *J. of Biomedical Materials Research. Pt B: Applied Biomaterials*, 68(**1**), 88–93. DOI: https://doi.org/10.1002/jbm.b.20004
38. Nomura, N., Oh, I.-H., Hanada, S. et al. (2005) Effect of nitrogen on mechanical properties of porous titanium compacts prepared by powder sintering. *Mat. Sc. Forum*, 475–479(**III**), 2313–2316. DOI: https://doi.org/10.4028/0-87849-960-1.2313
39. Torres, Y., Pavón, J.J., Nieto, I., Rodríguez, J.A. (2011) Conventional powder metallurgy process and characterization of porous titanium for biomedical applications. *Metallurg. and Mater. Transact. B: Process Metallurgy and Materials Proc. Sci.*, 42(**4**), 891–900. DOI: https://doi.org/10.1007/s11663-011-9521-6
40. Weng, F., Chen, C.Z., Yu, H.J. (2014) Research status of laser cladding on titanium and its alloys: A review. *Materials and Design*, **58**, 412–425. DOI: https://doi.org/10.1016/j.matdes.2014.01.077
41. Mohseni, E., Zalnezhad, E., Bushroa, A.R. (2014) Comparative investigation on the adhesion of hydroxyapatite coating on Ti–6Al–4V implant: A review paper. *Inter. J. of Adhesion and Adhesives*, **48**, 238–257. DOI: https://doi.org/10.1016/j.ijadhadh.2013.09.030
42. Christie, M.J. (2002) Clinical applications of trabecular metal. *American J. of Orthopedics (Belle Mead, N.J.)*, 31(**4**), 219–220. PubMed ID: https://pubmed.ncbi.nlm.nih.gov/12008854
43. Levine, B.R., Sporer, S., Poggie R.A. et al. (2006) Experimental and clinical performance of porous tantalum in orthopedic surgery. *Biomaterials*, 27(**27**), 4671–4681. DOI: https://doi.org/10.1016/j.biomaterials.2006.04.041
44. Darwich, A., Nazha, H., Daoud, M. (2020) Effect of coating materials on the fatigue behavior of hip implants: A three-dimensional finite element analysis. *J. of Applied and Computational Mechanics*, **2**, 284–295. DOI: https://doi.org/10.22055/JACM.2019.30017.1659
45. Jemat, A., Ghazali, M.J., Razali, M., Otsuka, Y. (2015) Surface modifications and their effects on titanium dental implants. *BioMed Research Int.*, Article number 791725. DOI: https://doi.org/10.1155/2015/791725
46. Sun, L. (2018) Thermal spray coatings on orthopedic devices: When and how the FDA reviews your coatings. *J. of Thermal Spray Technol.*, 27(**8**), 1280–1290. DOI: https://doi.org/10.1007/s11666-018-0759-2
47. Alontseva, D., Voinarovych,, S., Ghassemieh, E. et al. (2020) Manufacturing and characterisation of robot assisted microplasma multilayer coating of titanium implants: Biocompatible coatings for medical implants with improved density and crystallinity. *Johnson Matthey Technology Review*, 64(**2**), 180–191. DOI: https://doi.org/10.1595/205651320x15737283268284
48. Cizek, J., Matejicek, J. (2018) Medicine meets thermal spray technology: A review of patents. *J. of Thermal Spray Technol.*, 27(**8**), 1251–1279. DOI: https://doi.org/10.1007/s11666-018-0798-8
49. Lyasnikov, V.N., Lepilin, A.V., Protasova, N.V. (2013) Scientific fundamentals of development of dental implants. *Saratovskii Nauchno-Meditsinskii Zhurnal,* 9(**3**), 431–434 [in Russian].
50. Borisov, Yu.S., Kislitsa, A.N., Vojnarovich, S.G. (2006) Peculiarities of the process of microplasma wire spraying. *The Paton Welding J.*, **4**, 21–25.
51. Voinarovych, S.G., Alontseva, D.L., Kyslytsia, O.M. et al. (2022) Microplasma spraying of coatings using zirconium wire. *The Paton Welding J.*, **9**, 41–46. DOI: https://doi.org/10.37434/tpwj2022.09.07
52. Gaiko, G.V., Panchenko, L.M., Pidgaetskyi, V.M. et al. (2008) Influence of different types of coatings for cementless endoprosthesis on clonogenic activity of stem stromal cells of bone marrow in patients with hip osteoarthrosis in vitro (Experimental investigation). *Visnyk Ortopedii, Travmatologii ta Protezuvanniya,* 59(**4**), 5–11 [in Ukrainian]. DOI: https://doi.org/10.37647/0132-2486-2018-59-4-5-11
53. Moltasov, A., Dyman, M., Kaliuzhnyi, S. et al. (2022) Dependence of the elasticity modulus of microplasma coatings made of titanium grade VT1-00 and zirconium grade KTC-110 on their porosity. *Series on Biomechanics*, 36(**2**), 142–153. DOI: http://doi.org/10.7546/sb.36.2022.02.14

ORCID

A.V. Moltasov: 0000-0002-5025-4055,
S.G. Voinarovych: 0000-0002-4329-9255,
M.M. Dyman: 0000-0002-5886-1124,
S.M. Kalyuzhnyi: 0000-0002-8132-3930,
S.V. Burburska: 0000-0002-1487-613X

CONFLICT OF INTEREST

The Authors declare no conflict of interest

CORRESPONDING AUTHOR

A.V. Moltasov:
E.O. Paton Electric Welding Institute of the NASU
11 Kazymyr Malevych Str., 03150, Kyiv, Ukraine.
E-mail: 2052382@gmail.com

SUGGESTED CITATION

A.V. Moltasov, S.G. Voinarovych, M.M. Dyman, S.M. Kalyuzhnyi, S.V. Burburska (2022) Methods to prevent the stress shielding effect in implant–bone system (Review). *The Paton Welding J.*, **1**, 31–38.

JOURNAL HOME PAGE

https://patonpublishinghouse.com/eng/journals/tpwj

Received: 02.01.2023
Accepted: 28.02.2023

DOI: https://doi.org/10.37434/tpwj2023.01.06

MODERN MODELS OF FORMATION OF WELDED JOINTS OF POLYMER MATERIALS (REVIEW)

M.G. Korab, M.V. Iurzhenko, V.L. Demchenko, Ye.P. Mamunya

E.O. Paton Electric Welding Institute of the NASU
11 Kazymyr Malevych Str., 03150, Kyiv, Ukraine

ABSTRACT

The process of welding plastics is determined as a gradual disappearance of the interface between parts to be joined and the formation of a transition layer between them, whose structure is significantly different from the structure of the base polymeric material. The models of formation of welded joints of polymers existing today are based on different physical phenomena: mutual adhesion of substrates, diffusion of macromolecules and melt rheology. The most common is the diffusion model of macromolecules reptation in the welding zone, which many researchers refer to in order to explain experimental data. Without denying the possibility of progressive diffusion of elements of the molecular chain through the fusion surface, the postulate that this diffusion provides the main mass transfer during the formation of welded joints of polymers is considered to be controversial. The theory of the formation of welded joints of polymers due to conformational transformations of macromolecule fragments, being developed by the Scientific School of the PWI, is more realistic. In the development of this conformational theory, the model of homogenization of the transition layer on the interface during welding of polymers is proposed based on a vacancy-conformational principle.

KEYWORDS: polymer materials, welding, diffusion of macromolecules, conformational transformations

INTRODUCTION

Understanding of the mechanism of polymer welded joint formation is required for adequate selection of welding technology and mode parameters, as well as methods of welded joint quality evaluation. However, there is still no common point of view and there exist several hypotheses for this mechanism. Since the 80s, the PWI Scientific School has introduced and has been developing the theory of formation of polymer welded joints due to conformational transformations of macromolecule fragments. The objective of this work is to review the currently available explanations of the mechanism of producing a welded joint of polymer materials, and to give additional arguments in favour of the conformational theory.

The physicochemical properties of metals and plastics differ cardinally. However, the processes of welding these material types have a lot in common, as both are solids from the physical point of view. The scientific definition of the welding process is as follows: producing a permanent joint of solids, the monolithic nature of which is achieved by ensuring the physicochemical, and atomic-molecular bonds between elementary particles of the bodies being joined [1]. Or the so-called thermodynamic definition of welding: welding is a process of producing a monolithic joint of materials due to supply and thermodynamically irreversible transformation of energy and substance in the joining point.

A common property of solids, in particular, plastics, is preservation of an interface between the contact surfaces of individual bodies. That is why the following definition of welding of plastics was formulated: it is a technological process of producing a permanent joint of structural elements by diffusion-rheological or chemical interaction of polymer macromolecules, resulting in disappearance of the interface and formation of a structural transition from one polymer element to another one [2]. Another variant of such a definition is as follows: polymer material welding is a technological process of producing a permanent joint of parts and elements of a structure, resulting in disappearance of the primary interface between the parts from polymer materials, transforming into a transition layer with a homogeneous or heterogeneous chemical structure [3].

The ISO International Standard gives a rather simple definition: “welding of plastics is a process of joining the softened surfaces of materials, as a rule, through application of heat” [4].

Thus, blurring and disappearance of the interface between the parts is regarded as the essence of the welded joint, unlike an adhesion joint, where the interface always remains and is clearly visible. With the start of application of the first methods of plastics welding, scientists began putting forward hypotheses of the mechanisms of formation of polymer material welded joints.

MAIN BODY OF THE ARTICLE

In work [5], the researchers when studying the features of thermal welding of polymethyl methacrylate (PMMA) suggested that the welded joint forms by the diffusion mechanism of autohesion (bonding of surfaces of one and the same polymer material brought into contact). Furtheron, the theory of diffusion autohesion was developed, mutual movement of macromolecular

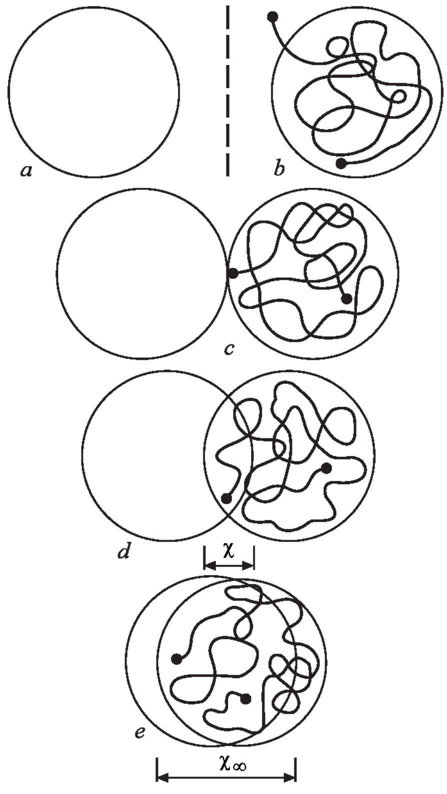

Figure 1. Block-diagram of stages of welded joint formation by R. Wool

fragments through the contact surface in welding was explained by thermal Brownian motion of molecular segments and their relative sliding in high-elastic (for amorphous polymers) and plastic states [6, 7].

Later on, US researcher R. Wool proposed the diffusion hypothesis of "crack healing in polymers", which consists of five stages, schematically shown in Figure 1 [8]. A dashed line marks the conditional dividing line of the joint, and inside the circle is the so-called random tangle of the macromolecular chain (shown only from one side for the sake of clarity). The first two stages are surface restructuring (usually melting under the impact of heat) and drawing of the surfaces together up to their contact (*a*, *b*). The third stage is mutual wetting of the surfaces (*c*), the fourth one is the start of diffusion to a certain distance (*d*) χ and the last fifth stage (*e*) is mutual diffusion to distance χ_∞ and blurring of the interface line.

The structure of amorphous polymers is schematically represented as a network structure of random bonds between the macromolecular chains. There exist alternative hypotheses of formation of such bonds: due to folded cluster structures [9, 10] and through the direct engagement of one molecular chain at least one with another — the theory of bridge bonds in a polymer massive [11]. In keeping with this theory, at formation of a welded joint, bridge bonds — engagements should also form between the macromolecules along the fusion line, which are schematically shown in Figure 2. A thick line shows a minimal structure of the molecular bridge through the interface line, which is required to form the weld. This model is used for explaining the mechanism of formation of structures of different strength along the fusion line, depending on thermophysical condition of the welding process [12].

In Western publications the "healing" term is used within the diffusion hypothesis for description of the process of formation of polymer welded joints, which is illustrated in Figure 3 [13]. After formation of contact between the partially melted surfaces of polymer elements being joined, the process of molecular chain diffusion through the butt surface and their entangling begins. It is shown that a rather long time of the polymer staying in the molten state, when the processes of macromolecule displacement are active, should be regarded as the main condition for "healing". However, the question of the very diffusion mechanism of "healing" (blurring, disappearance) of the fusion boundary in the welded joint is still debatable.

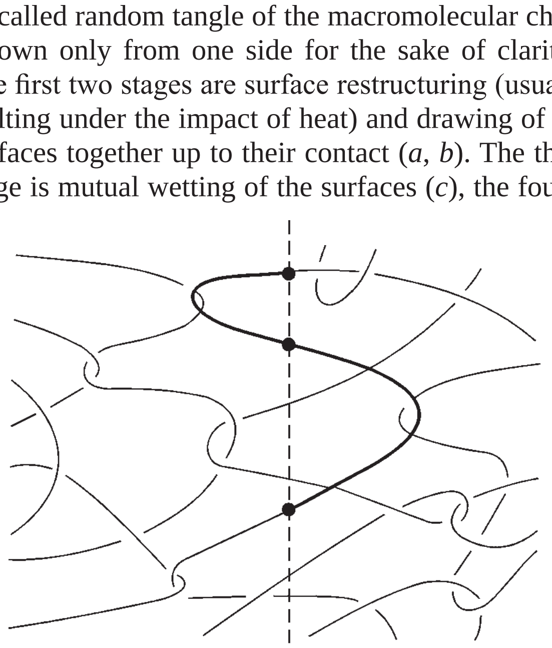

Figure 2. Illustration of a model of polymer welded joint formation due to macromolecule engagement in work [11]

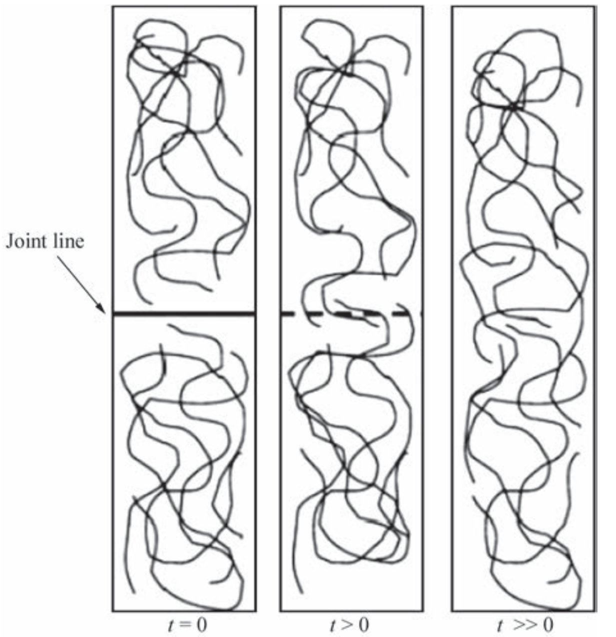

Figure 3. Illustration of the diffusion model of polymer welded joint formation in work [13]

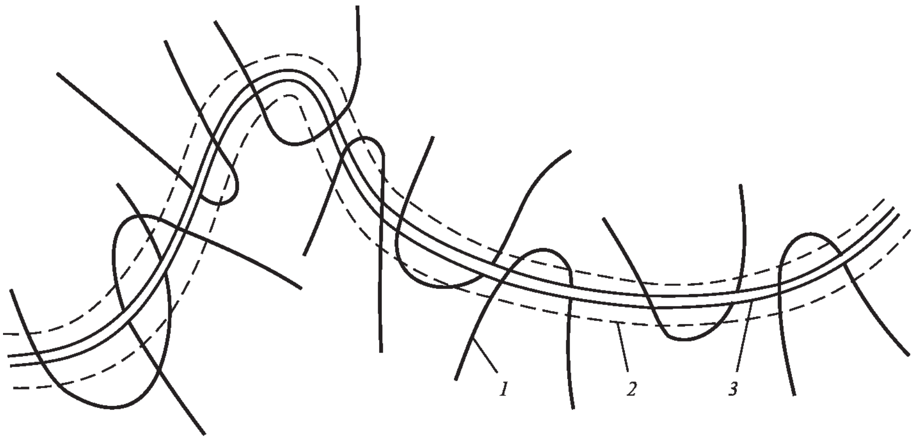

Figure 4. Schematic of formation of a "tube" from molecular chains by reptation theory: *1* — surrounding molecules; *2* — conditional boundaries of the tube; *3* — chain, capable of reptation

To clarify the mechanism of possible self-diffusion of the polymer chain, French physicist Pierre de Gennes with colleagues developed the reptation theory. It is believed that the macromolecule is surrounded by other chains on all sides, and it cannot move to the side, but can move in the longitudinally through such a medium as though through a kind of tube or tunnel (Figure 4). Such a movement of the macromolecule was called reptation, and it was conditionally compared with that of a snake crawling through a bunch of branches [14]. As under the melt conditions, all the molecules are in thermal Brownian motion, the chains forming the tube walls are constantly renewed.

It is believed that the main factor influencing the reptation tube parameters, is density of fluctuation network of engagements of macromolecules, present in the polymer melt. For flexible polymer chains, the distance between individual engagements is estimated to be in the range from 50 to 500 statistical molecular segments. It corresponds to rather long segments of the chain of length within 10^4–10^5. Therefore, it was assumed that such long segments add up to form a sequence of submolecular tangles, which is located inside the reptation tube (Figure 5). The characteristic size of the tangle (1) is what determines the average tube diameter *d*.

It should be noted that within the reptation theory the macromolecule mobility essentially depends on its length, i.e. molecular mass. It is believed that the time of molecule movement during reptation grows in proportion to the cube of its molecular mass. Therefore, such movements are most likely to be observed for short molecular chains. However, also considered is the possibility of reptation movement of fragments of molecular chains of a complex structure, namely branched, starlike and cyclic ones. So, a branched polymer chain can draw a side branch into the reptation tube during movement with its subsequent new random conformation outside. Cyclic polymer chains can fold into a linear conformation and can perform reptation movements in such a form. Owing to a high complexity of movement mechanisms of chains of a non-linear shape in the melt, the reptation displacement of macromolecules of complex shapes can proceed very slowly.

Let us consider the possible alternative mechanisms of formation of polymer welded joints. The processes of welding polymer materials and metals are similar in many cases. In flash-butt welding of metal parts, a structure forms which is similar to polymer material welds made by hot plate butt welding. Figure 6 shows the microstructure of a flash-butt welded joint of hot-rolled layered ferritic-pearlitic steel. In welding without flashing (*a*) the horizontal layered steel structure changes its orientation, deviating in the vertical direction along the joint line. In welding with flashing (*b*) a continuous layer of molten material forms on the end faces as a mixture of the melts of both parts, the

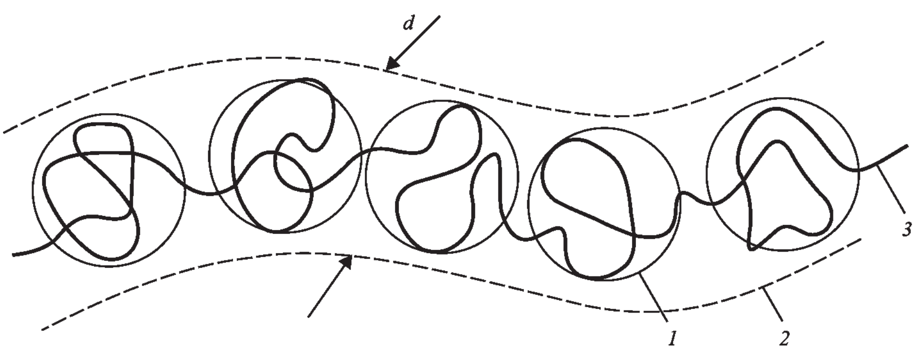

Figure 5. Molecule, consisting of a sequence of small tangles (submolecules) inside a "tube": *1* — molecular tangle; *2* — conditional boundary of the tube; *3* — polymer chain

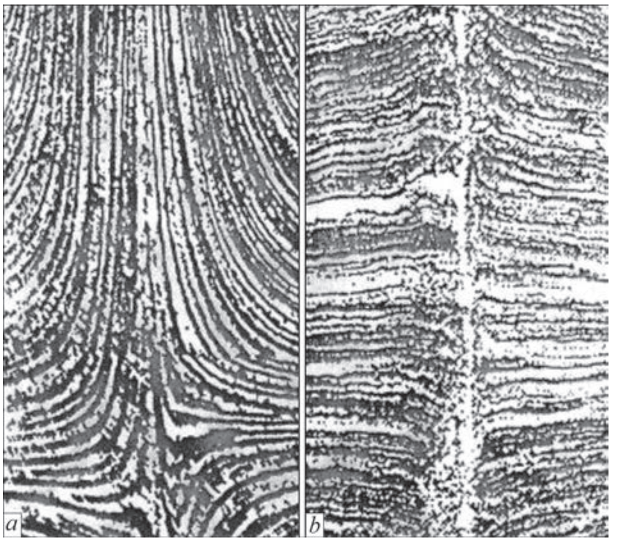

Figure 6. Macrostructure of flash-butt welded joints of pipe steel: *a* — welding without flashing; *b* — welding with flashing [15]

greater part of which is pressed out into flash by upset force. At cooling, the metal solidifies to form a welded joint. It is believed that the first butt joints form in the solid phase and the second ones — in a combined manner in the solid-liquid phase of the heated material [15]. In the latter case, the welded joint forms due to solidification of a thin layer of molten metal on the interface. A "rheological concept" of formation of welded joints of thermoplastic polymers was proposed by analogy with this mechanism. It was believed that the determinant role in the joint formation is played by "rheology": polymer melt flow at part upsetting under the impact of working pressure. Here, all the ingredients, hindering the intermolecular drawing together, namely gases, oxidized and contaminated areas, are driven out of the contact zone. As the shear rate of individual melt layers differs because of a nonuniform distribution of temperature and pressure, it causes the melt mixing, particularly on the fusion surface. Diffusion of macromolecule segments which occurs at the joint cooling, has little influence on the butt joint formation and is of a secondary nature [16].

A photo of the cross-section of a butt joint of layered polymer material cooled at the initial upsetting stage, is given to confirm mixing of melt microvolumes (Figure 7, *a*). Indeed, one can see from the photo that the polymer material layers are strongly deformed, but nothing points to their significant mixing. Similar work on hot plate butt welding of coloured layered samples of thermoplastics was conducted at PWI. In the cross-section of the layered welded joint (Figure 7, *b*, *c*) one can see that all the base material layers of the samples completely preserve their sequence, even in outer flash, changing just their thickness [2]. Thus, we cannot talk about any significant mixing of the melt during melting and deposition.

Yu.S. Lipatov with colleagues studied the specifics of interphase phenomena in heterogeneous systems of polymer-filler and polymer-polymer [17]. It was noted that different types of polymers are thermodynamically incompatible and they cannot form common crystalline shapes. However, different polymers are compatible morphologically, and at contact in the molten state they form common supermolecular structures as a transition layer. This layer is formed both by interdiffusion of the components through the interface, and due to one component adsorption on the surface of the other.

A polymer is a mixture of molecular chains of different size. Thermal fluctuations on the fusion surface lead to molecule differentiation by size and enrichment of the transition zone by molecules of smaller mass. Local diffusion through the surface of interfacial contact usually goes to a small depth and forms a transition layer of the thickness of several nanometers. On the other hand, different studies report the presence of the transition zones in polymer-polymer joints of 0.1–1.0 μm thickness. It is probable that alongside regular diffusion, transfer of rather significant volumes of one polymer into the interstructural regions of the adjacent polymer takes place in polymer melts at higher temperatures due to segmental mobility of macromolecules.

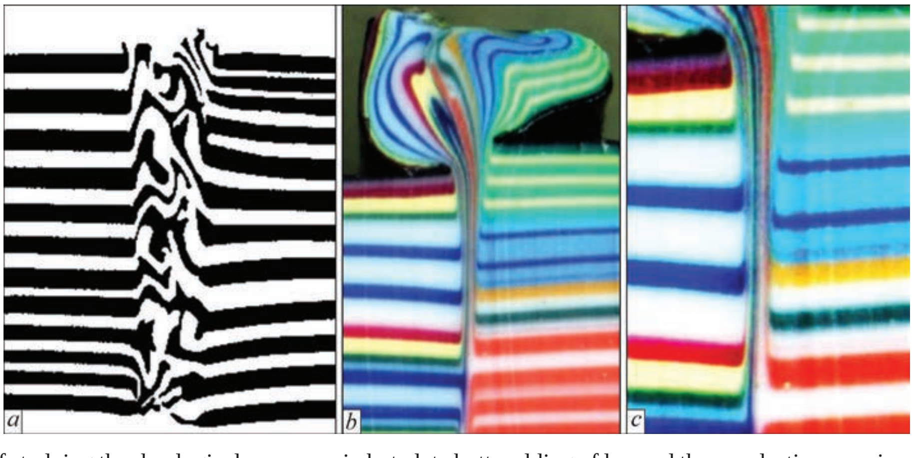

Figure 7. Results of studying the rheological processes in hot plate butt welding of layered thermoplastics: *a* — in work [16]; *b*, *c* — by PWI data [2]

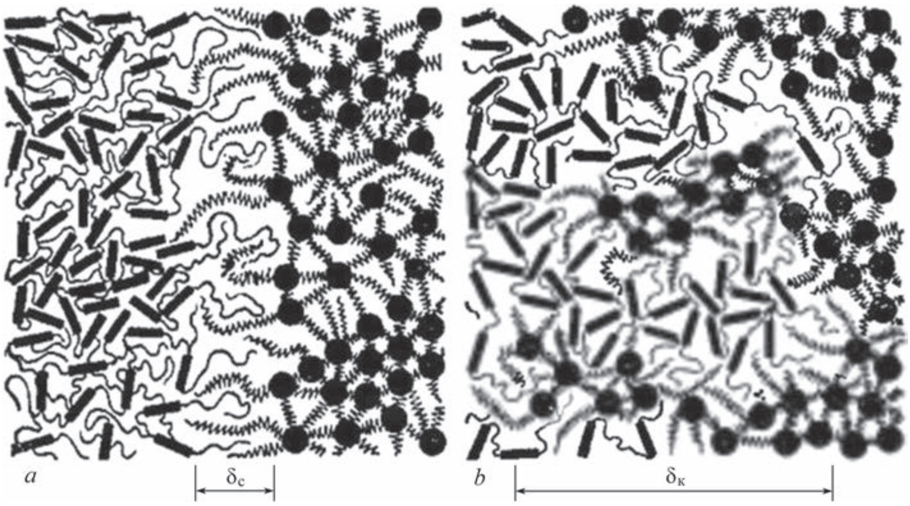

Figure 8. Model of the transition layer on the interface of different objects: *a* — allowing for only segmental diffusion; *b* — at displacement of structural elements [17]

Based on experimental data analysis, Yu.S. Lipatov developed a model of stage-by-stage formation of a transition zone on the contact boundary of the two polymers (Figure 8). At the initial stage, a thin transition layer forms at contact of molten surfaces due to conformational turns of macromolecule segments. If the temperature in the contact zone remains high enough for a certain time, the second stage comes, where not only segments, but whole macromolecules move through the fusion surface in the form of small supermolecular objects, under the impact of thermal motion. As a result, a much wider layer forms instead of a primary thin transition layer, where microvolumes of one polymer are immersed into the structure of the other one.

Similar processes, apparently, can take place also at formation of the welded joint between the contacting surfaces of the same polymers. While at joining different types of polymers, even with formation of a wide transition layer, a pronounced interface always remains, in polymers of one type this boundary disappears and is blurred during autohesion and diffusion. The welded joint strength is mainly influenced exactly by the properties of this transition structure in the fusion zone.

The general theory of diffusion in any environments, in particular, in polymers, treats this process as a totality of elementary acts of molecular particle movement. It is understandable that movement of any molecules or its fragment requires free space, into which it will be displaced. Therefore, the vacancy (hole) mechanism is believed to be the base of the diffusion process [18]. The elementary act of diffusion consists in formation of a microvoid (hole) near the molecule as a result of thermal motion, and their subsequent exchange of places. In high-molecular polymers the microvoids usually form owing to conformational turns of individual chain segments — so-called kinetic segments. Accordingly, assumptions are made that formation of a transition structure between the polymer parts in welding takes place mainly due to segmental interpenetration of macromolecules through the joint surface [19]. Here, the determinant role of temperature in the welding zone and working pressure is emphasized, which ensures the necessary viscous contact between the molten surfaces.

The conformational theory of polymer welded joints was formulated, proceeding from the results of investigations by Yu.S. Lipatov and PWI scientists [20]. The theory is based on the idea that the thermal movement of macromolecules occurs mainly due to conformational turns of molecular chains segments, not by translational movement of their ends. Therefore, polymer melting and solidification should be regarded as disordering and subsequent ordering by the conformational mechanism. Interpenetration of macromolecule fragments through the joint surface in polymer welding (interface "healing") also occurs due to molecular conformational turns. Macromolecule diffusion by translational movement of their ends through the joint surface practically does not influence the "healing"process, because of short welding time and small number of free ends of molecular chains, compared to the number of segmental atomic groups, capable of conformation.

An assumption was also made that the number of spherolitization nuclei on the fusion surface has a determinant influence of the final crystalline structure of the polymer. In keeping with this statement, a criterion of formation of a sound butt welded joint of polymers was formulated. In Figure 9, *a*, an optimal number of crystallite nuclei is present along the fusion line. It results in formation of a continuous complete spherulitic structure of strength equal to that of the base polymer material. Figure 9, *b* shows the case when the thermophysical conditions at butt joint formation promoted appearance of an excess number of spherulite nuclei. It results in formation of a large number of fine incomplete spherulites, and of the so-called transcrystalline

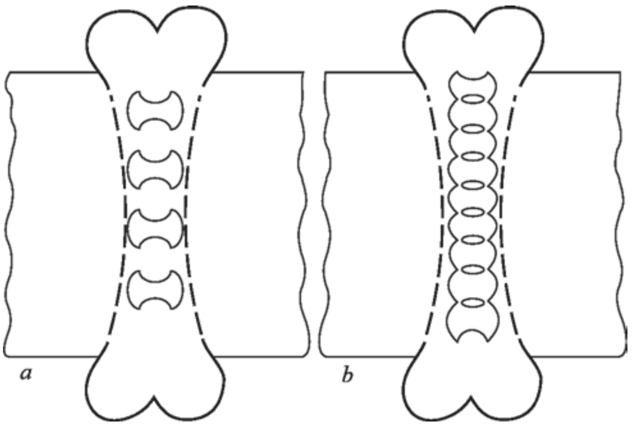

Figure 9. Formation of spherulitic structure along the polymer fusion line [20]

layer along the fusion line. Such a joint has lower strength and it fails along the weld line.

The recent studies performed at PWI, allowed complementing the conformational theory of polymer welded joint formation by new data [21, 22].

It is shown that the welded joint formation is influenced by two main factors — thermal energy T and force field P (external pressure and other factors) (Figure 10). Based on the results of comprehensive studies of the structure and properties of polymer welded joints it was assumed that in welding macromolecule orientation along the interface takes place in the thin melt layer with subsequent blurring of this surface due to rotational movements of macromolecule segments, i.e. change of their conformations in the transition layer volume [23]. The proposed concept does not deny the possibility of interdiffusion of polymer macromolecules, in particular due to reptation. It is believed, however, that statistically the conformational rotational movements of macromolecule segments occur much more frequently, compared to the diffusion ones, so that they have a decisive influence on blurring of the interface for the short-term joining process (Figure 11), which polymer welding is in most cases [2]. The base of the process of macromolecule fragment movement in the melt at thermal motion is exactly the vacancy (hole) mechanism. Presence of such vacancies in the polymer crystalline structure is envisaged by the closest to reality Hosemann paracrystalline model [24].

In keeping with this model, the polymer structure contains voids, amorphous regions, single-crystals, fragments of straightened chains and other formations. After melting or transition into a viscous state the voids remain on the molecular level, similar to some folded or disordered formations capable of conformational transformations. Figure 12 shows a model of gradual disappearance of the interface in polymer welding by vacancy-conformational principle. At the stage of wetting and contact of the molten surfaces ($t = 0$) the number of vacancies is the greatest exactly near the contact plane. After some time ($t > 0$), the vacancies on the interface are gradually filled owing to thermal motion of molecular segments (conformations), moving in-depth of the material. If the polymer material is in the molten state for some minimal time required, vacancy distribution in the melt will become almost uniform, and the interface will be "blurred" and will disappear. After solidification of the homogeneous melt layer a strong tight welded joint forms. We will call this minimum time T_g the homogenization time.

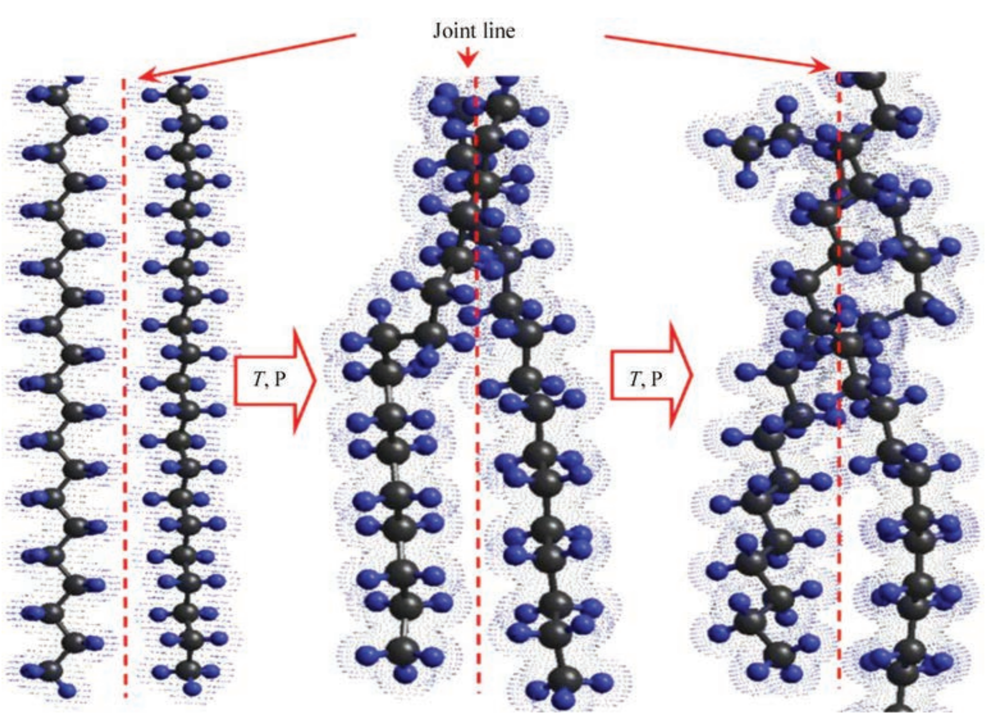

Figure 10. Process of segmental mobility with the change of macromolecule conformations under the impact of thermal and force fields in welding [23, 24]

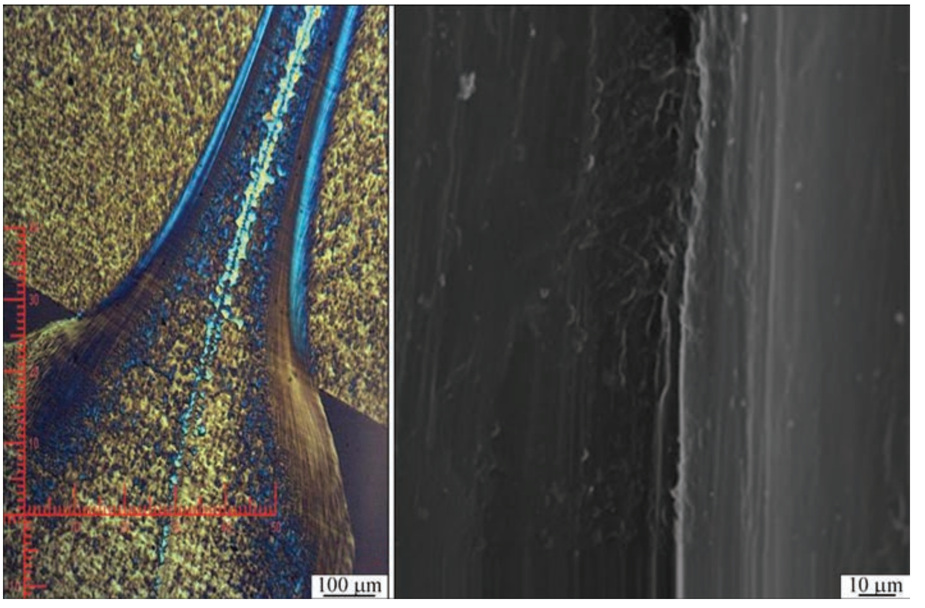

Figure 11. Optical and electron micrographs of polymer welds [25]

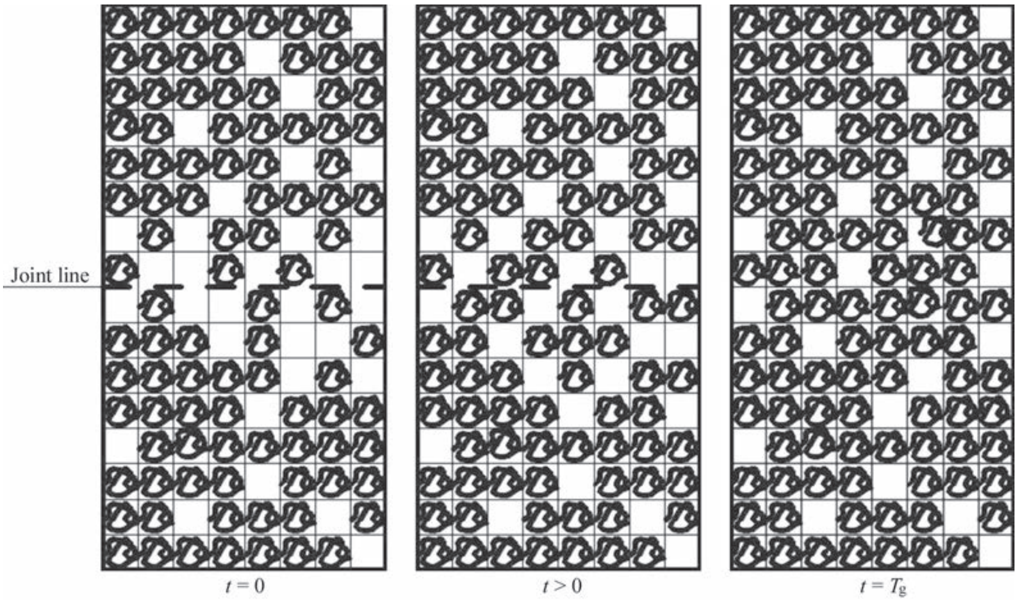

Figure 12. Model of transition layer homogenization on the interface in polymer welding by vacation-conformational principle

We believe that the terms “healing”, and “sealing” for the process of disappearance of the interface between the melts of contacting polymers of one type are insufficiently accurate. In reality, even though incomplete but still equalizing of volume-spatial properties of molecular structure of molten polymer takes place, macromolecule fragment distribution becomes more uniform and homogeneous. That is why, the process occurring in the thin layer of the transition zone should be regarded as equalizing of the melt properties. i.e. “homogenization”.

It was noted above that in order to produce a crystalline formation at polymer melt cooling, individual molecular chains should have the ability to move in the melt relative to their neighbours. Macromolecular chain movement can have two forms: conformational turns of individual parts of the molecule relative to its own chemical bonds, and translational movement of the chain relative to the common molecular tangle. Both the movements can be regarded as the phenomenon of self-diffusion, initiated by the thermal processes.

Note that the proposed model of the transition layer homogenization on the interface in polymer welding by the vacancy-conformational principle can be complemented by development of a mathematical model for determination of the appropriate modes of welding diverse polymer materials.

CONCLUSIONS

1. It was determined that the process of welding plastics is the gradual disappearance at the molecular level of the gap between the parts being joined and the formation of a transition layer (welded seam) between them, the

structure of which is strong, but significantly different from the structure of the main polymer material.

2. Nowadays there are several theories as to the nature and mechanisms of the process of plastics welding. Each of them has indirect experimental substantiation, but is not of a general nature. Therefore, at present continuation of investigations of the structure and properties of plastics welded joints is timely, in order to obtain fundamental data for complementing the theoretical fundamentals of polymer material welding.

3. A question which remains to be debatable is the possibility and mechanism of diffusion of molecular chain fragments, which is a decisive point for understanding the process of polymer welding. It is obvious that “homogenization”, i.e. equalizing of properties, will be a more accurate definition for the process of “blurring” of the interface in polymer welding, instead of the common definition of “healing”.

4. The currently available models of polymer welded joint formation are based on different physical phenomena — mutual adhesion of the substrates, macromolecule diffusion and melt rheology. We believe that the most realistic is the theory of polymer welded joint formation due to conformational transformations of macromolecule fragments. In development of the conformational theory, being elaborated by PWI Scientific School, a model was proposed of homogenization of the transition layer on the interface in polymer welding by the vacancy-conformational principle.

REFERENCES

1. Nikolaev, G.A. (1978) *Welding in machine-building*: Handbook in 4 Vol. Moscow, Mashinostroenie [in Russian].
2. Paton, B.E. (2018) *Dictionary and reference book on welding and gluing of plastics*. Kyiv, Naukova Dumka [in Ukrainian].
3. Komarov, G.V. (2006) Connections of parts from polymer materials. Moscow, Professiya [in Russian].
4. ISO 472:2013: *Plastics — Vocabulary*. Geneva.
5. Grishin, N.A., Voyutskii, S.S., Gudimov, M.M. (1957) On mechanism of welding of organic glasses. *Doklady AN SSSR*, 116(**4**), 629–632 [in Russian].
6. Voyutsii, S.S. (1960) *Autohesion and adhesion of high polymers*. Moscow, Rostekhizdat [in Russian].
7. Grishin, N.A., (1963) Weldability of thermoplasts. *Vysokomolekulyarnye Soyedineniya*, **3**, 33–35.
8. Wool, R.P., O’Connor, K.M. (1981) A theory of crack healing in polymers. *J. of Applied Physics*, 52(**10**), 5953–5963.
9. Lipatov, Yu.S., Privalko, V.P. (1976) On possibility of folding of marcomolecules in amorphous polymers. *Vysokomolekulyarnye Soiedineniya*, 18, A(**5**), 991–996 [in Russian].
10. Yeh, G.S.Y. (1972) A structural model for the amorphous state of polymers. Folded-chain fringed micellar grain model. *J. of Macromolecular Sci.*, 6, 2(**3**), 465–468.
11. Wool, R.P. (1995) *Polymer Interfaces: Structure and Strength*. Hanser Publishers.
12. Volynsky, A.L., Bakeev, N.F. (2009) Healing of interphase surface in polymer systems. *Vysokomolekulyarnye Soiedineniya, Series* A, 51(**10**), 1783–1816 [in Russian].
13. Grevell, D. (2007) Welding of plastics: Fundamentals and new developments. *Int. Polymer Processing*, **XXII**, 43–46.
14. Gennes de P. (1982) Ideas of scaling in polymer world. Moscow, Mir [in Russian].
15. Gubenko, S.I., Zhuravlev, S.I., Konovalov, N.A. (2014) On physical nature of appearance of “dead spot” type defects in resistance welding of main pipelines from ferritic-pearlitic steels. *Metallofizika i Novejshie Tekhnologii*, 36(**5**), 661–688 [in Russian].
16. Zajtsev, K.I. (1973) Mechanism of joint formation in flash butt welding. *Avtomatich. Svarka*, **9**, 29–30 [in Russian].
17. Lipatov, Yu.S. (1977) *Physical chemistry of filled polymers*. Moscow, Khimiya [in Russian].
18. Chalykh, A.E. (2015) *Diffusion in polymer systems*. Moscow, Khimiya [in Russian].
19. Komarov, G.V. (2015) Composition and properties of polymer materials affecting their weldability. *Polimernye Materialy*, **9**, 44–48 [in Russian].
20. Grinyuk, V.D., Shadrin, A.A., Korab, G.N. (1992) Molecular mechanism of formation of thermoplastic material welded joints. *Avtomatich. Svarka*, **7–8,** 33–36 [in Russian].
21. Galchun, A., Korab, N., Kondratenko, V. et al. (2015) Nanostructurization and thermal properties of polyethylenes’ welds. *Nanoscale Research Letters*, **10**, 138–144. DOI: https://doi.org/10.1186/s11671-015-0832-4
22. Demchenko, V., Iurzhenko, M., Shadrin, A. et al. (2017) Relaxation behavior of polyethylene welded joints. *Nanoscale Research Letters*, **12**, 280–285. DOI: https://doi.org/10.1186/s11671-017-2059-z
23. Iurzhenko, M. (2018) Novel theory of plastics welding and its application. In: *Proc. of 10th Int. Conf. Advanced Materials and Technologies: From Idea to Market (Ningbo, China, 24–26 October 2018*).
24. Hosemann, R. (1882) Dependence of the change in the free enthalpy on the lattice number with the formation of microparacrystals. *Colloid and Polymer Sci.*, **9**, 864–870.

ORCID

M.G. Korab: 0000-0001-8030-1468,
M.V. Iurzhenko: 0000-0002-5535-731X,
V.L. Demchenko: 0000-0001-9146-8984,
Ye.P. Mamunya: 0000-0003-3855-2786

CONFLICT OF INTEREST

The Authors declare no conflict of interest

CORRESPONDING AUTHOR

M.V. Iurzhenko
E.O. Paton Electric Welding Institute of the NASU
11 Kazymyr Malevych Str., 03150, Kyiv, Ukraine.
E-mail: 4chewip@gmail.com

SUGGESTED CITATION

M.G. Korab, M.V. Iurzhenko, V.L. Demchenko, Ye.P. Mamunya (2022) Modern models of formation of welded joints of polymer materials (Review). *The Paton Welding J.*, **1**, 39–46.

JOURNAL HOME PAGE

https://patonpublishinghouse.com/eng/journals/tpwj

Received: 02.01.2023
Accepted: 28.02.2023

DOI: https://doi.org/10.37434/tpwj2022.01.07

CONSUMABLE ELECTRODE WELDING OF D16 ALUMINIUM ALLOY WITH WELD METAL MICROALLOYING

T.M. Labur, V.A. Koval, M.R. Yavorska

E.O. Paton Electric Welding Institute of the NASU
11 Kazymyr Malevych Str., 03150, Kyiv, Ukraine

ABSTRACT

The paper gives the results of investigation of the influence of application of two isolated filler wires or embedded elements of different chemical composition on the features of formation of D16 aluminium alloy welds in consumable electrode welding. Wires of Zv1201, ZvAK5, ZvAK12 grades of 1.6 mm diameter and embedded elements cut out of V92, V96 and 7056 alloy blanks with different content of zinc were evaluated. It is shown that ZvAK5 wire ensures reduction of the length of solidification cracks and number of pores in welded joints, and welded joint strength becomes higher at addition of zinc into the weld.

KEYWORDS: aluminium alloy, arc welding, consumable electrode, welded joints, filler wires, structure, solidification cracks, mechanical properties, investigations

INTRODUCTION

At nonconsumable electrode welding of D16 alloy of Al–Cu alloying system solidification cracks are observed along the weld axis and in the zone of fusion with the base metal. The joint quality deteriorates. The causes for such a phenomenon are the dimensions of brittleness temperature range and low ductility of metal in this region, particularly, when the alloy is in T1 condition, i.e. after artificial aging [1–8]. At the same time, wide industrial application of this alloy in flying vehicle structures necessitates a more thorough study of the technological capabilities of consumable electrode welding of this alloy.

Note that the presence of some elements (iron, copper, silicon, etc.) causes a nonuniform distribution in the aluminium alloy structure, which is often found in their semifinished products, and at welding it leads to formation of low-melting eutectics in the intergranular and intercrystalline space, expands the solidification range, and this way causes higher sensitivity of the alloy to the thermal cycle of welding. Weld metal proneness to solidification crack formation becomes greater. Crack dimensions depend on thermophysical conditions of consumable or nonconsumable electrode welding, which determine the nature of primary phase precipitate distribution.

It is known [4, 9, 10] that the process of weld metal solidification is of an intermittent nature, related to an abrupt change of the solidification rate and temperature gradient. Increase of process dynamics leads to initiation of sites of transition from one kind of solidification to another one not only in the weld center, but also in the fusion zone. The main precipitation phases at process heating of the alloy are $CuAl_2$ (θ)-phase and Al_2CuMg (S)-phase. In the case of the ratio of Cu/Mg alloying elements ≤ 2.6 formation of S-phase is observed in the structure, which is necessary for D16 alloy hardening by phase formation. At the ratio of Mg/Si = 1.73 also Mg_2Si phase precipitates. Such transitions usually arise in welding alloys with relatively high content of alloying elements and admixtures. The latter, in their turn, influence the shape and dispersity of eutectic precipitates in the weld structure [1–7]. The shape and dispersity of the precipitates are due to metal pool solidification rate. In case of its increase, the process of admixtures diffusion on the interphase becomes shorter, narrowing the wall of crystallite cells. Eutectic phase precipitation occurs predominantly on the intercrystalline boundary, particularly at a low welding speed. At the specified welding mode the solidification rate varies in a wide range relative to the weld width. The nature of phase precipitates changes considerably at crystallite growth. In this case, eutectic precipitates with thinner walls of intercrystallite layers are observed in the weld center, where the solidification rate is higher, and the cell width is smaller than that at the fusion line.

The weld metal solidification process is influenced by the pattern of distribution of primary phase precipitates in the base metal and thermophysical conditions of consumable electrode welding [4–13]. The dynamic nature of the solidification process at weld pool cooling leads to formation of centers of transition from one kind of solidification to another one. Such transitions take place at welding alloys with a relatively high content of alloying elements and admixtures that affects the shape and dispersity of phase precipitates in the weld structure.

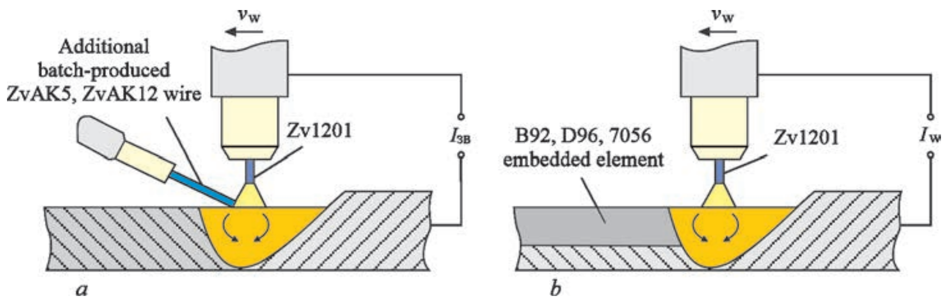

Figure 1. Technology variants of welding D16 alloy with two filler wires (*a*) and embedded elements (*b*) for weld metal alloying and improvement of the mechanical properties

OBJECTIVE OF THE STUDY AND EXPERIMENTAL PROCEDURE

One of the possible ways of improvement of structural homogeneity of welds on 6 mm D16 aluminium alloy (Table 1) can be simultaneous application of two isolated filler wires or embedded elements of different chemical composition in the weld pool. Here, conditions are in place for physicochemical interaction of alloying elements and admixtures of base metal and filler wires, which promotes formation of eutectics of a balanced composition and improves the homogeneity of the weld structure. Therefore, the objective of this work is revealing the structural features of welds produced using two filler wires or embedded elements (Figure 1). One wire of Zv1201 grade, the chemical composition of which is close to that of D16 alloy, will be fed directly into the arc burning zone, and the other — into the weld pool head part, which corresponds to the technology of nonconsumable electrode welding.

Transfer of liquid metal drops to the common pool will form the required weld volume, and feeding additional filler wire will allow modifying its structure. The effectiveness of such a technological solution was evaluated by comparison with the structure produced by the traditional method. The influence of several variants of batch-produced filler materials was studied to determine the components of rational modification of the weld structure and to produce the necessary ratio of alloying elements, and the most effective, substantiated by the investigation methodology, parameters of strength and ductility of the welded joints were selected, which ensure the welded structure reliability.

Variants of the studied materials from alloys of different alloying systems were selected, namely: batch-produced ZvAK5, AVAK12 wires of Al–Si alloying system, which retain silicon, as well as embedded elements from V92, V96 and 7056 alloys, which retain zinc. Availability of low-melting silicon in the additional wire composition will allow a certain increase of the nonequilibrium solidus temperature and a reduction of the range of the metal solid-liquid state. Zinc presence will promote an increase in the level of weld strength in the joints.

During studies the following technological variants were used: Zv1201 + ZvAK5; Zv1201-AvAK12; Zv1201 + V92; Zv1201 + V96; Zv1201-7056. The results were compared with joints produced using one batch-produced alloy of Al–Cu alloying system of Zv1201 grade. Proceeding from analysis of the features of the structure and mechanical properties of specimens cut out in different regions of welds, it is intended to determine an optimal combination of the compositions of filler wires, used for welding. Their application will allow producing permanent joints of D16 alloy in keeping with the requirements and structure purpose.

In order to implement the process, the technological equipment for simultaneous mechanical feeding of two wires into a common pool and the conditions of wire feed synchronization were improved, and the modes of the process of joining D16 alloy were retrofitted. Analysis of chemical composition of the wires and embedded elements was conducted by the spectral method, using Sprectrovak-1000 equipment of Baird Company (Table 2).

Before welding the blanks were treated by 10 % NaOH solution and clarified in 13 % HNO_3 solution. Blanks were welded by a consumable electrode in the horizontal position, using studied consumables. The wires were fed into the pool in keeping with the standard requirements, i.e. directly from the face surface.

To diversify the technology variants, embedded elements of 2×2×2.5 mm size were used, which were placed in the lower section of the butt, as zinc-containing wires do not exist. V92, V96 and 7056 alloys with different zinc content were selected. Chemical elements (zinc, magnesium, copper, manganese, zir-

Table 1. Chemical composition (wt.%) and mechanical properties of 6 mm D16 alloy

Mg	Cu	Mn	Si	Fe	Zn	*E*, GPa	σ_t	$\sigma_{0.2}$	$\sigma_{0,01}$	δ_5, %
							MPa			
1.4–1.7	4.0–4.5	0.34–0.53	0.16–0.19	0.21–0.22	0.07–0.11	67–71	217–221	106–115	79–89	16–18

Table 2. Chemical composition of studied filler materials, wt.%

Filler material grade	Si	Fe	Cu	Mn	Mg	Zr	Ti	Zn
Zv1201(Al–Cu)	0.16	0.14	3.8	0.42	0.7	0.08	0.02–0.1	–
ZvAK5 (Al–Cu)	0.70	0.15	3.8	0.42	0.63	0.08	0.15	–
ZvAK12 (Al–Cu)	1.8	0.23	3.0	0.37	0.60	0.07	0.15	–
Embedded element from V92 alloy (Al–Cu–Mg)	0.17	0.35	2.80	0.31	1.0	–	0.01	0.50
V96 (Al–Zn–Cu–Mg)	0.15	0.14	2.90	0.32	1.0	–	0.04	2.6
7056 (Al–Zn–Cu–Mg)	0.13	0.10	2.80	0.31	0.76	–	0.06	2.4

conium) present in these alloys, ensure the physico-chemical conditions for formation of fine-grained structure of weld metal in welding, and a significant effect of their hardening under the conditions of their further heat treatment [4–9].

The welding heat input was selected from the condition of minimal value of electric current, required for complete penetration of the alloy. That is why, this process was performed in the following mode: $I_w =$ $= 240–250$ A, $U_a = 20–21$ V; $v_w = 31–33$ m/h. The weld width from the face and penetration side was almost the same, being in the range of 9–11 mm. The process was conducted with application of the forming backing, as it is known that in case of its presence the process of crystallization and growth of columnar crystallites is two-dimensional, influencing the weld quality. Modulation of the main mode parameters with cycle time of 2.2 ± 0.2 s created certain thermophysical conditions for improved control of the process of drop transfer from the main wire, producing the appropriate shape of the weld pool and weld structure formation. All together, it ensured a greater amount of oversaturated solid solution, higher density of precipitation of the dispersed hardening phase particles during the next stage (solid solution decomposition), and improvement of the joint mechanical properties [5–7].

The quality of weld formation in butt joints of D16 alloy was assessed visually and by X-ray technique (GOST 7512 [13]) in RAP-150/300 X-ray unit. Weld metal density was controlled in Densitometer DP-30 instrument.

Specimens for mechanical tests were cut out of the welded butt joints in keeping with the normative documents. Mechanical tests were conducted to GOST 1497 [14] and GOST 6996–66 [15] in Instron-1126 machine with 6 mm/min traverse travel speed. During testing, a personal computer was used for continuous recording of the loading and deformation values. These results were used for calculation of the respective parameters of ultimate rupture strength (ultimate strength of welded joints ($\sigma_t^{w.j}$) and weld metal ($\sigma_t^{w.m}$).

Metallogrpahic analysis of base metal and welded joints was performed in MMT-1600V microscope. Investigations were conducted on microsections cut out across the sheet rolling direction. The microstructure was revealed by electrolytic polishing in a solution of the following composition: chloric acid — 1000 cm^3 + ice acetic acid — 75 cm^3.

RESULTS AND THEIR DISCUSSION

Analysis of the obtained results was the base to determine the effectiveness of the studied filler wires for welding D16 alloy, their influence on weld formation mechanism, weld form factor, level of mechanical properties and features of welded joint structure, depending on chemical composition.

Metallographic studies of welded joint microstructure revealed the presence of a considerable amount of precipitates of oversaturated phases, retaining copper. Their decomposition occurs under the impact of the thermal cycle, which is accompanied by formation and coagulation of hardening phases, as well as their dissolution in aluminium solid solution.

Welds are tight, no coarse porosity is observed in the weld metal or fusion zone (Figures 2–4), but presence of low-melting eutectics in the intergranular or intercrystalline space is reported, which may be indicative of the heterogeneity of iron, copper and silicon distribution in the structure. Eutectic formation temperature, their composition and amount are the decisive factors at selection of the heating temperature for hardening and hot deformation [1–4]. They are also the main factors, which determine the behaviour of these alloys in fusion welding [1, 3, 11, 12]. According to the data of microstructural analysis, the eutectic phase precipitates are recorded predominantly on the intercrystalline boundary. As the solidification rate changes in wide ranges relative to weld width at the specified welding mode, a significant change of the nature of phase precipitates with crystallite growth is observed. Eutectic precipitates in the weld center, where the solidification rate is higher, have thinner walls of intercrystalline layers, and the cell width is smaller than near the fusion boundary. Partial melting is observed near the zone of fusion with the base metal, increase of the amount of low-melting eutectics is reported, which is a feature of duralumin class.

Comparative analysis of the structure of D16 alloy welds produced by both the technology variants, shows that a change of liquid eutectic phase distribu-

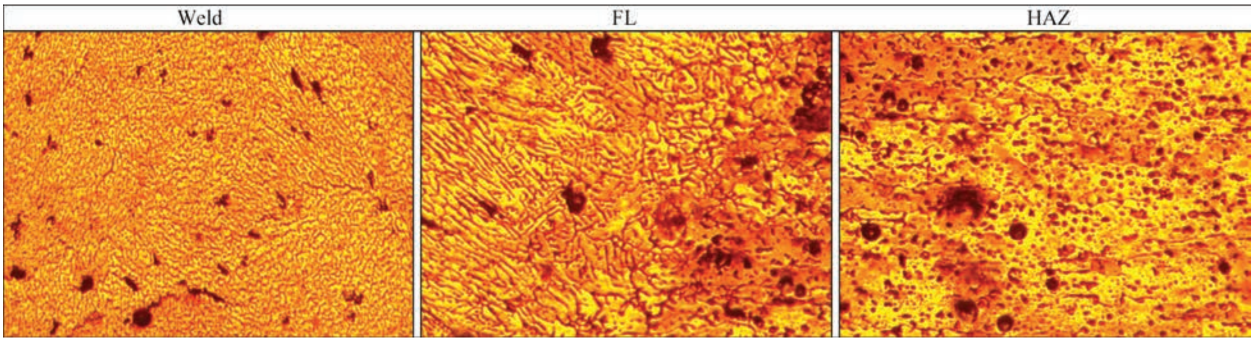

Figure 2. Microstructure of D16 alloy welded joints made with batch-produced Zv1201 wire in consumable electrode welding (×320)

tion takes place in the studied welds (Figures 2–4). It may be due to a change in the temperature intervals of their solidification due to additional modifying of weld structure. The length of solidification cracks and number of pores in welded joints decreases. Silicon addition in the amount of 5 % enabled avoiding cracking both in welds and along the fusion line, due to a balanced amount of low-melting eutectic (Figure 3). This is, probably, due to silicon promoting a higher mobility of the liquid eutectic and lowering of the temperature of primary dendrite formation in the welds [4–9, 12]. Application of ZvAK12 wire with a greater amount of silicon (12 %) does not provide the appropriate conditions for producing a permanent joint that may be due to an intensive enrichment of liquid intergranular interlayers in silicon during welding of the alloy. It results in widening of eutectic interlayers in this weld region.

Analysis of the features of welded joint structure showed that zinc addition into the weld metal, having the melting temperature of 419 °C, also influenced the ability to form a sound joint. Such chemical elements as zinc, magnesium, copper, manganese, zirconium, present in the composition of embedded elements, have different effect on the structure (Figure 4). The eutectic phase volume is also increased, limiting D16 alloy susceptibility to solidification cracking both in the weld, and in the fusion zone. Owing to an increase of the amount of low-melting eutectic and its balanced composition, conditions are provided for healing the solidification cracks and pores (Table 3). When V92 and V96 alloys are used, which have 0.50 and 2.4 % zinc, respectively, increase of its amount in the fusion zone leads to enrichment of the eutectic in the HAZ subzone where partial melting occurs during welding. It widens the eutectic interlayer between the grains. A similar effect is also observed at 2.6 % zinc (in technology variant of Zv1201 + 7056). A fine-grained structure forms in all the welds (Figure 4). Although the quantity of copper varies in the range from 4.8 to

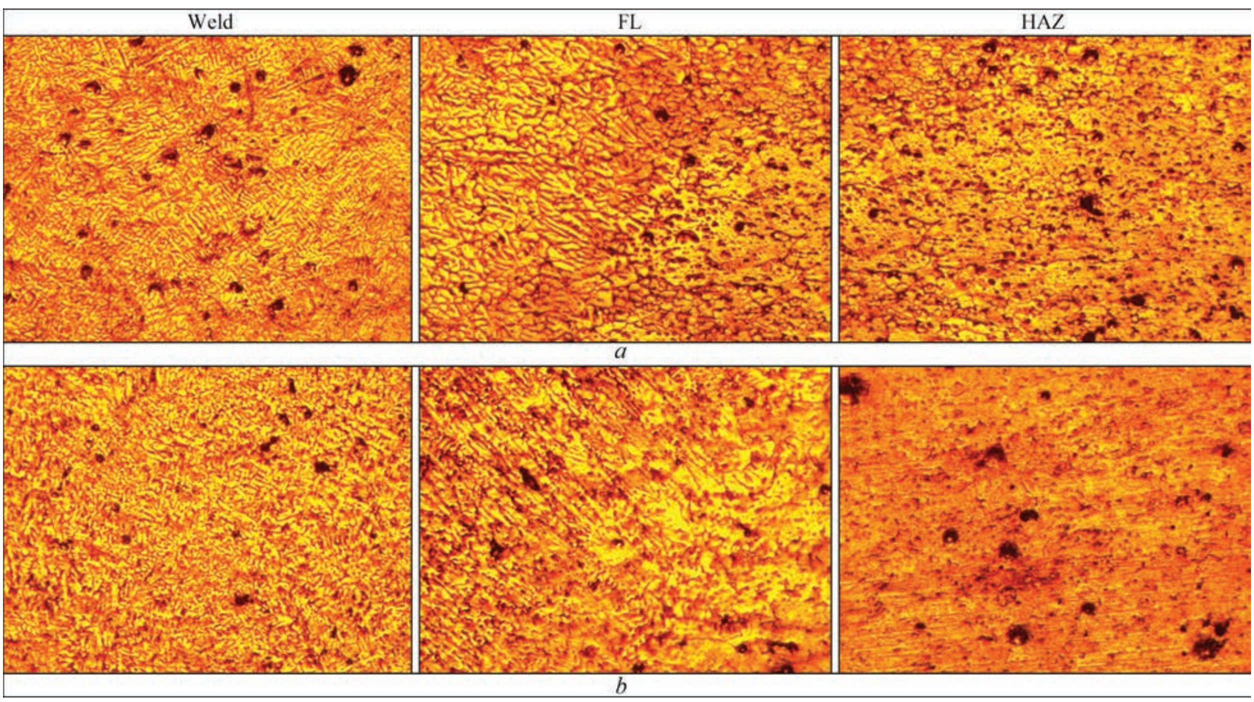

Figure 3. Microstructure of D16 alloy welded joints made by batch-produced wire Zv1201 + ZvAK5 (*a*) and Zv1201 + ZvAK12 (*b*) in consumable electrode welding (×320)

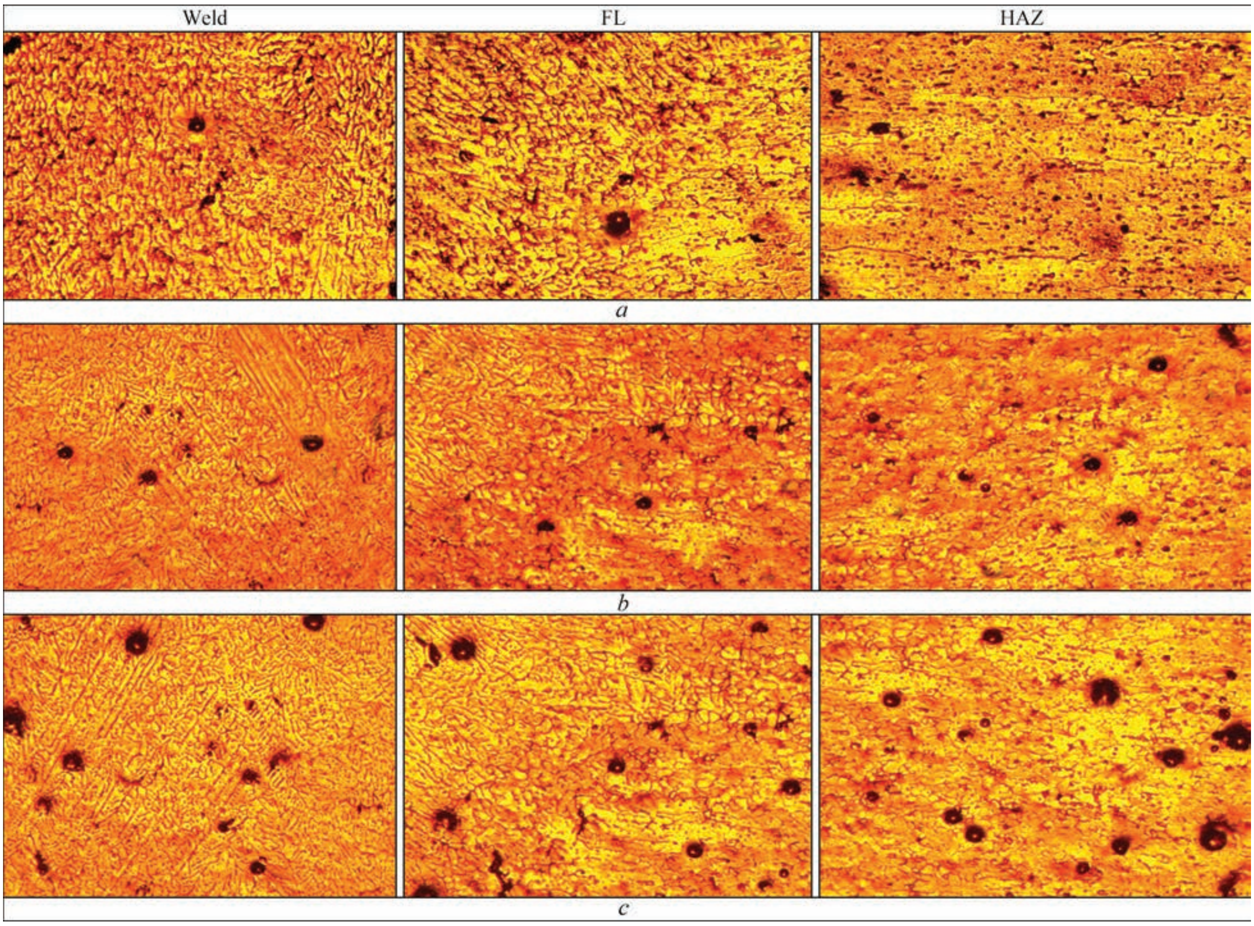

Figure 4. Microstructure of D16 alloy welded joints made with batch-produced Zv1201 wire and embedded element from B92 (*a*), B96 (*b*) and 7056 (*c*) alloys in consumable electrode welding (×320)

6.2 %, that of silicon from 0.27 to 2.2 %, and that of zinc from 0.99 to 3.2 %, their combination ensures a significant effect of weld structure hardening under the condition of further heat treatment of welded joints (Table 4) that coincides with the results obtained in works [7 – 10]. Comparative evaluation showed that the welded joint strength is equal to 186–188 MPa at application of batch-produced ZvAK5 and ZvAK12 wires with silicon. Weld metal strength here varies in the range of 180–187 MPa (Table 4). Note that Table 4 gives the average values of welded joint strength and ductility after mechanical tests of three specimens. Ductility value (bend angle) is equal to 44° for specimens made by the technological scheme of Zv1201 + SvAK5, and 27° with Zv1201 + ZvAK12 that may be due to formation of wider eutectic interlayers with low cohesion strength between the weld crystallites.

An essential increase of welded joint strength is observed, when embedded elements from V92, V96 and 7056 alloys, which retain zinc, are used as additional materials. The greatest increase of strength (up to 200.0 MPa) of both D16 alloy welded joints and weld metal (up to 194.0 MPa) is in place at application of V96 alloy, provided the ductility characteristic (bend angle) remains on the level of 23°. This is promoted by presence of zinc, which forms such complex intermetallic phase compounds as $Mg(Zn_2AlCu)$ ad $Mg_3Al_2Zn_3$ during weld metal solidification. The strength value limit depends on chemical composition of embedded element material.

Table 3. Content of the main chemical elements in the weld metal in D16 alloy consumable electrode welding with two isolated filler materials into a common pool, wt.%

Technology variants	Fe	Zn	Mn	Si	Mg	Cu	Zr
Zv1201	0.31	–	0.48	0.27	0.93	6.01	0.08
ZvAK5	0.26	–	0.34	1.02	0.73	4.95	0.08
ZvAK12	0.32	–	0.37	2.2	0.79	5.29	0.07
Embedded element from V92 alloy	0.65	0.99	0.51	0.21	1.12	5.18	–
V96	0.2	2.25	0.36	0.21	1.16	4.9	–
7056	0.27	3.2	0.3	0.46	1.51	4.81	–

Table 4. Influence of technology variants on mechanical properties of D16 alloy welded joints, depending on chemical composition of embedded elements* and filler wires**

Technology variants	$\sigma_t^{w.j}$, MPa	$\sigma_t^{w.m}$, MPa	α, deg
Zv1201 (Al–6.3 % Cu–0.3 % Mn) – base	193.0	186.0	40
Zv1201 + ZvAK5 (Al–5.5 % Si)	188.0	187.0	44
Zv1201 + ZvAK12 (Al–12 % Si)	186.0	180.0	27
Zv1201 + B92 alloy (Al–0.5 % Cu–4.2 % Mg–3.5 % Zn)	190.0	191.0	27
Zv1201 + B96 alloy (Al–2.3 % Cu–2.6 % Mg–8.5 % Zn)	200.0	194.0	36
Zv1201 + 7056 alloy (Al–1.65 % Cu–1.8 % Mg–9.5 % Zn)	190.0	194.0	31

*Fracture occurs through base metal in the HAZ.
**Fracture occurs along weld axis and fusion boundary of D16 alloy.

The nature of strength change in different regions of welded joints was studied by measuring the hardness value in these zones, namely: in the weld, fusion zone and HAZ (Table 5). This is due to the known correlation of metal strength and hardness in welding aluminium alloys [2–4, 9]. As shown by their analysis in as-welded butt joints, i.e. without heat treatment, use of batch-produced wires ZvAK5 and ZvAK12 containing 5 and 12 % silicon, respectively, has almost no influence on hardness level in different zones of the joints.

When welding with application of embedded elements from V92, V96 and 7056 alloys as additional materials, metal hardness in different zones of the joint rises by 2–5 units, compared to joints made with batch-produced ZvAK5 and ZvAK12 wires, containing silicon. The greatest difference is found in the weld metal. Hardness value is determined by the amount of zinc in the respective additional materials.

In the fusion zone the difference in the hardness values is equal to 1–2 units, and in the HAZ these values are almost the same (Table 5). Similar to the previous case, a 3–5 % increase in the hardness level is observed after artificial aging, in keeping with the amount of zinc in the additional material. Hardness increases even more after performance of the operations of full heat treatment of welded joints. Analysis of hardness measurement results shows that such a treatment mode is the most suitable for producing high values of mechanical properties, namely appropriate level of strength alongside sufficient ductility, which will ensure the welded structure performance. This is also indicated by the microstructure of specimens of welded joints made with two batch-produced silicon-containing wires and embedded elements from metals alloyed by zinc (Figures 2–4).

Table 5. Influence of chemical composition of silicon-containing filler wires and embedded elements from zinc-containing alloys on hardness of D16 alloy welded joints (65–67 *HB*) made by consumable electrode, MPa

Technology variants	Weld	FZ	HAZ
Zv1201	88–89	60–89	59–65
Zv1201 + ZvAK5	89–90	62–87	60–65
Zv1201 + ZvAK12	88–90	62–87	59–65
Zv1201 + (7056)	90–91	61–87	59–65
Zv1201 + (V96)	89–90	61–85	59–65
Zv1201 + (V2)	89–90	62–88	60–65

Notes. 1. Brinell hardness *HB* of welded joints was measured in Rockwell instrument at load P = 600 N by 1/16″ sphere. 2. The grade of the alloy used as embedded element is shown in brackets.

Relief of welded joint fracture surface after mechanical tests can be conditionally divided into characteristic structural zones: initial, where the microcrack initiates, region of its stable growth and region of its accelerated growth up to the main crack formation, the appearance of which leads to complete destruction of the specimens. Microrelief of each of the mentioned regions changed under the influence of the above technology factors. Realisation of this process is due to a considerable intensity of metal plastic deformation, when the stress level exceeds the value of the forces of cohesion of the matrix and the inclusion in the direction, normal to their boundary [9, 12]. Microcracks initiate on coarse phase particles and intermetallics located along the crystallite boundaries. The crack length is determined by its volume fraction in the base metal. Partially-melted grains of the base metal located near the zone of its fusion with the weld, point to a slight overheating of the metal in welding. Here, development of heterogeneity as to the dimensions of excess phases and clusters of intermetallic compounds is noted. The above-said is due to the respective amount of alloying elements and admixtures as a result of their segregation along the weld crystallite boundaries and base metal grains, as well as formation of individual regions of intergranular interlayers from oversaturated phases.

Weakly-developed deformation bands are visible on the fracture of a flat-ridge region. Cells of predominantly medium size (6–8 μm) are limited by tear ridges and retain broken inclusions of intermetallic phases on their bottom. Formation of such local centers of destruction in the form of cells can be associated with relaxation of compact high-density dislocation clusters and microvoid formation during plastic deformation. Fracture surface relief near the main crack mouth

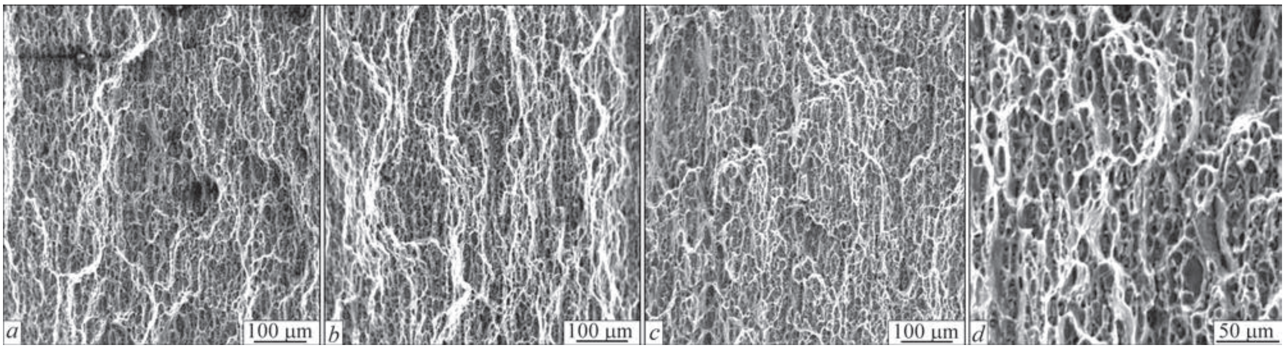

Figure 5. Panorama of fracture surface along the weld axis from technological convexity (*a*), medium regions (*b*, *c*) to the root (*d*) of a D16 alloy joint produced by consumable electrode welding, after mechanical testing (×500)

also contains microtears, arising along the crystallite boundaries during deceleration of crack propagation (see Figure 5). Centers of crack initiation are inclusions which do not dissolve at heating in welding and form intermetallic conglomerates. Considerable localization of stresses, particularly in the grain joining areas, leads to their destruction. Tough cells on the relief retain quasicleavage elements that may be indicative of ductile shear concentration in individual most stressed regions of D16 alloy structure. The size of facets on the fracture surface varies from 2 to 5 μm. Their small dimensions are determined by the rate of solid solution decomposition under the welding conditions, when phase transformations do not have enough time to develop.

CONCLUSIONS

1. Preliminary studies of consumable electrode welding of 6 mm D16 aluminium alloy were performed using two 1.6 mm filler wires of Zv1201, ZvAK5, ZvAK12 grade, as well as embedded elements from V92, V96 and 7056 alloys,. Wires were fed into the weld pool directly from its face surface. Optimal parameters of welding mode were determined as follows: I_w = 240–250 A; U_a = 20–21 V; v_w = 31–33 m/h. Weld width from the welding face and penetration side was almost the same in all the welds. Presence of silicon and zinc in the fillers promotes formation of a considerable amount of low-melting component in the structure that lowers the risks of appearance of solidification cracks and pores in the welds.

2. Structural analysis of D16 alloy welds produced by different fillers showed that a sufficient amount of the low-melting component forms at application of ZvAK5 wire (5 % Si) and it allows avoiding defects in welds. In case of application of ZvAK12 wire (12 % Si) no sound formation of the weld is observed that is due to greater width of intergranular eutectic interlayers due to enrichment in silicon. A similar phenomenon also takes place at application of embedded elements from V92, V96 alloys (0.50 and 2.4 %, respectively) and 7056 (Zn = 2.6 %). The amount of zinc influences the interlayer width.

3. A dependence of mechanical properties of D16 alloy joints on chemical composition of the wires and embedded elements was established. At application of ZvAK5 and ZvAK12 wires the joint strength is equal to 186 to 188 MPa, and that of weld metal — 180–187 MPa. Ductility value (bend angle) is equal to 44 and 27°, respectively, which may be associated with low cohesion strength of the eutectic interlayers. The joint fails in the HAZ, near the weld, where a brittle intermetallic network is observed along the grain boundaries, because of coagulation of the strengthening phases. More over, metal overheating takes place with partial melting of the individual components, as well as a series of structural transformations, namely low-temperature recovery, annealing, recrystallization, partial hardening. Zinc presence in the embedded elements increases the joint strength level to 190–200 MPa and of weld metal in the range of 191–194 MPa, compared to silicon-retaining wires.

4. Joints fail through coarse phase particles and intermetallics located along the boundaries of weld crystallites in the zone of fusion with the base metal. The above phenomenon is determined by volume fraction in the base metal and the effect of modifying by fillers, which is due to the presence of the respective amount of alloying elements and admixtures, their segregation, formation of individual regions of intergranular interlayers from oversaturated phases in the structure and inhomogeneity of excess phases and intermetallic clusters. Partially-melted base metal grains, located near the zone of D16 alloy fusion with the weld, point to a slight metal overheating in consumable electrode welding.

REFERENCES

1. (1998) *Welding in aircraft construction*. Ed. by B.E. Paton. Kyiv, MIIVTs [in Russian].
2. Beletsky, V.M., Krivov, G.A. (2005) *Aluminium alloys (composition, properties, technology, application)*: Handbook. Ed. by I.N. Fridlyander. Kyiv, Komintekh [in Russian].

3. Ishchenko, A.Ya., Labur, T.M. (2013) *Welding of modern structures of aluminium alloys*. Kyiv, Naukova Dumka [in Russian].
4. Ishchenko, A.Ya. (2003) *Aluminium high-strength alloys for welded structures. Progresyvni Materialy i Tekhnologii*. Vol. 1.Kyiv, Akademperiodyka, 50–82 [in Russian].
5. Lebedev, V.A. (2007) Some peculiarities of mechanized arc welding of aluminium with controlled pulse feed of electrode wire. *Svarochn. Proizvodstvo*, **11**, 26–30 [in Russian].
6. Wenez, A. (2005) Hundertfuntzig Jahre Aluminium. *Der Praktiker*, **5**, 74–75.
7. Kononenko, V.Ya. (2010) *Welding of aluminium alloys*: Handbook. Kyiv, Ekotekhnologiya [in Russian].
8. Ishchenko, A.Ya., Lozovskaya, A.V. (2001) Improvement of weldability of aluminium alloys by optimization of amount of additives. In: *Proc. of 5th Session of Sci. Council on New Materials of Int. Ass. of Sci. Acad. (12 May, 2000, Kyiv)*. Gomel, NANB, 72–77.
9. Teh, N.J. (2006) Small joints make a big difference. *TWI Connect*, 143(**4**), 1–7.
10. Norlin, A. (2000) A century of aluminium — a product of the future. *Svetsaren*, **2**, 31–33.
11. Labur, T.M. (2021) Tendencies of technological development of arc welding processes for joining of modern aluminium alloys. *Zvarnyk*, **6**, 6–17 [in Ukrainian].
12. Golovatyuk, Yu.V., Poklyatskyi, A.G., Labur, T.M., Ostash, O.P. (2018) Increase in structural strength of welded joints of Al–Cu–Mg system alloy. *Fiz.-Chim. Mekhanika Materialiv*, 54(**3**), 112–119 [in Ukrainian].
13. GOST 7512–82: *Nondestructive testing. Welded joints. Radiography method* [in Russian].
14. GOST 1497–84 (ISO 6892–84, CT CMEA 471–88): *Metals. Tensile test methods*.
15. GOST 6996–66: *Welded joints. Methods of mechanical tests*. Introd. 01.1967. Moscow, Izd-vo Standartov [in Russian].

ORCID

T.M. Labur: 0000-0002-4064-2644,
V.A. Koval: 0000-0001-5154-1446,
M.R. Yavorska: 0000-0003-2016-6289

CONFLICT OF INTEREST

The Authors declare no conflict of interest

CORRESPONDING AUTHOR

T.M. Labur
E.O. Paton Electric Welding Institute of the NASU
11 Kazymyr Malevych Str., 03150, Kyiv, Ukraine.
E-mail: tanyalabur@gmail.com

SUGGESTED CITATION

T.M. Labur, V.A. Koval, M.R. Yavorska (2022) Consumable electrode welding of D16 aluminium alloy with weld metal microalloying. *The Paton Welding J*., **1**, 47–54.

JOURNAL HOME PAGE

https://patonpublishinghouse.com/eng/journals/tpwj

Received: 03.09.2022
Accepted: 28.02.2023

DOI: https://doi.org/10.37434/tpwj2023.01.08

INFLUENCE OF RESIDUAL PROCESS STRESSES ON BRITTLE FRACTURE RESISTANCE OF WWER-1000 REACTOR BAFFLE IN CASE OF AN EMERGENCY

O.V. Makhnenko, S.M. Kandala

E.O. Paton Electric Welding Institute of the NASU
11 Kazymyr Malevych Str., 03150, Kyiv, Ukraine

ABSTRACT

At present, the majority of WWER-1000 reactors in Ukrainian NPPs are going through the procedure of extension of their service life. Reactor internals (RI) are one of the key elements of the structure, which limit the NPP beyond design life. Physical control of RI condition is rather difficult, and even impossible for some areas, so that mathematical modeling is the main method of prediction and analysis of the technical condition. Note that most of the studies in this area are limited to modeling the normal operation mode, but the project also envisages emergency situations (ES), characterized by a rather abrupt change of boundary conditions and loads that promotes formation of quite high stresses. The work analyzes how the residual process stresses generated during RI baffle manufacture, can affect the values of stress intensity factor on the contour of postulated cracks during ES. A significant influence of RPS on the baffle brittle fracture resistance during ES was revealed that should be taken into account at calculation-based substantiation of extension of service life of WWER-1000 type power units.

KEYWORDS: WWER-1000, reactor internals, baffle, residual process stresses, emergency situation, crack-like defect, stress intensity factor

INTRODUCTION

Improvement of the methods of extension of the life of currently operating nuclear power plants in Ukraine is one of the urgent tasks in nuclear power sector. An emergency situation (ES) is the operation mode with stringent loading conditions [1]. In some cases the project envisages not more than one such scenario during the entire term of operation (including operation beyond the design life). Reactor internals (RI), such as the reactor baffle and internal shaft, are some of the key structural elements of WWER-1000 power unit, limiting the NPP term of operation beyond the design life. Similar problems of calculation-based prediction of brittle fracture resistance (BFR) of RI elements in ES [1] and under normal operation conditions were considered earlier [2], but the residual process stresses RDS arising during baffle manufacture were not taken into account. Proceeding from published results of similar calculations [1], *J*-integral values, close to the critical ones, were derived for crack-like defects postulated in the baffle. Considering the results of recent studies in this field, namely a significant influence of RPS on the stress-strain state (SSS) of RI baffle under the normal operation conditions [3], analysis of RPS influence on SSS and BFR of RI baffle under ES conditions will be timely.

EMERGENCY MODE

A big leak at rupture of primary circuit piping of 100–850 mm conditional diameter was considered as an ES. The mathematical model of baffle SSS includes allowing for RPS [4], radiation dose accumulated over 60 years of operation, as well as temperature distributions. An emergency situation, considered in this work, is accompanied by an abrupt drop of coolant pressure and temperature. The initial parameters used were the temperature field, generated as a result of gamma radiation and contact of the coolant with the baffle surface [4], and SSS distribution without allowing for SSS (Figure 1, *a*, *c*) and allowing for SSS (Figure 1, *b*, *d*), which correspond to the normal operating mode of the reactor and are described in [3]. Proceeding from the conditions of conservatism, it was assumed in the computation model that the ES mode occurs after 60 year of reactor operation. Allowing for radiation swelling and creep for the entire term of operation is described by mathematical models [5], the correctness of which was considered in [6].

Development of an emergency situation is accompanied by a change in boundary conditions (heat transfer coefficient and coolant temperature) and loading (pressure) in time. The laws of boundary condition change are shown in Figure 2.

At modeling of the considered ES it was determined that the maximum stress values are observed at moment of time t = 100 s from ES start. The temperature field is sown in Figure 3. Stress distributions in the axial direction allowing for RPS and without allowing for them were also derived (Figure 4).

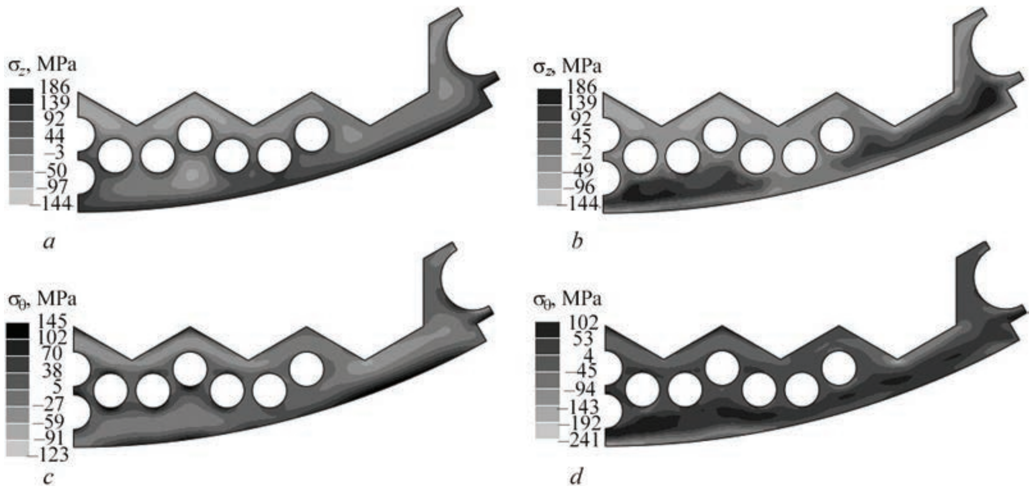

Figure 1. Stress distribution in the baffle in the 60th year of operation: *a* — axial component without allowing for RPS; *b* — axial component allowing for RPS; *c* — circumferential component without allowing for RPS; *d* — circumferential component allowing for RPS

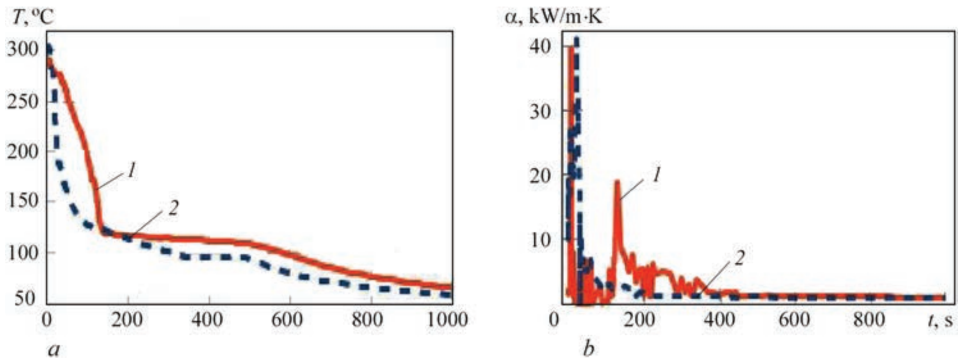

Figure 2. Temperature change (*a*) and heat transfer coefficient (*b*) of baffle walls during ES: *1* — inner surface; *2* — outer surface

Figure 3. Temperature field at moment of time t = 100 s since ES start

As one can see from Figure 4, allowing for RTS essentially influences the stress distribution. So, the maximal level of axial stresses on the baffle inner surface, when allowing for RPS, decreases from 488 to 416 MPa. However, in the baffle volume near the outer surface the compressive stresses (to 200 MPa), when allowing for RPS, turn into tensile stresses (to 50 MPa).

In [1] it was determined that at ES developing in zones 1 and 2 (Figure 4) of the baffle cross-section under consideration the value of *J*-integral for the postulated cracks is in the critical range. It should be noted that the residual process stresses were not taken into account here. In this work, the influence of RPS on the values of stress intensity factor (SIF) on the contour of postulated cracks, which are located in the plane of the baffle cross-section, is considered under the impact of axial stresses in an ES.

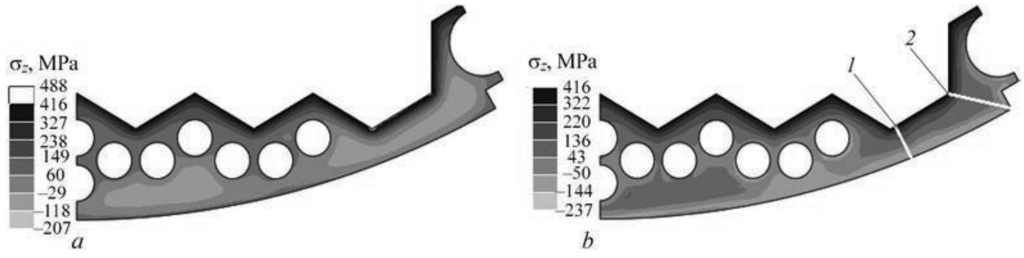

Figure 4. Distributions of axial stresses at t = 100 s since ES start without allowing for (*a*) and allowing for (*b*) RPS

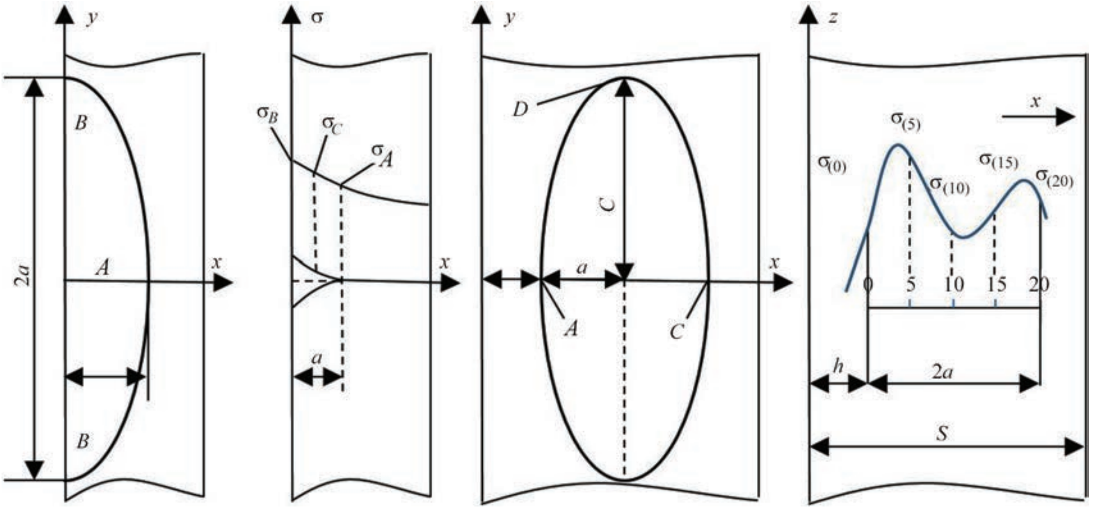

Figure 5. Geometrical parameters of semi-elliptical surface (*a*) and elliptical subsurface crack (*c*) with stress distribution (*b*, *d*)

DETERMINATION OF STRESS INTENSITY FACTOR

SIF determination was performed according to the procedures, described in [7] and [8]:

$$K_I = \sigma_K Y \sqrt{a}, \quad (1)$$

where K_1 is the stress intensity factor, MPa·m$^{0.5}$; σ_K are the stresses reduced to the uniform value, MPa; Y is the crack form factor, mm; a — minor half-axis of the crack, mm.

As the zone of maximum tensile stresses in the axial direction is located on the baffle inner surface, and when allowing for RPS this zone extends in the direction of the outer surface, the postulated defects were incorporated in the form of a surface semi-elliptical and subsurface elliptical crack (Figure 5), which are located at minimal depth ($h \geq a/9$). The ratio of the minor half-axis to the major one, in keeping with the requirements of [5], is equal to $a/c = 1/3$.

Stress distribution in the case of postulation of an elliptical subsurface crack, given in an arbitrary form, in keeping with [7], is calculated for the following coordinates across the thickness $x_j = h + a/10$, where $j = 0, 1, 2, \ldots, 20$, h is the depth of defect location. Stresses $\sigma_j = \sigma_K(x_j)$ are determined in each point x_j. Values reduced to uniform stresses $\sigma_K(A)$ and $\sigma_K(C)$ are calculated by the following dependencies:

$$\sigma_K(A) = \sum_{j=0}^{20}\left(A_j + \frac{a}{c}B_j\right)\sigma_j,$$
$$\sigma_K(C) = \sum_{j=0}^{20}\left(A_{20-j} + \frac{a}{c}B_{20-j}\right)\sigma_j, \quad (2)$$

where A_j and B_j are the tabulated values [7].

Determination of stresses σ reduced to the uniform value, at their parabolic distribution for a surface semi-elliptical crack was performed using the method described in [8]:

$$\sigma_K = 0.61\sigma_A + 0.39\sigma_B +$$
$$+\left\{0.11a/c - 0.28a/s\left[1-(a/c)^{1/2}\right]\right\}(\sigma_A - \sigma_B); \quad (3)$$
$$\sigma_K = 0.18\,\sigma_A + 0.82\,\sigma_B.$$

Form factors for each of the considered cases were also determined by different procedures. So, in keeping with [7], for elliptical subsurface cracks:

$$Y_{A,C} = \left[1-\left(\frac{a}{h+a}\right)^{1.8}\left(1-0.4\frac{a}{c}-\gamma_{A,C}\right)\right]^{-0.54} \times$$
$$\times\left[\frac{\pi}{1+1.464(a/c)^{1.65}}\right]^{0.5} \quad (4)$$

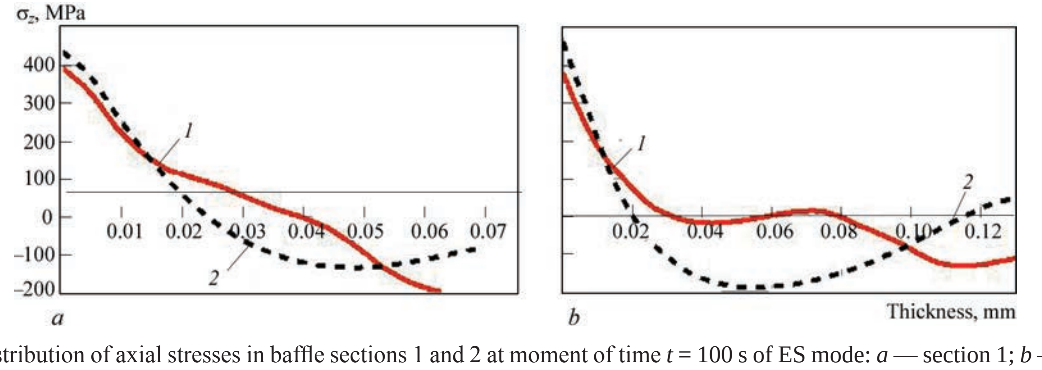

Figure 6. Distribution of axial stresses in baffle sections 1 and 2 at moment of time t = 100 s of ES mode: *a* — section 1; *b* — section 2; *1* — allowing for RPS; *2* — without allowing for RPS

Table 1. Geometrical parameters of postulated defects

Section number	a, mm	c, mm	h, mm	s, mm	Y_A	Y_C/Y_B^*	Y_D
Surface semi-elliptical crack							
1 (without RPS)	21.3	63.9	–	71	1.9	1.24	–
1 (from RPS)	35.5	106.5	–	71	2.13	1.46	–
2 (without RPS)	16.375	49.125	–	131	1.77	1.13	–
2 (from RPS)	35.5	106.5	–	131	1.87	1.22	–
Subsurface elliptical crack							
1 (without RPS)	8.875	26.75	1.7	71	2.43	1.86	2.6
1 (from RPS)	17.75	53.25	1.7	71	3.0	2.03	3.52
2 (without RPS)	8.125	24.375	3.3	131	2.06	1.76	2.08
2 (from RPS)	32.75	70.0	3.3	131	2.59	1.82	3.23
Note. $^*Y_B$ – for surface semi-elliptical crack; Y_C for subsurface elliptical crack (Figure 5).							

Table 2. Results of studying maximal SIF

Section number	$\sigma_K(A)$, MPa	$\sigma_K(C)$, $\sigma_K(B)$, MPa	$\sigma_K(D)$, MPa	K_A, MPa·m$^{0.5}$	K_C, K_B, MPa·m$^{0.5}$	K_D, MPa·m$^{0.5}$
Surface semi-elliptical crack						
1 (without RPS)	157.9	364.7	–	43.8	66.1	–
1 (from RPS)	76.4	296.5	–	30.6	81.5	–
2 (without RPS)	238.1	403.2	–	54.0	58.3	–
2 (from RPS)	100.6	294.1	–	35.5	67.5	–
Subsurface elliptical crack						
1 (without RPS)	320.5	83.8	202.2	77.8	24.9	59.1
1 (from RPS)	255.2	55.6	155.4	102.2	17.3	74.8
2 (without RPS)	284.7	68.6	176.6	52.8	12.2	34.0
2 (from RPS)	213.8	45.3	129.6	72.2	3.3	48.0

at $a \le c$, $a \le 9h$, $h + a \le s/2$;

$$\gamma_A = \left(0.5 - \frac{h+a}{s}\right)^2, \gamma_C = 0.8\left(0.5 - \frac{h+a}{s}\right)^{0.4}, \qquad (5)$$

where s is the baffle thickness, mm.

At postulation of the subsurface semi-elliptical cracks in keeping with [8], the form factors were determined by the following dependencies:

$$Y_A = \frac{2 - 0.82a/c}{\left\{1 - \left[0.89 - 0.57(a/c)^{1/2}\right]^3 (a/s)^{1.5}\right\}^{3.25}};$$
$$Y_B = \left[1.1 + 0.35\,(a/s)^2\right](a/c)^{1/2} Y_A. \qquad (6)$$

CALCULATION RESULTS

In order to determine the influence of RPS on BFR in two sections (Figure 4), two defects were postulated in the form of elliptical subsurface cracks. The geometrical parameters, as well as form factors, derived from expressions (*) for each of the defects, are given in Table 1. Figure 6 shows the distribution of axial stresses at moment of time t = 100 s since the emergency start, from which we can see an essential influence of RPS on the stress level in the considered sections 1 and 2.

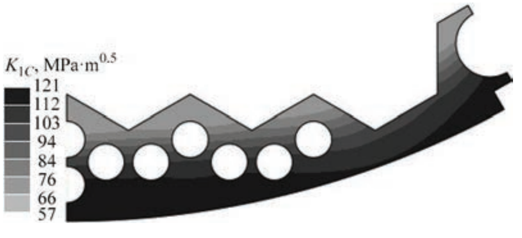

Figure 7. Distribution of critical SIF values in the baffle material at moment of time t = 100 s since ES start

Table 2 shows the results of calculation of maximum equivalent stresses and SIF for three characteristic points of the defects being postulated, at moment of time t = 100 s in ES mode.

As one can see from Table 2, allowing for RPS, on the whole, lowers the values of equivalent stresses, irrespective of the location of characteristic points (A, B, C and D) and type of postulated defect, leading to lowering of SIF value. It should be noted, however, that in the case of allowing for RPS, the tensile stress zone becomes greater, due to redistribution of stresses, permitting the postulated crack dimensions to be increased. Increase in the dimensions of the postulated defect can lead to a higher SIF value.

At postulation of a surface semi-elliptical crack, it was determined that in each of the considered sections when allowing for RPS in points A, SIF values decrease significantly, by 30 % for section No. 1 and by 34 % for section No. 2. However, an increase by 23 and 16 % is observed in points B. Note that the maximal SIF values were determined in points B, so that from the viewpoint of BFR evaluation the model allowing for RPS is more conservative.

At consideration of a subsurface elliptical crack it was determined that when allowing for RPS the SIF level for points *A* and *D* becomes higher, and its slight decrease is characteristic for point *C*. An increase in SIF value is observed for points: *A* and *D* by 31 and 27 % in section No. 1, and by 37 % and 41 % in section No. 2, respectively (Table 2).

The elliptical subsurface crack is more hazardous in terms of BFR, and its dimensions may reach critical values in an emergency (in section No. 1 at moment of time $t = 100$ s since ES start, $K_1 = 102.2$ MPa·m$^{0.5}$ allowing for RPS). Distribution of SIF critical values in the baffle material is shown in Figure 7.

An ES with harder boundary conditions is considered in [1]. Here, in one of the sections, which is in an area of significant impact of RPS and corresponds to the considered section No. 2, *J*-integral level reaches 12420 J/m^2 at critical value $J_c = 15400$ J/m^2. In keeping with the data (Table 2), SIF value, when allowing for RPS, can rise by approximately 40 %, i.e. *J*-integral values, derived in [1], can be much higher than the critical value, when allowing for RPS ($J \approx \approx 17000$ J/m^2). That is, allowing for RPS can enhance the conservatism of the approach for BFR evaluation and determination of RI baffle life.

CONCLUSIONS

Results of the conducted modeling of SSS and evaluation of BFR in WWER-1000 reactor RI baffle during an emergency in the mode of a big leak at rupture of primary circuit piping with the conditional diameter of 100–850 mm, allowing for and without allowing for RPS in the baffle showed that:

● at the most hazardous moment of time $t = 100$ s from ES start rather high stresses form in the axial direction in the baffle. Allowing for RPS decreases the value of total stresses, but the zone of tensile stresses becomes larger due to their redistribution, which permits increasing the size of the postulated crack and can lead to SIF increase, respectively;

● subsurface elliptical cracks are more hazardous in terms of BFR than the surface semi-elliptical cracks. Allowing for RPS leads to an increase in SIF for subsurface elliptical cracks up to 40 % at moment of time $t = 100$ s since ES start.

Thus, an essential influence of RPS on brittle fracture resistance of the baffle during ES was found, which should be taken into account at calculation-based substantiation of extension of operating life of WWER-1000 type power units.

REFERENCES

1. Pištora, V., Švrček, M., Ferko, P., Mirzov, I. (2018) Fracture Mechanical Assessment of VVER Reactor Internals. *ASME 2018 Pressure Vessels and Piping Conf. (July 15–20 2018, Prague, Czech Republic)*. DOI: https://doi.org/10.1115/PVP2018-84589
2. Orynyak, A.I. (2021) Methods of stress intensity factor calculation allowing for geometrical nonlinearity and arbitrary shape of the crack*: Syn. of Thesis for Cand. of Tekh. Sci. Degree*, 05.02.09, Kyiv [in Ukrainian].
3. Makhnenko, O.V., Kandala, S.M. (2022) Evaluation of brittle fracture resistance of WWER-1000 reactor baffle during long-term service, taking into account the residual technological stresses. *Tekh. Diahnost. ta Neruiniv. Kontrol*, **3**, 3–11 [in Ukrainian]. DOI: https://doi.org/10.37434/tdnk2022.03.01
4. Makhnenko, O., Kandala, S., Basistyuk, N. (2021) Influence of the heat transfer coefficient on the level of residual stress after heat treatment of the VVER-1000 reactor baffle. *Mechanics and Advanced Technologies*, 5(**2**), 254–259. DOI: https://doi.org/10.20535/2521-1943.2021.5.2.245074
5. PM-T.0.03.333–15: *Typical program on evaluation of the technical condition and extension of service life of WWER-1000 reactor internals* [in Russian].
6. Chirkov, A.Yu. (2020) On correctness of the known mathematical model of radiation swelling allowing for the effect of stresses in the problems of elastoplastic deformation mechanics. *Problemy Mitsnosti*, **2**, 5–22 [in Russian].
7. RD EO 1.1.2.05.0330–2012: *Guide on strength analysis of equipment and piping of RBMK, WWER and EGP reactor units at the stage of operation including operation beyond the design life* [in Russian].
8. (2013) *Guidelines for integrity and lifetime assessment of components and piping in WWER nuclear power plants (VERLIFE)*. Vienna, Int. At. Energy Agency.

ORCID

O.V. Makhnenko: 0000-0002-8583-0163,
S.M. Kandala: 0000-0002-2036-0498

CONFLICT OF INTEREST

The Authors declare no conflict of interest

CORRESPONDING AUTHOR

O.V. Makhnenko
E.O. Paton Electric Welding Institute of the NASU
11 Kazymyr Malevych Str., 03150, Kyiv, Ukraine.
E-mail: makhnenko@paton.kiev.ua

SUGGESTED CITATION

O.V. Makhnenko, S.M. Kandala (2022) Influence of residual process stresses on brittle fracture resistance of WWER-1000 reactor baffle in case of an emergency. *The Paton Welding J.*, **1**, 55–59.

JOURNAL HOME PAGE

https://patonpublishinghouse.com/eng/journals/tpwj

Received: 09.09.2022
Accepted: 28.02.2023

SUBSCRIPTION–2023

«The Paton Welding Journal» is Published Monthly Since 2000 in English, ISSN 0957-798X, doi.org/10.37434/tpwj.

«The Paton Welding Journal» can be also subscribed worldwide from catalogues subscription agency EBSCO.

If You are interested in making subscription directly via Editorial Board, fill, please, the coupon and send application by Fax or E-mail.

12 issues per year, back issues available.

$384, subscriptions for the printed (hard copy) version, air postage and packaging included.

$312, subscriptions for the electronic version (sending issues of Journal in pdf format or providing access to IP addresses).

Institutions with current subscriptions on printed version can purchase online access to the electronic versions of any back issues that they have not subscribed to. Issues of the Journal (more than two years old) are available at a substantially reduced price.

Subscription Coupon			
Address for Journal Delivery			
Term of Subscription Since	**20**	**Till**	**20**
Name, Initials			
Affiliation			
Position			
Tel., Fax, E-mail			

The archives for 2009–2020 are free of charge on www://patonpublishinghouse.com/eng/journals/tpwj

ADVERTISING
in «The Paton Welding Journal»

External cover, fully-colored:
First page of cover
(200×200 mm) — $700
Second page of cover
(200×290 mm) — $550
Third page of cover
(200×290 mm) — $500
Fourth page of cover
(200×290 mm) — $600

Internal cover, fully-colored:
First/second/third/fourth page
(200×290 mm) — $400

Internal insert:
(200×290 mm) — $340
(400×290 mm) — $500

- Article in the form of advertising is 50 % of the cost of advertising area
- When the sum of advertising contracts exceeds $1001, a flexible system of discounts is envisaged
- Size of Journal after cutting is 200Í290 mm

Address
11 Kazymyr Malevych Str., 03150, Kyiv, Ukraine
Tel./Fax: (38044) 205 23 90
E-mail: journal@paton.kiev.ua
www://patonpublishinghouse.com/eng/journals/tpwj